COMPUTATIONAL STUDIES OF CRUSTAL FLUIDS AND EARTHQUAKES

A DISSERTATION
SUBMITTED TO THE DEPARTMENT OF GEOPHYSICS
AND THE COMMITTEE ON GRADUATE STUDIES
OF STANFORD UNIVERSITY
IN PARTIAL FULFILLMENT OF THE REQUIREMENTS
FOR THE DEGREE OF
DOCTOR OF PHILOSOPHY

By
William Joseph Bosl
March 1999

I certify that I have read this thesis and that in my opinion it is fully adequate, in scope and in quality, as a dissertation for the degree of Doctor of Philosophy.

Dr. Amos Nur
(Principal Advisor)

I certify that I have read this thesis and that in my opinion it is fully adequate, in scope and in quality, as a dissertation for the degree of Doctor of Philosophy.

Dr. Paul Segall

I certify that I have read this thesis and that in my opinion it is fully adequate, in scope and in quality, as a dissertation for the degree of Doctor of Philosophy.

Dr. Gregory Beroza

Approved for the University Committee on Graduate Studies:

Dean of Graduate Studies

Preface

The study of crustal fluids, particularly groundwater, has generally been confined to studies of the movement of dissolved chemical species through a static porous crust. Mechanical aspects of crustal dynamics have tended to relegate pore fluid effects to a secondary role, except perhaps in situations where fluids are being actively pumped into or extracted from wells. It has long been suspected that pore fluids might play a more active role in the mechanical evolution of the crust. Unfortunately, it is difficult to measure pore pressures over broad regions in order to find correlations with measured deformation, faulting processes and earthquakes, or stress changes. Thus, theories about the involvement of pore fluids in crustal dynamics have remained in the realm of qualitative hypotheses.

Computer simulation has emerged in the past few decades as a 'third way' of doing science, taking a place alongside field and laboratory measurement and theoretical analysis. Simulation allows researchers to experiment with various complex dynamical theories about phenomena and to test the consequences of different theories. Because all parameters are controlled in numerical experiments, it is possible to determine the relative importance of different physical processes or properties on the system behavior.

Phenomena of interest to geoscientists tend to differ from those of interest to traditional physicists in that they often involve several dynamical processes that operate simultaneously in a coupled fashion. The phenomenon of interest may be viewed as a complex system, which integrates many more fundamental processes. The dynamical behavior of the whole system may be totally unlike the behavior of any of the component processes. Thus predictions about the future states of the system of interest

(which is the goal of all science) are impossible to make on the basis of solutions to equations for individual components of the system. Earthquakes are an example of a complex system such as this.

Earthquakes and related effects such as deformation and aftershocks, are often studied as the consequence of elastic or viscoelastic and elastic behavior of a fractured material crust. This approach allows the use of well-developed mathematical tools for solving elastic equations with given boundary conditions and perhaps friction laws in faults. Recent theories postulate a key role for pore fluids in the earthquake cycle. Pore fluids are involved in two ways. First, pore pressure is fully coupled dynamically to the elastic behavior of a saturated, porous material. Pore pressure might be considered the seventh component of the stress tensor, the time-dependent component. Secondly, pore fluids are chemically reactive and can change the material properties of rocks on geologically short time scales. This requires that the evolution of material properties of crustal rocks, such as permeability and elastic moduli, be considered. Computer simulation is the only way to test the consequences of all these processes working together to produce the complex system behavior we call earthquakes.

This thesis is an attempt to examine several aspects of the role of crustal fluids in the earthquake process through computer simulation. Scales ranging from pore-scale evolution of the rock matrix by various diagenetic processes, through large scale deformation due to fluid flow in a poroelastic crust are considered. My goal is two-fold: the specific geophysical results contribute to our understanding of the role of fluids in crustal dynamics. The second goal is that the computational experimentation methodology and the software tools used for this research will advance the field of computational geosciences and encourage others to expand the scope of this approach to geodynamics.

The ultimate goal of any scientific research is understanding. By this we mean the ability to make predictions about the future based on present observations. A computer model or algorithm, in the form of software, may one day become accepted as readily as a written partial differential equation, as a scientific "law" through which we make predictions about complex systems. Traditional mathematics, so

effective in advancing physics in the first half of this century, has been powerless to encapsulate the surprising behavior of complex systems. This is the reason that geological sciences have tended toward description rather that quantitative prediction. But a new paradigm is emerging which includes quantitative models that are more appropriate for the kinds of coupled, nonlinear, surprising, *complex* behavior that characterizes earth systems. This dissertation is written in the spirit of the new paradigm.

Acknowledgements

Many people have contributed to my success in graduate school under unusually difficult circumstances. Amos Nur, my advisor, has been a great teacher and inspiration. To me he exemplifies the Stanford motto, "Stanford - die Luft der Freiheit weht" (Stanford - [where] the wind of freedom blows). Amos gave me the freedom to pursue my sometimes unorthodox approaches to geophysical research and was always there to gently lead me back onto more fruitful paths when I naively strayed into intellectual quagmires. Though I was told by many of my scientific colleagues graduate school had been a painful ordeal for them, my graduate studies at Stanford have truly been an enjoyable and wonderfully exciting experience. The most important lessons I learned in my years at Stanford were learned from Amos outside of the classroom: first, in scientific research one must always have clearly in mind what question one is trying to answer. A great deal of muddled thinking can be avoided by adherence to this simple principle Second, no idea is solely one's own, no matter how brilliant, so share credit generously. It will not take away from one's accomplishments to acknowledge the help of others.

My dear wife and childhood sweetheart, Judy, has been at my side through all of my college and graduate studies. She has put up with seemingly endless nights of study, the clickety-clack of my keyboard in the night, and the inevitable mood swings and frustrations that accompany academic endeavors. And she is still at my side providing love and encouragement for all of my restless pursuits. She has developed an uncanny ability to look through my eyes and know if her words are registering, or if they have been pre-empted by an unresolved scientific puzzle that still occupies my limited CPU resources. Unfortunately, the latter flaw will not be cured by the

completion of this dissertation. Thanks for everything ...

My children have known, shared and even encouraged my exhuberent love for science and have patiently tolerated my absence while I lived a dual life as Livermore computer scientist and Stanford graduate student. Justin, Brian, Janelle, and Kevin, I love you all very much and am thankful for your wide-eyed fascination with nature that has helped to keep alive my own child-like enthusiasm for science. Even if you never become scientists, I hope I will pass on to you a love for nature and my enjoyment in understanding its secrets.

My father encouraged my earliest interest in science and never failed to support me along the way. I only wish he could be here now to see the completion of my formal education. Thanks especially to my mother, who is a constant source of encouragement and support.

Many professors, colleagues and friends have contributed to my development as a scientist. Gary Mavko helped me to learn to push off fearlessly into the unknown with his admonition to "stop talking about what you think you can do and just do something". His prodding, generousity with ideas, and encouraging discussions will always be remembered. Thanks to Jack Dvorkin, who worked closely with me in my earliest research projects. A special thanks to Steve Ashby at LLNL for his constant support as I tried to balance project goals at work with my academic interests. Steve Smith, who is one of the most far-sighted computer scientists I know, provided many enjoyable discussions of complex systems and computational science and helped to keep my imagination alive. Thanks to all my friends and colleagues for whom there is not space to mention individually. Thanks also to Margaret Muir for guiding me through many of the details of graduate work while at Stanford and for many pleasant and stimulating conversations. I have enjoyed your friendship immensely.

Finally, I would be remiss if I was not to acknowledge my gratitude to the Creator of this intriguing universe. I've been granted the freedom to earn a living by exploring this world, a priviledge that the vast majority of humanity has never had and perhaps will never have. I can only hope that my labors will reach beyond my own personal gain and contribute something of lasting value to the world.

Contents

Preface **iv**

Acknowledgements **vii**

1 Introduction **1**

1.1 Earthquakes, Crustal Fluids, and Computer Modeling 2

1.1.1 Complexity in the Geosciences 2

1.2 Summary of this Dissertation 7

1.2.1 General and Specific Goals 7

1.2.2 The Evolving Crust: Material Properties 7

1.2.3 Poroelasticity 8

1.2.4 The 1992 Landers Earthquake 9

1.2.5 Pore Fluids and Aftershocks 10

1.2.6 A General Earthquake Model Strategy 10

Bibliography 11

2 Permeability Models for Crustal Simulation **12**

2.1 Introduction 12

2.2 Pore Structure and Permeability 13

2.3 Permeability representation in porous materials 15

2.4 Implications for Crustal Fluids 17

Bibliography 17

3 Permeability-Porosity Relationships in Granular Rocks **19**

3.1 Introduction 19
3.2 Lattice-Boltzmann Flow Model 20
3.3 Pore-Space Models and Simulated Diagenetic Processes 22
3.4 Scale and boundary conditions 26
3.4.1 Effect of sample size 26
3.4.2 Effect of grid size 27
3.4.3 Effect of Boundary Conditions 28
3.5 Numerical Results 29
3.5.1 Four Basic Diagenetic Processes 29
3.5.2 North Sea Sandstones 30
3.5.3 Fontainebleau Sandstone 33
3.6 Conclusions 34
3.7 Appendix: A Digital Rock Physics Laboratory 35
3.7.1 Pore Geometry and Structure 36
3.7.2 Permeability Calculator 36
3.7.3 Other Rock Properties 38
3.7.4 Software Organization and Design 39
Bibliography 40

4 Computer Simulation of the Complex Crust: Theory **42**

4.1 Introduction 42
4.2 Complexity and Computer Modeling 45
4.2.1 Coupled Processes 46
4.2.2 Heterogeneous Properties 47
4.2.3 Nonlinearities 48
4.2.4 Time Evolution of Material Properties 48
4.2.5 Computational Science versus Engineering Computing 49
4.3 Theoretical Development: Thermoporoelasticity 50
4.3.1 Mass Balance Equations 52
4.3.2 Heat Transport 57

4.3.3 Elastic Deformation 58
4.3.4 Summary of Thermoporoelastic Equations 59
4.3.5 Constitutive Relations 60
4.3.6 Material Properties 61
4.3.7 Representation of Faults 61
4.4 Computational Method 62
4.4.1 Gridding 63
4.4.2 Finite Element Spatial Discretization 63
4.4.3 Time Discretization 65
4.4.4 Linear and Nonlinear Solution Methods 66
4.4.5 Boundary Conditions 67
4.4.6 Initial Conditions 68
4.5 Some Special Cases 68
4.5.1 Pressure Diffusion and Deformation 68
4.5.2 Coupled Isothermal Poroelasticity 70
4.5.3 Poroelasticity with Thermal Diffusion 70
4.6 Software Implementation 71
4.6.1 Managing Complexity in Sofware 71
4.7 Summary 75
4.8 Proposal for a General Earthquake Model 75
4.8.1 Goals 75
4.8.2 Earthquake Physics 75
4.8.3 Fault Mechanics 77
Bibliography 78

5 The Mandel-Cryer Effect **81**

5.1 Introduction 81
5.2 Review of poroelastic equations 82
5.3 The Mandel-Cryer effect 83
5.4 Fluid Flow in Fault Zones 90
5.5 Conclusions 93

Bibliography 96

6 Landers Postseismic Deformation **97**

6.1 Introduction 97

6.2 The 1992 Landers Earthquake 99

6.3 Computational Model 101

6.3.1 Induced Pore Pressure Due to Fault Slip 101

6.3.2 Pore Fluid Diffusion and Elastic Deformation 103

6.4 Postseismic Vertical Displacement 109

6.4.1 SAR Measurements of Postseismic Rebound 109

6.4.2 Computed Postseismic Rebound 110

6.5 Postseismic Horizontal Deformation 110

6.6 Discussion 126

6.7 Conclusions 127

6.8 Acknowledgemets 128

Bibliography 128

7 Aftershocks and Pore Fluid Diffusion **131**

7.1 Introduction 131

7.2 Nur and Booker Hypothesis 132

7.3 The Coulomb Fracture Criterion 134

7.4 Equations for Fluid Diffusion in a Porous Medium 136

7.5 Aftershocks of the 1992 Landers Earthquake 139

7.5.1 Description of the 28 June 1992 event 139

7.5.2 Slip models and fluid flow simulation 140

7.5.3 Regional aftershock frequencies 140

7.5.4 Pore pressure tendency at aftershock locations 144

7.5.5 Coulomb stress due to pore pressure 146

7.6 Summary and Conclusions 150

7.7 Acknowledgements 151

Bibliography 151

List of Tables

4.1 The most common dynamical variables 44
4.2 Examples of complex or *surprising* dynamics that can arise in the crust 46

6.1 Model of Landers fault rupture 102
6.2 Material parameters for Landers simulation 109
6.3 Time intervals over which vertical displacement changes were measured 110

List of Figures

2.1 Kozeny-Carmen curves 14

3.1 Schematic diagram of digital rock 22
3.2 Simulated granular rock with superimposed lattice points 23
3.3 Digital Finney pack 24
3.4 REVs in a random dense pack of spheres. 26
3.5 Effect of the cube size on porosity and permeability 27
3.6 Permeability as a function of grid spacing and boundary conditions . 28
3.7 Laboratory measurements of permeability and porosity 30
3.8 Normalized perm versus porosity from simulations 31
3.9 Computed curves for uniform expansion and random filling 32
3.10 Computed curves derived by filling high-flow pores and uniform expansion 33
3.11 Computed uniform expansion curve and Fontainebleau 34
3.12 Organization of a digital rock physics laboratory 40

4.1 Diagram of the PorousMedium class hierarchy. 72
4.2 Diagram of FaultSystem class. 73
4.3 Material properties and reactive chemistry class 73
4.4 Diagram of the SimQuake simulator 74
4.5 Class structure for a proposed GEM model 76

5.1 Cryer's sphere 84
5.2 Mandel-Cryer effect for several values of the parameter a 85

5.3 Mandel-Cryer effect for several diffusivity values 86
5.4 Snapshots of pore pressure evolution 87
5.5 Mandel-Cryer effect for several domain sizes 88
5.6 Pore pressure with isolated low-permeability pocket 89
5.7 Random values of the diffusivity parameter D 91
5.8 Schematic picture of Byerlee's fault model 92
5.9 Illustration of a simple two-permeability fault zone model 94
5.10 Plots of pore pressure along a line and at the center of the domain . . 95

6.1 Map of the Mohave region 99
6.2 Landers coseismic stress field 104
6.3 SAR measurements of Landers postseismic vertical displacement. . . 111
6.4 Computed postseismic vertical displacements 112
6.5 Computed postseismic vertical displacements using Biot diffusion . . 113
6.6 Pressure changes 115
6.7 Vertical displacement 116
6.8 Horizontal strain 117
6.9 Surface trace of the Landers earthquake and GPS postseismic monitoring stations 118
6.10 GPS baseline solutions from Shen, et al. (1994) 119
6.11 Computed horizontal (east and north) displacement differences. . . . 120
6.12 Geodetic array used by Savage and Svarc 121
6.13 Computed displacements relative to Sanh 122
6.14 Map of the Landers region showing total displacement relative to Gold 124
6.15 Changes in pore pressure and horizontal displacement 125

7.1 Coseismic mean stress field computed from Hudnut, et al. (1994) . . 142
7.2 Regional aftershock frequency following the 1992 Landers earthquake 143
7.3 Fraction of aftershocks that occur where pore pressure is rising. . . . 145
7.4 Aftershocks of the Landers earthquake and pore pressure. 147
7.5 Aftershocks of the Landers earthquake and Coulomb stress increase. . 149

Chapter 1

Introduction

> "The use of simulation is an activity that is as natural as a child who role plays with toy objects. To understand reality and all of its complexity, we must build artificial objects and dynamically act out roles with them. Computer simulation is the electronic equivalent of this type of role playing." (Fishwick, 1995)

The earth's crust is a complex, dynamical system. It is complex because future states depend very sensitively on current states. This is so because the physical laws which govern the fundamental processes in the crust are nonlinear. Furthermore, although the fundamental physical and chemical laws are generally well-known in an isolated laboratory setting, many processes operate simultaneously and in a coupled, inter-dependent fashion in the earth. The result is seemingly random behavior that may at times bear little resemblance to the processes that are observed in the laboratory. The methods of classical mathematical physics, which have enjoyed tremendous success in the pursuit of basic, fundamental physics, are generally powerless when faced with complex systems that involve coupled, nonlinear processes.

The crust is dynamic because it is in a state of permanent disequilibrium. This is because the two primary energy systems which drive crustal physics, the tectonic system and the hydrologic system (Hamblin, 1992) will continue to operate until the earth's core cools completely and the Sun burns the last of its hydrogen fuel. Heat energy in the earth, whether from nuclear decay or residual heat from the primordial

universe, ultimately manifests iteself in kinetic energy: thermal convection currents in the mantle are the engine that drives plate tectonic motion. The hydrologic cycle, driven by energy from the Sun as well as from tectonic processes, can significantly alter crustal properties quickly on geologic time scales. The coupling of these two dynamical systems results in complex behavior which requires quantitative computer simulation to sort out the role of all the parameters and variables in this coupled system.

1.1 Earthquakes, Crustal Fluids, and Computer Modeling

1.1.1 Complexity in the Geosciences

The earthquake cycle is a complex process. Though only well-known classical laws are involved, the combined effects of nonlinear, spatially heterogeneous properties, chemical alteration, and coupled effects result in surprising emergent phenomena. By this I mean that phenomena appear in coupled systems which cannot be predicted by observing the physics of isolated processes. A simple example of this is Cryer's poroelastic sphere, which will be discussed in a later chapter on the Mandel-Cryer effect. Earthquakes may be an example of emergent phenomena. Rather than looking for a single law to explain the observed pattern of seismic behavior on a certain fault, perhaps we need to examine more carefully all of the relevant processes that are operative and how they behave as a coupled system. For example, attempts to reproduce Omori's law, which relates earthquake size (magnitude) to frequency, focus on finding a friction law which, when applied in a sterile and isolated theoretical setting, give the right statistics. Why must complex dynamics find it's source in a single nonlinear equation?

In this thesis I will proceed from the belief that complex dynamics on one scale can result from the simultaneous operation of many processes which, when isolated, might be rather simple and well-understood. However, when coupled together, surprising behavior results. This kind of complex behavior, emergent complexity rather than

reductionist complexity, may also result or be enhanced by spatially heterogeneous material properties, which may evolve in time, and which may be nonlinear functions of the state variables.

The struggle of quantitative geologists and geophysicists to define mathematical models of the earth's dynamics is illustrated by physicist Philip Anderson, who wrote in a 1991 *Physics Today* editorial:

> "As one probes deeper into the origin of the universe or the interior of the quark, it will never be questioned that one is doing physics. By contrast, the traditional, reductionist physicist and, for sure, the funding agencies can be left vaguely disturbed or hostile as new fields lead us up the hierarchy of complexity toward sciences such as geology, developmental biology, computer science, artificial intelligence or even economics. There can be a somewhat surprising lack of understanding of what those of us working in these new fields are doing. It is still possible, for instance, to find Marvin L. Goldberger and Wolfgang Panofsky, who are relatively enlightened physicists, saying, in an op-ed piece for *The New York Times*: 'Other branches of physics [than particle physics] ... are interesting, challenging, and of great importance.... The objectives are not a search for fundamental laws as such, these having been known... since the 1920s. Rather, they are the application of these laws.' ... Is complexity physics? Is it science? What is it?" (Anderson, 1991).

Of course, geology is not a "new field" as Anderson seems to imply. But the study of geological processes as a rigorously quantitative field is rather new. The problem to which Anderson alludes, I believe, is that the model of atomic physics is not appropriate for the study of geological systems. Just as a thorough understanding of English grammar is not enough to analyze Shakepearean poetry, so an aquaintance with classical mechanics and aqueous geochemistry may not be enough to understand the behavior of the coupled effects of a fractured, thermoporoelastic system whose material properties evolve chemically.

In my research, I proceed with several assumptions, which I will lay out now.

First, crustal processes are the result of fundamental classical physics.The dynamics of the earth, including faulting and earthquakes, is governed by well-known, classical physics. Second, spatial heterogeneity on many scales, time-varying and possibly nonlinear parameters, and the coupling of two or more simpler dynamical processes together produce dynamical behavior that is complex and exhibits emergent phenonmena. That is, studying any of these processes in isolation may miss a significant part of the system dynamics. And finally, the methods of classical mathematical analysis, based on assumptions of continuity and infinitesimals, must give way to new quantitative approaches. Computational science, in which computer software that implements discrete simulations of dynamical processes, is the appropriate theory for complex earth processes. This is so because the class of processes that can be represented by differential or algebraic equations is rather limited.

Wolfram (1994) has demonstrated that any physical process may be represented by a computational algorithm. Differential equations and their discrete approximations represent two types of algorithms for computing a future state from a preceding state. But there are many processes, which Wolfram refers to as computationally irreducible processes, which cannot be written as an equation. An example of such a physical process is given later in this dissertation in the chapter on lattice Boltzmann simulations. There, we introduce an algorithm that simulates the filling of pore spaces in a granular rock on the basis of fluid flow velocites in the spaces. The flow velocities change as the pore spaces are filled. The simulated diagenesis cannot be modeled a priori by any equations, no matter how complex. Yet the process can be modeled rather easily by prescribing a rule for carrying out the simulation in time. This is an example of a computationally irreducible process. Faulting processes, perhaps controlled by geochemical, mechanical, and fluid processes may be computationally irreducible processes. They can only be modeled by prescribed dynamically rules, which may not be reducible to differential or algebraic equations.

Discretized partial differential equations are a step in this direction and provide a powerful means for studying complex systems. But more radical approaches are also being developed which re-examine our continuum physical models. An example of this is the lattice gas or lattice Boltzmann model for fluid flow. As Toffoli suggests

(Toffoli, 1987), our physical models reflect to a large extent the analytical tools we have available. The computer has hardly begun to impact our quantitative models.

Computational experimentation with a hierarchy of increasingly complex numerical models is perhaps the only way to sort out which effects are of greatest importance for modeling earthquakes and fault dynamics. The purpose of this thesis is to examine the role of crustal fluids as an important element in the evolution of crustal stress and the earthquake process through computer simulation. A strategy for constructing a General Earthquake Model, based on the software component strategy used for this thesis, will be outlined. It is hoped that this research, and the proposed design for simulating crustal processes, will spur further research in the study of the crust as a fascinating complex system.

What does it mean to understand a physical process in a scientific sense? This is, of course, at the very heart of our definition of science. Science is much more than simply a collection of data. It is also fundamentally a set of rules that coherently connect the data into a logical pattern. It is this pattern that allows us to make predictions about the future behavior of a dynamical process, given some current configuration. For the past three hundred years or so, these rules have generally been written in a mathematical form that uses constructs from differential calculus to form differential equations. Enormous energy has been spent in devising solutions to these equations using the methods of differential and analytical calculus. The return on this investment of effort has been correspondingly high. We "understand" many things about nature that we not understood in the pre-calculus days.

An example is found in Maxwell's equations, which describe the dynamical behavior of electromagnetic fields. We still do not understand what an electromagnetic field *is* in its essence. But all of science is at base phenomenological. What we call *laws* in science are mental constructs about an underlying reality which we only infer from our observations. Another example is Newton's laws of mechanics. These are quite good descriptions of how rigid bodies behave. Nevertheless, they are wrong. Newton's laws are merely an approximation to the more accurate dynamical model given by relativistic quantum mechanics. So, we see that in common usage, scientific laws are simply rules about the behavior of nature that are well-established and

predict dynamical behavior fairly accurately, to within some acceptable tolerance.

What does all this have to do with the earth sciences? I believe the earth sciences are just beginning to reach a golden period, much as physics did in the period between Newton and the early 20^{th}century when the foundations of quantum mechanics were laid. The reason for this, I believe, has to do with the development of digital computing technology and new mathematical ideas in the fields of nonlinear dynamics and numerical simulation methods. These new developments have provided the scientific community with tools that are more appropriate for dealing with the kinds of processes encountered in the solid earth than were previously available.

The quantitative study of the earth involves the integration of many fundamental processes. These fundamental processes derive from classical physics and generally well-known chemistry. However, even if we can write down the differential equations that might describe each of the processes that are important in the earth, they are not tractable by analytical methods. In fact, we can safely say that they never will be. This is because the equations involve nonlinearites, spatially heterogeneous coefficients, temporally evolving parameters, and couplings that result in *complex* behavior. For now, let us simply define complex behavior to be surprising behavior. That is, the resulting dynamics is not only quantitatively unpredictable by analytical means (we can't write down a formula from which we can derive all future states of a system) but it is also non-intuitive qualitatively.

I wish to argue in this essay that we can claim to understand some process in the earth if we can make a computer simulation code that predicts the behavior of that earth system to within some acceptable degree of accuracy. Such a theoretical model is conceptually no different from a differential equation model from which we can draw analytical solutions. Both are rules for predicting the future state of a system, to within some tolerance, from a starting state. It should be emphasized that I am not restricting computer codes to discrete approximations of differential equations, though these are an important part of the class of computer models which I am describing. Also included are discrete models of the fundamental physics, such as cellular automata, lattice gas models of fluids, and other alternatives to differential equations.

The point of my dissertation is to begin studying the dynamics of the crust and the role that fluids play in it. The equations which describe this behavior include all the characteristics of complex phenomena: nonlinearities, heterogeneities, and coupled processes. Systematic classification of when each of these complex deviations from simple linear theory is a large undertaking that must be done in order for earth scientists to begin to recognize characteristic patterns in observed data.

1.2 Summary of this Dissertation

1.2.1 General and Specific Goals

This thesis has a dual purpose. It presents specific results about crustal fluids, permeability, postseismic deformation and aftershocks. It also presents a general methodology for a quantitative study of the physics of the earth based on computational models whose dynamical consequences can only be observed through the use of digital computers.

1.2.2 The Evolving Crust: Material Properties

The ubiquitous presence of water in the crust provides a dynamic mechanism by which the fundamental material properties of the crust can be profoundly altered in geologically short time spans. The mechanical, thermal, and chemical properties of the crust are thus in a constant state of disequilibrium, even on human time scales.

One of the most important controlling parameters for the hydrologic engine is permeability. An understanding of permeability is vital for practical concerns such as producing a petroleum reservoir or cleaning up a contaminated aquifer. Permeability heterogeneity and evolution have been invoked as playing a critical role in some theories of the earthquake cycle. The construction of computer models which include evolving porosity must have some means of relating permeability to the changing pore structure of rocks. It is not yet well understood in a quantitative, predictive sense how permeability is related to porosity and pore structure. A knowledge of this relationship might be the key to relating permeability to other physical properties of

rocks, such as electrical conductivity and seismic wave velocity, which are measureable quantities.

A first attempt, and more importantly, a strategy for future work, is made here to clarify the relationship between permeability and pore structure. The method is to make pore-scale computer models of rocks, *digital rocks*, and then compute the permeability of the model rock. Various methods for filling the pore space are used to generate porosity - permeability curves for the various synthetic diagenetic schemes. The results are compared to laboratory measurements of different natural and artificial granular materials to determine what pore-filling mechanisms might possibly explain observed trends in the real materials. This kind of numerical experimentation was made possible by the implementation of a new method for fluid flow simulation based on a microscopic statistical mechanical approach. The first such model, called a lattice gas model, is a type of cellular automaton which can be shown theoretically to reproduce the macroscopic Navier-Stokes equations.

I implemented a modification of the discrete lattice gas model, based on the Boltzmann equation and called a lattice Boltzmann model for fluid flow in a computer program. Continuing with the common theme for all of the numerical modeling work presented in this thesis, I encapsulated complex processes into separate components so that I was free to experiment with one process whilst being unencumbered by other complex processes. Once the lattice Boltzmann "permeability calculator" was implemented, I was then free to experiment with various methods for evolving the pore space in my digital rocks. Future work following this general strategy will involve the computation of other rock properties from the same pore geometries used for the permeability calculations. New schemes for generating and evolving pore geometries will also be developed in order to allow more realistic simulations of real materials.

1.2.3 Poroelasticity

To a large extent, the upper 10 km of the Earth's crust, behaves as a fluid-saturated elastic material. Though the equations of linear elasticity are often used to compute stress changes in the crust due to fault dislocations, pore fluids add a time element to

the equations that describe stress in the brittle crust. The coupled equations for fluid flow in a saturated porous medium and elastic deformation were first formulated by Maurice A. Biot in 1941 and have been formulated and presented by many authors in various forms since then. The equations are presented here in a more general form that does not assume material properties are constants. Rather, spatial heterogeneity, inelastic evolution due to diagenesis, and nonlinearities are allowed and assumed. Permeability, which controls the movement of fluid, is assumed to be a full rank 2 tensor, which permits anisotropy in the direction of fluid flow. The resulting equations cannot be solved analytically, so a numerical algorithm is presented for their solution by computer.

Under certain conditions, poroelastic materials can exhibit rather surprising and unexpected dynamical behavior. One definition of complexity or complex dynamics might be dynamical processes that do not evolve according to our usual linear ways of thinking; that is, they behave in surprising and unexpected ways. One example of this kind of complex behavior is the Cryer-Mandel effect in a poroelastic sphere or cylinder. After reproducing this effect numerically and discussing the physical reasons for the effect, I show that the effect is not limited to simple spherical geometry, but may also arise in contexts that have important implications for faults. The combination of coupled poroelastic effects together with heterogeneous permeability are necessary ingredients for this phenomenon to occur. All of these ingredients and more are always present in the earth. It is only by computer experiments with models that include many processes that we can hope to begin to understand quantitatively the dynamics of a complex process such as earthquakes.

1.2.4 The 1992 Landers Earthquake

Considerable data was collected following the 1992 Landers earthquake, which makes it an ideal earthquake for research. Using the poroelastic model which was mentioned in the preceeding section, postseismic vertical and horizontal deformation was simulated. The goal was to determine how significant poroelastic deformation caused by

pore fluid diffusion following the earthquake, was in explaining the measured deformation in the region of the Landers earthquake. Simulations with reasonable parameters strongly suggest that pore fluid movement must be included in considerations of postseismic deformation. Even simulations with simple models of the local material properties exhibited complicated patterns of deformation, indicating that considerably more research should be done when more information about permeability and elastic anisotropy become available.

1.2.5 Pore Fluids and Aftershocks

It is well-known that many hydrologic effects may be observed following large earthquakes. Nur and Booker (1972) proposed that aftershocks were controlled to a large extent by pore pressure diffusion following earthquakes. A general theory was proposed for why this was so. I take a new look at this idea using computer simulation with the model developed for studies of deformation following the Landers earthquake. Aftershock frequencies are computed and aftershock locations are correlated with pore pressure tendencies. These correlations are reasonably good. Better results are achieved by looking at the Coulomb stress perturbation caused by pore pressure diffusion following the earthquake. These results indicate that coupled poroelastic stress changes caused by pore fluid movement following an earthquake may play a significant role in aftershock occurrence.

1.2.6 A General Earthquake Model Strategy

Of course, more general physical models are possible, including viscoelasticity, various nonlinear elastic theories, and multiphase fluid flow. Incorporation of reactive chemistry models which modify the material properties, fault models which behave, during rupture, at least, according to their own dynamical laws, and interactions with other physical systems, such as lower boundary conditions created by mantle convection, are all possible extensions to a model of crustal dynamics. A strategy is presented by which the complex physical and mathematical models required by each of these

processes can be encapsulated for use in more complex simulators. Software components, each corresponding to a particular dynamical process, can be designed which allow more and more complex models to be built from tested simpler components. This allows for considerable flexibility in designing computer experiments to test and compare various physical theories about phenomena such as earthquakes which involve numerous complicated, coupled processes operating simultaneously. A system for rapid numerical experimentation with complex systems can be constructed in this way. The rudiments of this system have been built for the numerical simulations carried out in this dissertation. By building on this system, tools for a whole generation of scientists to use can be made available, making the computer a playground for scientific creativity.

Bibliography

Biot, M. A., Generalized theory of 3-dimensional consolidation, *J. Appl. Phys.*, *12*, 155–164, 1941.

Fishwick, P. A., *Simulation Model Design and Execution: Building Digital Worlds*, Prentice Hall, Englewood Cliffs, NJ, 1995.

Hamblin, W. K., *Earth's Dynamic Systems, Sixth Edition*, MacMillan Publishing Co., New York, 1992.

Nur, A., and J. R. Booker, Aftershocks caused by pore fluid flow?, *Science*, *175*, 885–887, 1972.

Toffoli, T., and N. Margolus, *Cellular Automata Machines: A New Environment for Modeling*, MIT Press, Boston, 1987.

Wolfram, S., *Cellular Automata And Complexity : Collected Papers*, Academic Press, New York, 1994.

Chapter 2

Permeability Models for Crustal Simulation

2.1 Introduction

Fluid flow in the crust is controlled by the permeability of the porous material through which the fluid flows. The rate at which permeability evolves due to precipitation/dissolution, the degree of permeability heterogeneity, and nonlinear response of permeability to pore pressure are all critical parameters. Seemingly small quantitative variation in the magnitude of these parameters can result in vastly different qualitative behavior of the system. In order to make quantitative predictions about the dynamics of a fluid-saturated porous medium it is necessary to understand the sensitivity of the system to the parameters that determine spatial and temporal permeability distribution. Computer simulation is the tool utilized to carry out the quantitative experiments here. These quantitative results can then be used to determine which field measurements are needed to differentiate between competing theories.

As indicated in the previous chapter, crustal processes are characterized by complexity: spatial heterogeneity and geometrical complexity, nonlinearities, and coupling of two or more processes. This makes computer simulation a non-trivial task and is perhaps one reason why large-scale computer modeling is less well developed in the solid earth sciences than in other earth sciences, such as meteorology and

oceanography. Some new algorithmic tools are employed in the investigations presented here. The lattice Boltzmann method is used for a pore scale investigation of permeability-porosity relationships in granular materials. The results of this study have implications for the functional representation of permeability in terms of porosity.

2.2 Pore Structure and Permeability

The permeability distribution of a porous medium represents the plumbing system that controls the flow of fluid in the medium. The evolution of permeability in a chemically reactive medium must be represented mathematically as a function of porosity in order to include this evolution in numerical simulation of fluid flow when chemical reactions which change the medium are included. The functional relationship between permeability and porosity may be critical for some processes where the rate at which permeability changes with porosity. Walder and Nur (1984) have shown, for example, that if permeability decreases faster than a critical rate, anomalously high pore pressure can develop in permeable rock. If permeability decreases slowly, fluid drains quickly enough to prevent high pore pressures from occurring. Some models of the earthquake cycle suggest that high pore pressures may develop in compartments in a fault zone when precipitation clogs the porosity. The rate at which permeability declines as porosity decreases determines whether or not the compartments of high fluid pressure will form or not.

One of the most common ways of representing the functional relationship between porosity and permeability is through a power law or Kozeny-Carmen relationship (Bourbie, 1987; Dullien, 1992):

$$k = c\phi^n \tag{2.1}$$

where k is the intrinsic (scalar) permeability, ϕ is the porosity, n is an exponent generally equal to 2 or 3, and c is an empirically determined coefficient. Several Kozeny-Carmen curves are shown in figure 2.1, superimposed on laboratory measurements of porosity and permeability for several types of sandstones. It is clear that the

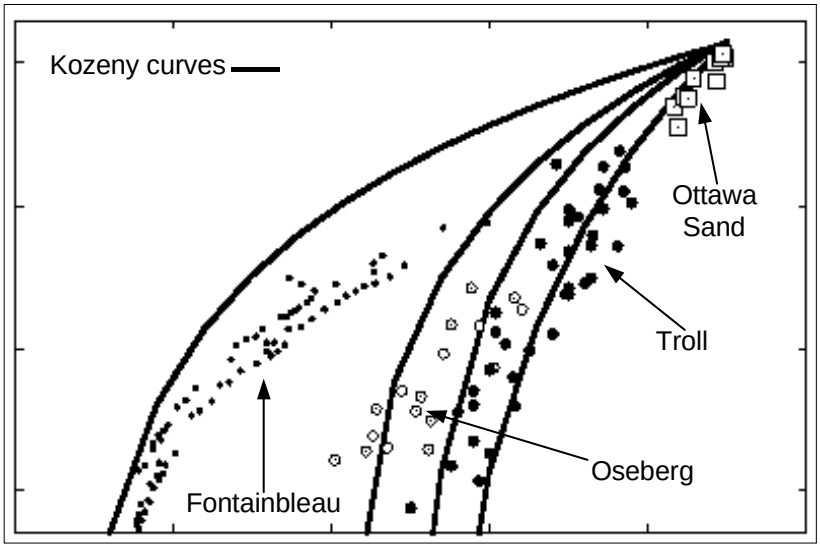

Figure 2.1: Kozeny-Carmen curves

curves do not follow the data trends very well for the North Sea sandstones, which appear to follow a linear trend on the semi-log plot.

Person, et al. (1996) suggest that the porosity may be linearly related to the log of permeability:

$$\log(k) = C\phi + D \tag{2.2}$$

This relationship is empirically based on laboratory measurements of cores from clastic sediments (Bethke, 1985). Such a relationship appears to be a good fit to the North Sea data which is shown in our plot of Kozeny-Carmen curves.

The particular functional relationship chosen for modeling pore pressure evolution might make a qualitative difference between the development of high pore pressure compartments and the lack of such development. To determine which functional relationship to use to compute permeability when the porosity evolution is due to uniform deposition of silicates by precipitation, for example, it will be necessary to investigate more precisely the physical and geometrical causes of the observed functional relationships.

2.3 Permeability representation in porous materials

Permeability is a macroscopic parameter which determines the flow characteristics of a porous medium. On scales larger than the pore scale, permeability is spatially heterogeneous in all real earth materials. It may be pressure dependent and anisotropic, particularly in fractured materials. When the fluid flowing through the rock matrix is chemically reactive, the pore space may be altered by mineral deposition or dissolution of the rock matrix. The permeability will then change with time as flow proceeds. We wish to characterize permeability mathematically in order to include it in a computer simulation of flow in reactive poroelastic media.

The general permeability tensor, k_{ij} appears in Darcy's equation in the following form:

$$q_i = \frac{k_{ij}}{\mu} \frac{\partial P}{\partial x_j} \tag{2.3}$$

where μ is the kinematic viscosity, P is the pore pressure, and q_i is the fluid flux across a unit surface area normal to the x_i direction.

In conceptual models of the subsurface, the functional dependence of k_{ij} must be represented quantitatively if it is to be used in computer simulations of porous media flow. It is convenient to decompose permeability into the following form:

$$\widetilde{k}_{ij} = k_{ij}(x) \cdot k_0(x,t) \cdot k_f(P,\sigma) \tag{2.4}$$

The tensorial factor, $k_{ij}(x)$, in this representation depends only on spatial location. For many simulations, it may be adequate to allow $k_{ij}(x)$ to vary on a larger scale with, for example, the lithologic unit. In general, the permeability anisotropy will not be known on a finer scale than this. Furthermore, memory requirements in computer simulations would be substantially increased if six components of the permeability tensor were required at every grid point.

The scalar quantity $k_0(x,t)$ varies spatially and temporally. The temporal variation is due to nonelastic evolution of the pore space, such as chemical alteration and diagenesis. $k_0(x,t)$ here is explicitly independent of the pore pressure and applied

stress. k_0 depends strongly on how the precipitating mineral is deposited in the pores. Results shown below suggest that uniform deposition causes a porosity-permeability relationship that follows a typical Kozeny-Carmen or exponential curve. Linear relationships on semi-log axes do not result from uniform depositional processes, but are apparently caused by the plugging of pore throats by clay particles or deposition that is related to the flux of fluid through the pore.

$k_f(P, \sigma)$ represents the pressure and stress dependence of permeability. This is particularly important in materials where the primary permeability is due to fractures. Yilmaz (1994) has shown that strongly nonlinear flow behavior can occur in reservoirs where the permeability is sensitive to pore pressure. Local stress has the same effect on permeability as pore pressure and so also must be considered in some cases. In fractured rocks, the permeability might depend on the full stress tensor. Typically, the pressure dependence of permeability is given by:

$$k_f(P, \sigma) = e^{\beta(P+\sigma)} \tag{2.5}$$

where β is the permeability compliance of the material. Note that β may vary spatially, perhaps with the lithologic unit, just as the anisotropy varies. The mean stress, represented here by σ, and P refer to the deviation from some reference value.

The above representation of permeability is intended primarily for matrix permeability, but may also be adequate for fractured media. Fractured media present particular modeling challenges because of their flow anisotropy and their anisotropic response to stress. The reader is referred to the study *Rock Fractures and Fluid Flow* (1996) written by the Committee on Fracture Characterization and Fluid Flow for a thorough review of flow in fractured rocks. Three of eight key recommendations made in this study deal with research into improved methods for modeling flow in fractured systems, and numerical studies of the effects of coupling between chemical processes, stress, temperature, and flow in fractured systems. Pore scale computer simulations, such as that presented in the next chapter for granular materials, may be easily be extended to fractures in order to understand the effects of chemical diagenesis on flow in fractures. Models of fracture permeability can also be easily implemented in the thermoporoelastic simulation software described in Chapter 4 in order to study

coupled effects. Fractured systems will not be considered further in this thesis.

2.4 Implications for Crustal Fluids

This short chapter is intended to show that permeability, which is often treated as a constant scalar in poroelastic models, can be quite complex in earth materials. The correct representation of permeability and its dependence on pore structure can have important implications for models of crustal pore pressure and stress evolution. The evolution of permeability over geologically short periods depends upon a number of factors which, ultimately, control the geometry of the pore structure. Simulation of crustal processes which include moving fluids requires that permeability be modeled quantitatively. In order to do this, a systematic study of each of the factors which affect permeability is required. In the next chapter, we study the affect of cement deposition in the pore spaces on permeability and porosity.

Bibliography

Bethke, C. M., A numerical model of compaction-driven groundwater flow and heat transfer and its application to the paleohydrology of intracratonic sedimentary basins, *Journal of Geophysical Research*, *90*, 6817–6828, 1985.

Bourbie, T., O. Coussy, and B. Zinszner, *Acoustics of Porous Media*, Gulf Publishing Co, Houston, Texas, 1987.

Committee on Fracture Characterization and Fluid Flow, ed., *Rock Fractures and Fluid Flow*, Washington, D. C., National Academy Press, 1996.

Dullien, F. A. L., *Porous Media: Fluid Transport and Pore Structure*, 2nd ed., Academic Press, New York, 1992.

Person, M., J. P. Raffensperger, S. Ge, and G. Garven, Basin-scale hydrogeologic modeling, *Reviews of Geophysics*, *34*(1), 61–87, 1996.

Walder, J., and A. Nur, Porosity reduction and crustal pore pressure development, *J. Geo. Res.*, *89*(B13), 11539–11548, 1984.

Yilmaz, O., R. Nolen-Hoeksema, and A. Nur, Pore pressure profiles in fractured and compliant rocks, *Geophysical Prospecting*, pp. 693–714, 1994.

Chapter 3

Permeability-Porosity Relationships in Granular Rocks

3.1 Introduction

A knowledge of characteristic porosity-permeability relationships in various reservoir rocks is important for several reasons. An understanding of how permeability depends on pore structure may play a role in the attempt to determine a physical relationship between permeability and acoustic velocity or other rock properties that can be measured in the field. This is because pore structure, not just porosity, determines many rock properties. For example, pore structure determines the stiffness of the rock matrix and thus controls the speed of seismic waves in the rock. Permeability changes due to chemical alteration of the pore space in rocks may be an important factor in many crustal processes that involve fluid flow. Geochemical evolution of permeability has been invoked as a critical factor in theories of earthquake cycles (Byerlee, 1994), the development of anomalously high pore pressure (Walder and Nur, 1984), and basin-scale hydrogeologic modeling (Person, 1996). In order to evaluate the importance of permeability evolution in these processes, the relationships among porosity, permeability, and mineral deposition patterns must be understood.

Further study of realistic diagenetic processes will be required for deeper insight

into the porosity permeability relationships in porous rocks. Digitized photomicrographs of thin sections may also be used for computations of permeability. Laboratory measurements of permeability from the actual rock sample can be taken and compared with computed values to determine how pore geometry affects permeability. The method presented here gives a means for computing permeability from pore geometry. This opens the door to further geological research which focuses on the pore structure of real sedimentary (or other) rocks.

Network models have been extensively used to simulate fluid flow at the pore scale. See Bryant (1993) and Cade (1994) for recent examples of the use of network models for pore-scale studies. In the network model approach, a complex pore space is represented by a set of idealized geometrical figures. Such approximations can be limiting and are often non-unique. The actual pore structure is obscured and it is rather difficult to model complex or irregular pore geometries. Furthermore, it is difficult by such approximations to experiment with various pore evolution schemes as we have done in this study.

3.2 Lattice-Boltzmann Flow Model

We take an alternative approach to modeling pore-scale fluid flow in complex media. We simulate fluid flow using the lattice Boltzmann model (LB). The particular model used here is the one developed by Ladd (1994a). In our simulations, we assume low Reynolds number, which is appropriate for groundwater flow in porous media. The second term on the left side, the inertial term, is then zero. The steady state flow field is of interest for permeability calculations. The full (nonlinear) Navier-Stokes equation

$$\rho\partial_t\left(\mathbf{u}\right) + \rho\mathrm{u}\cdot\nabla\mathrm{u} = -\nabla p + \eta\nabla^2\mathbf{u} \tag{3.1}$$

reduces to

$$\nabla p = \eta\nabla^2\mathbf{u} \tag{3.2}$$

Equation 3.2 describes flow in the creeping or Darcy regime. The fluid is also assumed to be incompressible. Since Ladd's paper contains extensive theoretical and numerical

discussions, as well as numerous computational results, we will not repeat details of our numerical code here. Continuing applications of our code by Ladd for related studies, including tests of simple Poisuelle flow, have confirmed the accuracy of our code (Ladd, personal communication). LB models are also becoming a common and accepted tool for pore-scale studies of fluid flow. Many theoretical and numerical studies of the lattice Boltzmann method and variations on it are available. See, for example, Ferreol (1995) and Qian (1992). The most appealing of feature of the LB model for pore-scale flow modeling is the decoupling of the computational complexity of the numerical scheme from the geometrical complexity of the pore structure. Once the numerical scheme is implemented, flow may be simulated in any pore geometry, regardless of complexity, merely by classifying grid points either as rock matrix or pore space.

The effective permeability of a simulated porous material can be computed from the fluid flux in the material by applying Darcy's law

$$q_x = -\frac{k}{\mu}\frac{\Delta P_x}{\Delta x} \tag{3.3}$$

where q_i is the mean fluid flux through the block of material in the x direction, k is the permeability which is to be computed, μ is the fluid viscosity and ΔP_x is the pressure gradient applied to the ends of the block over the length Δx to drive the flow. A schematic diagram of the computational concept used to model the rocks is shown in figure 3.1.

A uniform rectangular grid is the computational grid. An array of 1's and 0's is used to characterize grid points as either pore space (0) or mineral grain (1). Fluid flow occurs only in the pore spaces. The lattice Boltzmann algorithm was used to compute flow vectors only in the pore spaces, since flow velocity in the mineral grain nodes is zero.

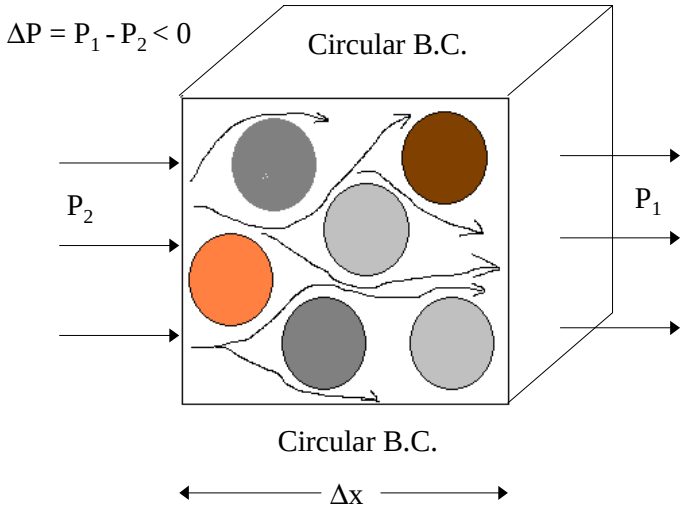

Figure 3.1: Schematic diagram of the digital rock used to compute permeability using a lattice Boltzmann flow simulation method.

3.3 Pore-Space Models and Simulated Diagenetic Processes

We use an LB simulation to compute permeability versus porosity in granular rocks for several pore evolution schemes. The starting pore structure is that of a dense random pack of identical spheres. The coordinates of the sphere centers have been experimentally measured by Finney (1970) and made available to us in digital form. For this numerical study we start with approximately 4000 sphere center coordinates, which correspond to a spherical volume of radius $20mm$. From this volume, we map the spheres which fall within our computational domain onto the rectangular computational domain.

Flow is simulated on a cube that is $6mm$ or more on each side. Figure 3.3 shows an image that was created by plotting the three-dimensional grid array of 1's and 0's which are used within our code to denote rock grains and pore spaces, respectively. The finite grid resolution is apparent in the figure. As our numerical simulations below demonstrate, a resolution of ten grid points per spherical grain appears to give

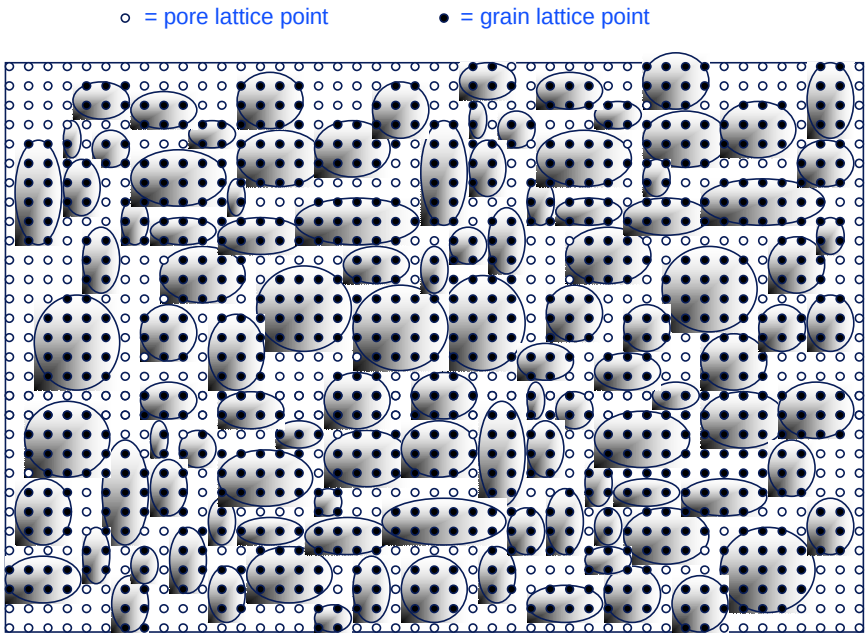

Figure 3.2: Simulated granular rock with superimposed lattice points. In the numerical simulation, flow occurs on pore nodes. Grain nodes are reflecting boundaries.

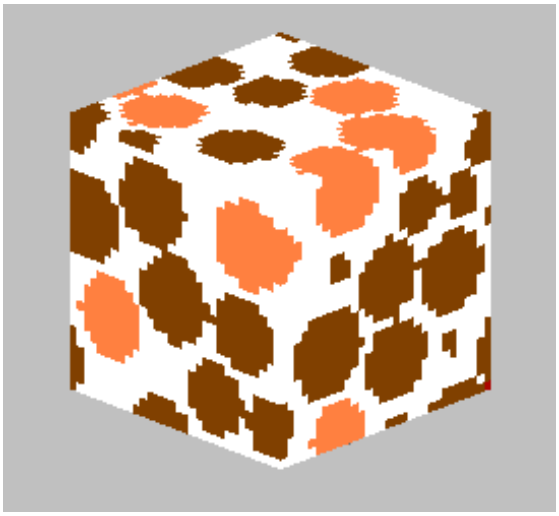

Figure 3.3: The array of 1's and 0's that represent rock grains and pore spaces on the computational grid result in a "digital rock" as shown here. This pore model is derived from the Finney pack, a random dense pack of identical spheres. The resolution in this 6mm cube is 0.2 mm; the computational grid is 30x30x30. Spherical grain edges show the effect of the digital representation.

adequate results with the random dense pack of identical spheres that we used.

Grains in sedimentary environments are generally well-sorted due to the physical processes that deposit them. Furthermore, the depositional process tends to cause grains to be clustered as a random dense pack, rather than in a regular packing. Thus, the use of uniform spheres in a random dense pack is a reasonable first approximation to real sandstones for studying granular materials.

Pore-space diagenesis is modeled in this study by (a) uniform growth of the grains,(b) cement deposition in low fluid flux regions, (c) cement deposition in high fluid flux regions, (d) random precipitation in the pore space, (e) static combinations of these processes; and (f) dynamic combinations of these processes which change during the diagenetic process.

Uniform expansion of the grains is accomplished by expanding the radius of the spheres in our simulation. In our code, grid points are initially assumed to be pore space grid points. As the simulated diagensis proceeds, appropriate grid points are

marked as grains. Thus, expanding the sphere radii uniformly, for example, causes no problems if the spheres overlap; a grid point in this case is simply marked as a grain node more than once. Geologically, uniform expansion of the spheres corresponds to uniform deposition of cement on grain surfaces. The cemented glass beads which we measured in the laboratory are also formed by a similar process. In contrast, random deposition was suggested by X-ray micrographs of thin sections of granular materials containing significant clay content.

The depositional schemes that depend on flow velocity are simulated by depositing cement in a specified fraction of the pore space where the fluid flow velocities are the lowest and the highest, respectively. We speculated initially that flow velocity might play a deterministic role in cement deposition in real sedimentary processes. We did not assume a particular process was responsible for deposition. Deposition in high flow regions in real rocks might be caused by precipitation as fluid moves into a different temperature region, for example. In this case, more material would be deposited where the most dissolved material flows; that is, where the fluid flux is highest. Alternatively, pore spaces might be clogged initially by smaller particles which are carried in the high flow channels of the pore space. This process might be expected to occur during early diagenesis, when burial and compaction are occuring. Other physical mechanisms that might result in high-flow pores being filled are certainly possible.

Random pore filling proceeded in a simple manner. A specified percentage of the pore spaces were filled randomly and the permeability was recalculated. This pore-filling mechanism is included as another entry in our catalog of porosity-permeability relationships. The manner in which clay appears to be distributed in the pore space of some sedimentary materials suggests that this scheme might have a physical basis.

In real systems, combinations of these processes might reasonably be expected to occur. For example, as diagenesis proceeds in sedimentary environments, the relative proportion of different processes that dominate might change. Thus, we investigated some combinations of our basic diagenetic algorithms and altered them as the simulated diagenesis progressed.

Though our primary goal was to find depositional schemes that would match our

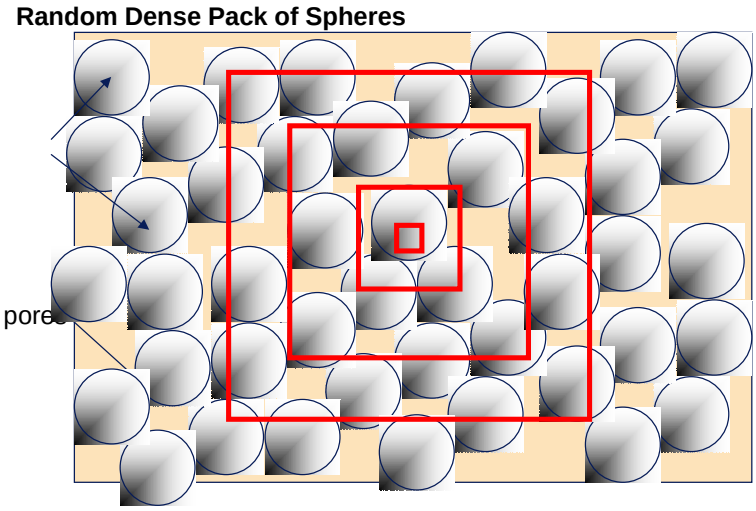

Figure 3.4: Illustration showing representative elementary volumes (red outlines) in a random dense pack of spheres. Porosity and permeability values as functions of REV cube sizes are shown in 3.5.

measured data, this study may also be used as a catalog of porosity-permeability relationships that result from the several geometrical algorithms that control the diagenesis in our simulations. We found that certain relationships that resulted from our diagenetic algorithms appear to correspond to various diagenetic patterns in natural rocks and cemented bead packs.

3.4 Scale and boundary conditions

3.4.1 Effect of sample size

All LB simulations are implemented on a cube which is a spatial subset of the full Finney pack dataset. In this section we investigate how the size of the cube and the grid spacing affect the resulting permeability and porosity values. In one simulation, the center of the cube is positioned in the pore space; in the other it falls inside a solid spherical grain. By expanding the walls of the cube, we calculated the resulting porosity and permeability (Figure 3.5). The results show that once the length of

the cube side exceeds four grain radii, the scale-related fluctuations in porosity and permeability become negligible. Porosity becomes 0.36 and permeability becomes $2.71 \times 10^6 mD$, which are the experimentally determined values for a random dense pack of identical spheres (Bourbie, 1987; Bryant, 1993).

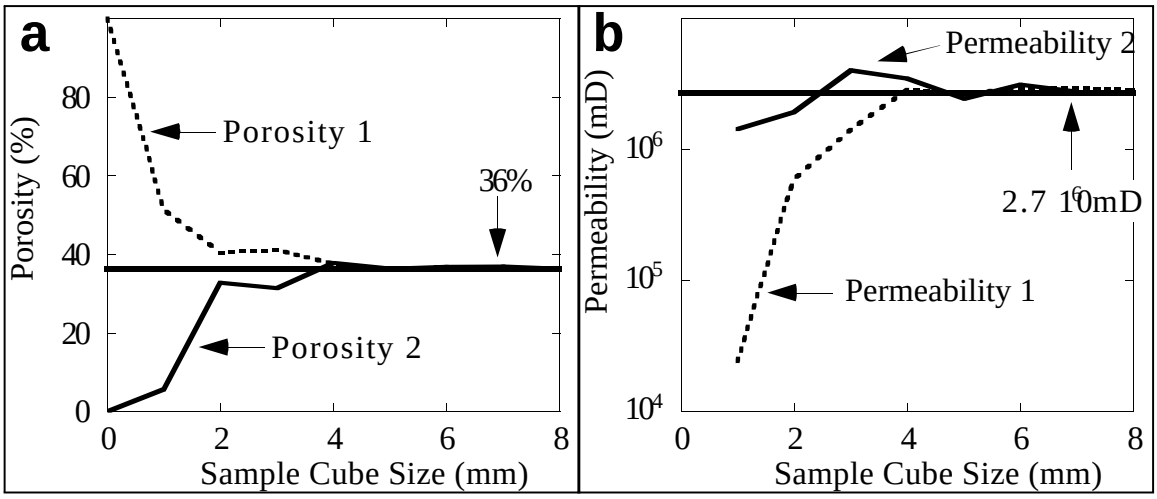

Figure 3.5: The effect of the cube size on porosity (a) and permeability (b). The grain diameter is 2 mm. The computational grid spacing is 0.2 mm. The solid curve is for the case where the cube center is in the spherical grain; the dotted curve is for the case where the cube center is in a pore; the horizontal line is the value for the entire pack.

3.4.2 Effect of grid size

In our numerical simulations we began with a 6 mm cube (the grain diameter is 2mm). For some of the pore-filling schemes, we found that a 10 mm cube gave smoother results at low porosities. This effect does not appear to be due to the grid spacing. Some pore filling schemes gave quite smooth results down to porosities of less than 5%. When porosity-permeability curves were not smooth, we found that using a larger sample size (8 or 10 mm) with the same grid spacing (10 grid points per sphere diameter) gave quite good results. A uniform (in space) pressure gradient is applied to the fluid particles along the flow direction. Then the flux is computed and the permeability obtained from Darcy's law. An important question is: how fine

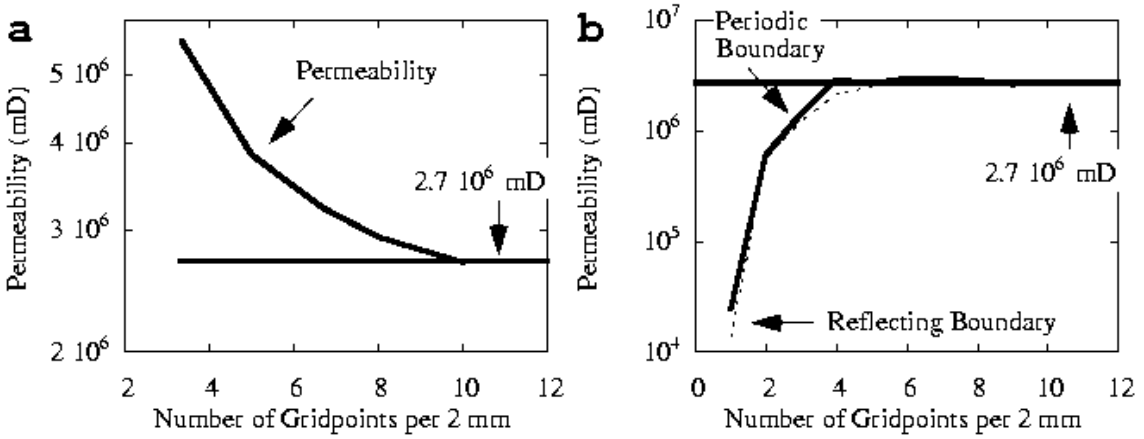

Figure 3.6: a. Calculated permeability of a 6 mm cube as a function of grid spacing. b. Circular and solid boundary conditions on sides of block. Both cases were computed using the Finney pack with spheres of diameter 2 mm.

the grid has to be to produce consistent and accurate results. In Figure 2a we show the permeability evolution as grid space becomes finer. The spacing of ten grid points per solid sphere diameter appears to be adequate. This resolution was also reported by Ladd (1994a) to be adequate.

3.4.3 Effect of Boundary Conditions

Another important issue is what boundary condition to use on the cube sides parallel to the flow. We consider two options. The first one is where the particles elastically bounce from the side walls (reflecting, or no-flow boundary condition). The second one is where the flux exiting one side of the cube equals that entering the cube from the opposite side (periodic boundary condition). Both conditions give similar results (Figure 3.6b). In all remaining calculations we use periodic boundary conditions. Reflecting boundary conditions occur on all interior solid (grain) boundaries.

3.5 Numerical Results

3.5.1 Four Basic Diagenetic Processes

Calculated porosity-permeability curves are shown below for several diagenetic schemes. In Figure 3.7, we display laboratory measurements for natural rocks: Fontainebleau sandstone (Bourbie, 1985) ; North Sea sandstones from the Troll (Blangy, 1992) and Oseberg (Strandenes, 1991) fields; and Ottawa sand (Estes, 1994) . Also shown are data for two artificial cemented sphere packs: epoxy-cemented glass beads and sintered glass beads, and calculated porosity-permeability curves for three pore-filling schemes: (a) uniform growth of the grains; (b) cement deposition in pore spaces where the fluid flow velocities are lowest; and (c) cement deposition in pore spaces where the fluid flow velocities are highest.

Laboratory measurements of permeability and porosity data are displayed in figure 3.7. All computed curves in figure 3.8 evolve from a single point which is computed from the initial Finney pack. The porosity is approximately 0.36 and the permeability, normalized by the grain diameter squared, is $6.8\,10^5 mD/mm^2$ at this point. These values correspond to laboratory values for the a dense random pack (Finney, 1970).

Note that all of our permeability values are normalized by either the sphere diameter (for theoretical or artificial sphere packs) or the estimated average grain size. This is the only way to compare permeability values between granular materials of different grain scales.

The curve obtained by filling low fluid flux pores does not appear to match any of the experimental data. Therefore, we do not investigate this diagenetic scheme further in this study.

The uniform expansion curve, for high porosities, appears to match experimental results obtained for the artificial cemented sphere packs, particularly the sintered glass beads. In figure 3.9, we display the computed uniform expansion and random-fill permeability curves with superimposed experimental values for artificial granular materials. The epoxy-cemented glass beads deviate from the uniform expansion curve and the sintered glass bead results for low porosities. A probable cause is the non-uniform epoxy distribution due to gravity – the accumulation of epoxy at the bottom

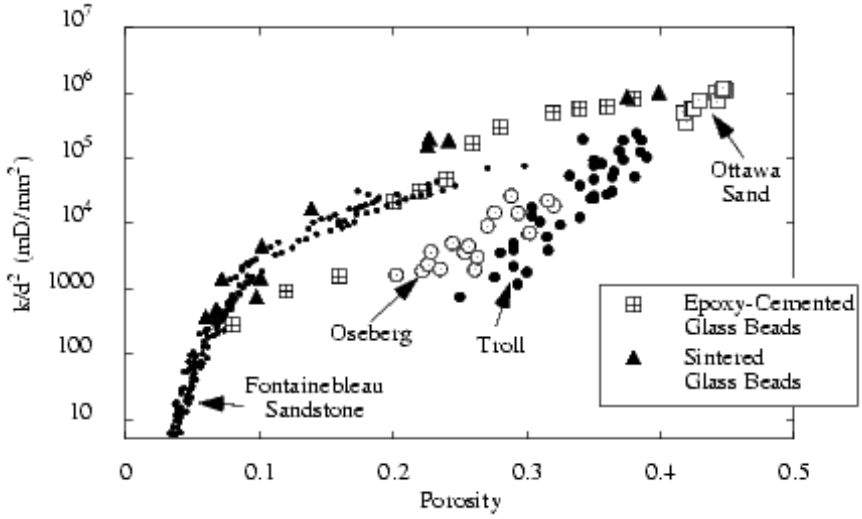

Figure 3.7: Laboratory measurements of permeability (normalized by grain diameter) versus porosity for several kinds of sandstone and for two glass bead packs (sintered glass beads and epoxy cemented glass beads).

of a cylindrical sample blocks the flow. The proximity of the theoretical uniform-expansion curve and experimental values indicates that the numerical scheme is an effective method for computing porosity-permeability relationships in complex porous materials. The simulated diagenetic scheme appears to approximate the evolution of the pore space in the artificial sphere packs.

3.5.2 North Sea Sandstones

Notice in Figure 3.7 that at high porosity, the data points for artificial materials appear to emanate from the random-dense-pack point ($6.8\,10^5 mD/mm^2$, 0.36) in the porosity-permeability plane. This does not appear to be the case for the North Sea sandstones (Oseberg, Troll) and the Ottawa sand. The curves for these materials appear to follow straight lines from the region of the Ottawa sand point of highest porosity and do not pass through the random-dense-pack point. The uniform expansion model appears to describe the porosity-permeability relationship for cemented and sintered glass beads, but overestimates the permeability of North Sea sandstones.

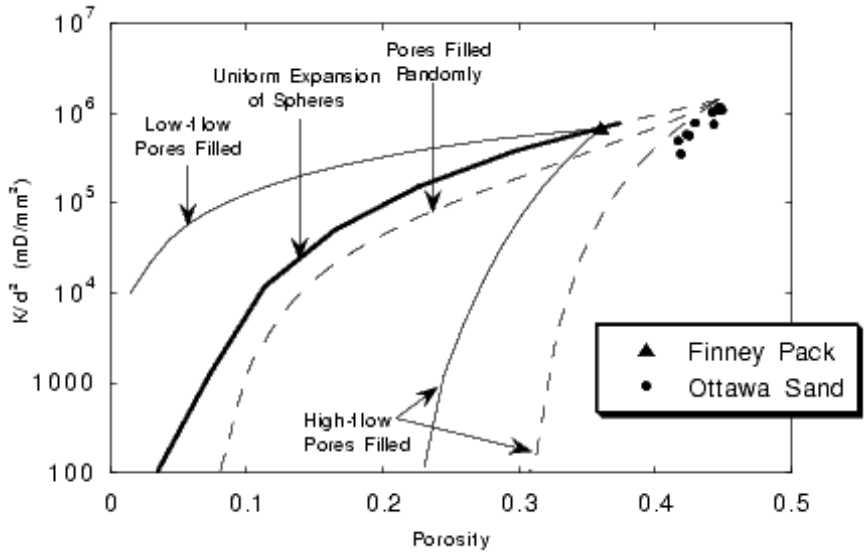

Figure 3.8: Normalized permeability versus porosity from our numerical simulations. Ottawa sand data points from figure 3.7 are shown for reference. The starting point for the Finney pack is marked by a triangle. Theoretical curves start either from the Finney pack point, or from the point that is computed by *contracting* the spheres until the porosity approximately matches that of Ottawa sand.

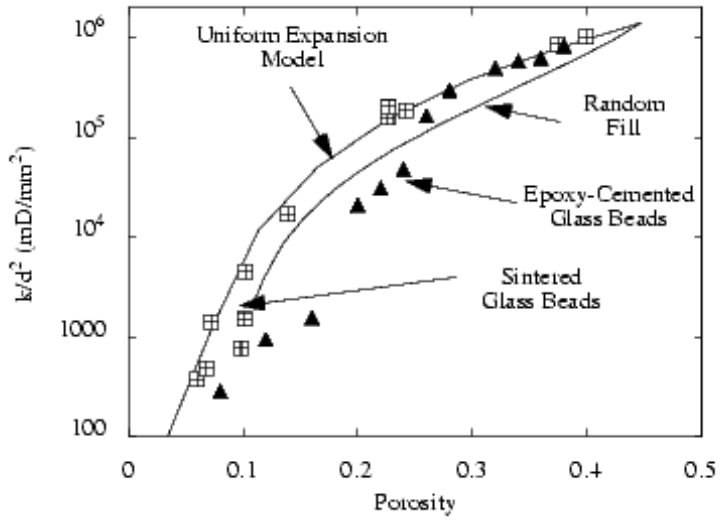

Figure 3.9: Computed porosity-permeability curves for uniform sphere expansion and random filling with superimposed data points for artificial sphere packs.

Physically, this suggests that North Sea sandstones begin as uncemented grains, similar to Ottawa sand, and then undergo a diagenetic process which is rather different from uniform expansion.

To test this hypothesis we attempted to find a theoretical diagenetic scheme which would model the North Sea curves. We begin by *contracting* the spheres in the simulated Finney pack uniformly until the porosity is approximately that of the most porous Ottawa data point. We then evolve the granular material using various diagenetic schemes. Note that the porosity-permeability trends for the North Sea sandstones are distinctively different from that of Fontainebleau sandstone, which will be considered separately.

In order to match the North Sea sandstone trends, we found it necessary to combine two different diagenetic schemes. In figure 3.10 we show curves for uniform expansion and filling of high-flow pores. These form the two extreme curves in the figure. The three curves that fall between the extremes were computed by allowing the rate of uniform expansion to increase as the diagenesis proceeded. That is, the initial pore cementation was due primarily to filling of high-flow pores. Later, uniform

expansion became the dominant process. Such a change in diagenesis is not unreasonable physically. The cementation process might be expected to alter as burial and compaction of sediments proceeds.

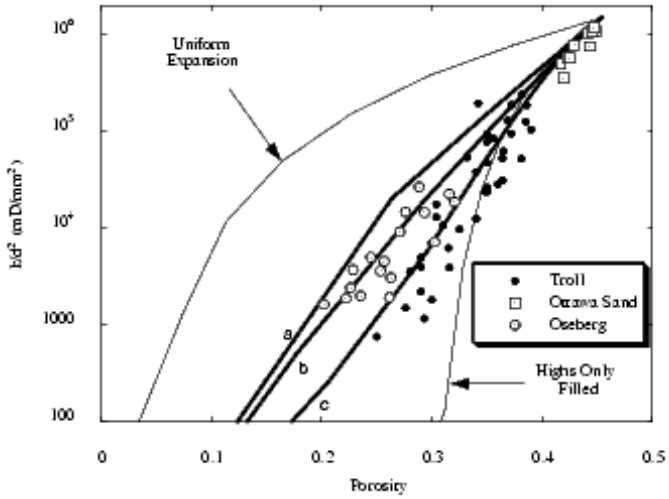

Figure 3.10: Computed porosity-permeability curves derived by filling high-flow pores and uniformly expanding the spheres simultaneously. The rates of these competing processes vary. The bold curves show increasing rates of high-pore filling relative to uniform expansion. At each diagenetic step, 4% of the high-flow pores are filled. Uniform expansion for the three bold curves starts at a) 0.0005 mm, b) 0.0003 mm, and c) 0.0001 mm per diagenetic step, respectively. This expansion is increased by a factor of 2.0 after each step.

3.5.3 Fontainebleau Sandstone

The Fontainebleau sandstone porosity-permeability data points are quite distinct from the North Sea sandstones. The shape of the Fontainebleau trend appears to be similar to the uniform expansion curve, as shown in Figure 3.11. The curve for random deposition of cement appears to also have a shape that is similar to the uniform expansion curve and to the Fontainebleau trend, but shifted downward.

An average grain diameter of 0.25 mm for Fontainebleau was obtained from Bourbie (1985). Photomicrographs of Fontainebleau thin sections taken by one of the authors reveals that the average grain diameter appears somewhat smaller in some

samples. We found that the Fontainebleau data points match the uniform expansion curve very well if we normalized using 0.125 mm for the average grain diameter. The match to the uniform expansion curve is so close, and so distinctly different from the North Sea sandstones, that we feel further study is needed on the manner in which scaling is done when comparing porosity-permeability relationships in granular materials with dissimilar mean grain sizes. We tried many combinations of the four basic diagenetic schemes discussed in this paper and none appeared to match the Fontainebleau data nearly as well as uniform grain expansion when the 0.125 mm grain diameter is used for normalizing the data.

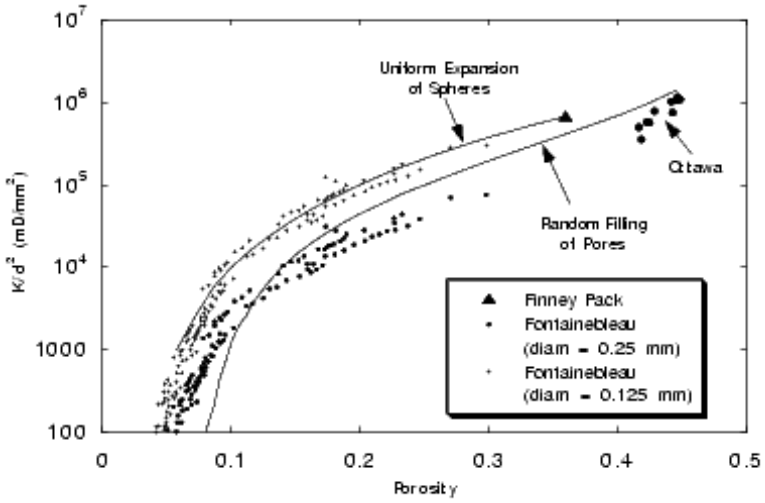

Figure 3.11: Computed uniform expansion porosity-permeability curve, data points for Fontainebleau sandstone, assuming grain size of 0.25 mm, and Fontainebleau assuming grains are 0.125 mm in diameter.

3.6 Conclusions

We have been able to compute porosity-permeability curves that match laboratory measurements for real and artificial granular rocks. The theoretical porosity-permeability relationships were computed using a lattice Boltzmann method to compute

the fluid flux in a simulated porous material, from which the permeability was determined. Several diagenetic schemes were used, alone and in combination, to achieve our results. Sintered glass beads were found to have a porosity-permeability relationship that was remarkably similar to our computed uniform expansion curve. Epoxy-cemented beads were similar at high porosities, but deviated from the sintered beads and the uniform expansion curve at low porosity.

North Sea sandstones had porosity-permeability characteristics that were quite distinct from Fontainebleau. These characteristics were matched by our simulations using a diagenetic scheme that started with the filling of high-flow pores predominating, then shifted to uniform expansion of the spherical grains. The starting point for these simulations was obtained by contracting the Finney pack spheres uniformly to the porosity of Ottawa sand. Fontainebleau data has a different porosity-permeability trend from the North Sea sandstones, and is similar in shape to the uniform expansion model. If the average grain size used to normalize the permeability measurements for Fontainebleau is 0.125 mm, the uniform expansion curve fits the Fontainebleau data very closely.

The porosity-permeability relationships computed in this study using various diagenetic schemes may also be used as a brief catalog of theoretical results to be compared with other laboratory measurements of real rocks. The lattice Boltzmann model used in this exercise for simulating flow in porous media with complicated pore geometries enabled us to focus on diagenetic rather than on computational difficulties that might have been a major distraction using more traditional numerical methods.

3.7 Appendix: A Digital Rock Physics Laboratory

Determination of rock properties by direct calculation is useful in conjunction with laboratory measurements. The primary advantage of a numerical simulation is that all parameters are known and controlled. This allows experimentation with one particular parameter which enables cause and effect to be determined. Together with laboratory measurements of rock properties, this combination is a powerful tool for quantitatively relating rock properties to basic pore structure and pore evolution

processes.

3.7.1 Pore Geometry and Structure

Pore geometry is determined by the rock structure and the particular processes which evolve the microstructure of the pores. Working together with sedimentologists, geochemists, and petrologists, realistic pore evolution schemes can be simulated. The computational methods proposed here separate the calculation of rock properties from the determination of pore structure, so these two lines of investigation may proceed rather independently. Many previously-used methods, such as the network models mentioned earlier, make the calculation of properties and the representation of the pore structure highly dependent upon one another. It can also be difficult to implement diagenetic schemes which are based primarily on geological or geochemical models using previous methods.

3.7.2 Permeability Calculator

The lattice Boltzmann method is ideally suited to computing fluid flow in a complex pore geometry. The method generally consists of two steps: propagation of fluid "particles" and collision relaxation. In a lattice gas simulation, integral numbers of particles are moved around the computational grid. Momentum and mass conservation laws are used in the collision step. The lattice Boltzmann method is a generalization of the lattice gas method in that real number particle *densities* are moved around the grid. From one point of view, the lattice Boltzmann method may be viewed as an alternative finite difference formulation of the equations for Stokes flow. When computing a steady-state flow field, such as when determining permeability, the usual procedure is to evolve the initial flow field until the flux change with each propagation/collision step is less than some tolerance. The particle density at any pore node after one step is a linear combination of the particle densities at neighboring pore nodes. Neighboring nodes include the node itself because of reflections off of neighboring grains nodes.

A possible method for computing permeability using the lattice Boltzmann method

would be to write the propagation and collision steps as a single matrix operation. Such a matrix would be sparse, as each node interacts only with 19 other nodes (including itself). Let us suppose that the particle densities in each direction, at each node, are represented by the variable u. u has 19 components (directional velocities) at each node. If there are N nodes in a grid or lattice, then there are a total of 19N independent variables to advance in time at each step. A propagation step may be written as:

$$\begin{pmatrix} u_{1,1} \\ u_{1,2} \\ \vdots \\ u_{1,19} \\ u_{2,1} \\ u_{2,2} \\ \vdots \\ u_{2,19} \\ \vdots \\ u_{N,1} \\ u_{N,2} \\ \vdots \\ u_{N,19} \end{pmatrix}^{n+1} = M \begin{pmatrix} u_{1,1} \\ u_{1,2} \\ \vdots \\ u_{1,19} \\ u_{2,1} \\ u_{2,2} \\ \vdots \\ u_{2,19} \\ \vdots \\ u_{N,1} \\ u_{N,2} \\ \vdots \\ u_{N,19} \end{pmatrix}^{n} \tag{3.4}$$

or, more succinctly,

$$\mathbf{u}^{t+1} = \mathbf{M}\mathbf{u}^{t} \tag{3.5}$$

Since only the stead state flow field is of interest, this can be written as an equilibrium equation $\mathbf{u}_s = \mathbf{M}\mathbf{u}_s$ or

$$(\mathbf{M} - \mathbf{I})\,\mathbf{u}_s = 0$$

The permeability can be computed directly from the flow field $\mathbf{u}_s$.

The purpose of the fluid flow simulation is the computation of the steady state flow field, from which the permeability can be calculated. If the intermediate flow

velocities are of interest as they develop in time, this matrix method will not be of interest. The matrix method described here has the advantage of allowing the highly-developed methods of numerical linear algebra to be used in solving the system of equations for the equilibrium flow field. This might be advantageous for low-porosity rocks where convergence by the traditional iterations was found to be quite slow.

3.7.3 Other Rock Properties

Electrical conductivity

Many effective or macroscopic rock properties besides permeability depend on the microstructure of the pores. It is desirable to compute effective rock properties from the same microstructure in order to find correlations between them. The primary motivation is to find ways to determine properties such as permeability and porosity, which control flow and transport in reservoirs and aquifers, from measureable properties such as electrical conductivity and acoustic wave velocity.

The effective (macroscopic) electrical conductivity of a porous material depends on the pore-scale geometry of the material. Ohm's law applies at the pore scale:

$$J(\mathbf{x}) = \sigma(\mathbf{x}) E(\mathbf{x}) = -\sigma(\mathbf{x}) \nabla V(\mathbf{x}) \tag{3.6}$$

where J is the electric flux vector, σ is the conductivity, and V is the electric potential. Each of these variables varies locally at the pore scale. The divergence of the flux vector is zero, so that

$$\nabla \cdot J(\mathbf{x}) = -\nabla \cdot (\sigma(\mathbf{x}) \nabla V(\mathbf{x})) = 0 \tag{3.7}$$

The pore-scale potential function $V(\mathbf{x})$ can be computed by solving equation 3.7 using values of $\sigma(\mathbf{x})$ for rock and water (pore conductivity) that are appropriate for the material. The effective conductivity is then found from

$$\sigma_{eff} = \frac{J_{avg} \Delta x}{\Delta V} \tag{3.8}$$

where J_{avg} is the arithmetic mean flux in the x-direction over the entire computational sample. Computationally, the same pore geometry and diagenetic schemes

may be used as for the permeability calculations. For effective electrical conductivity calculations, the 1's and 0's that indicate pore space or rock grain must be mapped to local conductivity values. Once this has been accomplished, the computation of the potential can be carried out using traditional finite difference or finite element methods. This software has been written and the accuracy of initial calculations has been confirmed by comparison with laboratory measurements and theory.

Elastic moduli and P wave velocity

The rock stiffness depends very strongly on the pore geometry and on the type of cement deposited at grain contacts. A method for computing elastic moduli using the pore geometry and diagenetic schemes which have been outlined already has to account for differing cement and grain properties. Various possibilities which may be considered for computing elastic moduli are finite element structural codes, discrete element methods for studying the interaction of discrete granular particles. Finite difference or finite element elastic wave codes may be useful for directly simulating wave propagation through complex media in order to determine wave velocities. This is an area for future research.

3.7.4 Software Organization and Design

The fundamental contribution of this paper is the isolation of initial pore geometry, diagenetic schemes, and effective property calculations. By designing our computational software to reflect these different physical dynamics, we are able to focus on the essential scientific problem of determining how pore structure determines the various rock properties. Combining these computational tools with laboratory measurements enables us to sort out cause and effect in complex porous rocks.

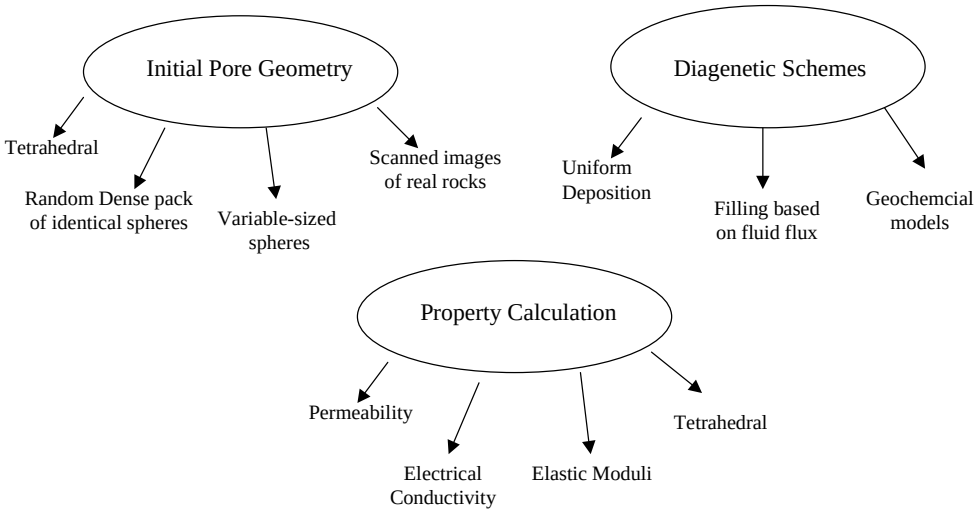

Figure 3.12: Schematic organization of software components for a digital rock physics laboratory.

Bibliography

Blangy, J. P., Integrated seismic lithologic interpretation: The petrophysical basis, Ph.D. thesis, Stanford University, Stanford, California, 1992.

Bosl, W. J., J. Dvorkin, and A. Nur, A study of porosity and permeability using a lattice boltzmann simulation, *Geophys. Res. Lett.*, *25*, 1475–1478, 1998.

Bourbie, T., and B. Zinszner, Hydraulic and acoustic properties as a function of porosity in fountainebleau sandstone, *Journal of Geophysical Research*, *90*, 11,524–11,532, 1985.

Bourbie, T., O. Coussy, and B. Zinszner, *Acoustics of Porous Media*, Gulf Publishing Co, Houston, Texas, 1987.

Bryant, S. L., D. W. Mellor, and C. A. Cade, Physically representative network models of transport in porous media, *AIChE Journal*, *39*(3), 387–396, 1993.

Byerlee, J., Earthquakes, *Journal of Geophysical Research*, 1994.

Cade, C. A., I. J. Evans, and S. L. Bryant, Analysis of permeability controls: A new approach, *Clay Minerals*, *29*, 491–501, 1994.

Estes, C. A., Elastic and transport properties of unconsolidated materials, *Stanford Rock and Borehole Geophysics Project Report*, 1994.

Ferreol, B., and D. H. Rothman, Lattice boltzmann fontainebleau sandstone, *Transport in Porous Media*, *20*(1), 3, 1995.

Finney, J., Random packings and the structure of simple liquids i. the geometry of random close packing, *Proc. Roy. Soc.*, *319A*, 479, 1970.

Ladd, A. J. C., Numerical simulations of particulate suspensions via a discretized boltzmann equation. part 1, theoretical foundation, *Journal of Fluid Mechanics*, *271*, 285–309, 1994.

Person, M., J. P. Raffensperger, S. Ge, and G. Garven, Basin-scale hydrogeologic modeling, *Reviews of Geophysics*, *34*(1), 61–87, 1996.

Qian, Y. H., D. d'Humieres, and P. Lallemand, Lattice BGK models for Navier-Stokes equation, *Europhys. Lett.*, *17*(6), 479–484, 1992.

Strandenes, S., Rock physics analysis of the brent group reservoir in the oseberg field, *Stanford Rock and Borehole Geophysics Project Report*, 1991.

Walder, J., and A. Nur, Porosity reduction and crustal pore pressure development, *J. Geo. Res.*, *89*(B13), 11539–11548, 1984.

Chapter 4

Computer Simulation of the Complex Crust: Theory

"When we try to pick out anything by itself, we find it hitched to everything else in the universe."

4.1 Introduction

The brittle crust is often modeled as an elastic solid for purposes of studying seismic waves, fault mechanics, and rock physics. Hydrologists and geochemists, who are generally interested in fluid dynamics or aqueous chemistry, treat the crust as a porous medium through which fluids flow. Faults can greatly complicate matters for both the mechanical and hydrologic aspects of crustal models. Of course, physical and chemical processes occur simultaneously and in a coupled fashion, resulting in dynamical behavior that is sometimes counter-intuitive, may even appear random, and is difficult to predict. Investigation of the complex dynamical behavior of crustal processes requires computer simulation. This is the only means by which the consequences of competing physical theories can be explored.

The purpose of this study is to present a general set of equations for thermal, mechanical, and hydrologic processes in a form that is intended for computer simulation.

More than just presenting a set of equations, a strategy is given for implementing numerical software that is designed for experimentation. General assumptions about the spatial and temporal variability of material properties are made so as to not dismiss heterogeneous coefficients and nonlinearities that might be important in some circumstances. Though geochemical modeling will not be considered in any detail here, the role of geochemical models in the general modeling framework is indicated. Though the framework outlined here is appropriate for general simulations on many scales, the specific intention is to build a simulation framework that can support computational experimentation with fault models and earthquake source mechanics embedded in a complex continuum model of the crust. The emphasis in the present paper is on the continuum equations for thermoporoelasticity. A discussion of fault modeling will be reserved for a future paper, though indications of how fault models fit into the general framework are given.

Table 4.1 lists some of the most common fundamental variables of interest when describing the physical state of the earth's crust. Along with each variable are the simplest (linear, uncoupled) equations which are used to model the variable and the most important material properties that effect its dynamics. Geochemistry is a vast subject and the modeling of geochemical systems is a complex undertaking in itself. Of primary interest for modeling the physical state and evolution of the crust is aqueous geochemistry as an agent for modifying the material properties of the crust, such as permeability and elastic moduli. Porosity is usually considered to be a material property rather than a dynamical variable. However, when the rock material that makes up the crust has evolving properties due to chemical changes, porosity can be considered a fundamental variable which depends primarily on the total solid phase fraction in any given cell volume. Key material properties, such as permeability, thermal diffusivity, and elastic moduli can be derived from porosity, given other parameters which define the quantitative relationship between porosity and other properties. The Kozeny-Carmen rule (Dullien, 1992) for computing permeability from porosity is an example. To use this rule, an exponent and a constant parameter must be specified in addition to porosity.

There are many equations which can be specified to govern the evolution of the

Dynamical variable	**Governing equations**	**Controlling parameters**
displacements, u_1, u_2, u_3	Navier equations	elastic moduli, G, ν
displacement rates	viscoelastic equations	moduli, rock viscosity
pore pressure, p	hydraulic diffusion	permeability k, viscosity μ
temperature, T	thermal diffusion	thermal conductivity, c_T
porosity, ϕ	solid phase fraction	chemical concentrations
chemical concentrations, c_s	geochemical system	activity coefficients

Table 4.1: The most common dynamical variables of interest which describe the physical state of the crust. Chemical species are considered here only as they pertain to the physical state of the crust.

relatively small set of dynamical variables shown in the preceding table. The basic governing equations listed in the table may be coupled into systems of equations. Or, nonlinear terms may be added to the simplest linear equations. In some situations, the material parameters may be nonlinear functions of the dynamical variables. For some materials, anisotropic elastic moduli may be appropriate. One of the primary tasks that must be accomplished by computer simulation is to determine which equations model the observed behavior of the crust by experimenting with different fundamental equations, couplings between equations, and spatial distributions of material properties. Complex dynamics can emerge from a combination of simple processes, each of which is understood in isolation.

One of the most important aspects of the crust which is not governed directly by any of the above equations is faulting. Fault movement may alter some or all of the primary variables listed above, as well as the material properties which govern the evolution of the primary variables. From a modeling point of view, faults may be considered geometrical regions, defined by grid points, which are governed by laws distinct from the continuum equations. For example, displacement along boundary points which make up opposing faces of a fault might be displaced by applying some friction law when shear stresses exceed some threshhold. At the same time, thermal conductivity equations might be unaltered by the presence of the fault, except that a heat source is added during sliding. The inclusion of faults in a simulation of the crust will necessarily involve complicated gridding and decision algorithms which will not be discussed in this paper. Faults can, however, be easily included in the general

framework presented here and this will be indicated where appropriate.

4.2 Complexity and Computer Modeling

The motivating assumption behind this paper is that the complexity typically observed in crustal dynamics is fundamentally due to physical processes that are well-known in terms of classical physics and chemistry. Quantitative description and, eventually, prediction are thus reasonable expections. This is the goal of all physical theory and is in fact the essence of science. However, the fundamental physical processes involved in such complex phenomena as earthquakes must be adequately modeled in simulations if we are to begin to understand the relative importance of each factor in controlling the total complex system. By this, I mean that all of the relevant physical processes must be included, they must be properly coupled, and the material properties must be modeled correctly. It is not sufficient to use a simple diffusion equation with constant coefficients, for example, to discuss the role of fluids in crustal processes if this model is not the correct description of how fluids flow in the thermoporoelastic, chemically evolving material that makes up the crust.

For example, immediately following an earthquake, excess pore fluid does not simply diffuse from the ends of the fault in the surrounding medium (this was suggested by Scholz, 1990, p. 209 as the reason earthquake-induced fluid flow cannot be the underlying explanation for aftershocks). Because of poroelastic effects, pore fluid pressures are almost instantly altered *everywhere* in the region of the fault and fluid diffusion occurs in rather complex patterns controlled by the initial mean stress and the permeability distribution in the fault region. There is a great temptation to simplify mathematical equations to make them amenable to solution by the methods which are available to us. Simplification is desirable only when insignificant terms can be excluded. It is one of the central themes of this paper that when seemingly simple processes occur together in media which vary spatially and temporally, the resulting behavior may be wholly unlike the dynamics of simple, uncoupled processes.

The tectonic and hydrologic forces that drive the dynamics of the crust are not independent of each other. Tectonic forces effect changes in pore pressure, which

Type	**Variables involved**	**Physical example**
Coupled processes	P, σ(mean stress)	Cryer-Mandel effect [1]
Spatial heterogeneity	P, σ, k	High p in fault zone [2]
Nonlinear parameters	$k = k(p)$	Piston-like pressure profile [3]
Chemical alteration	p, ϕ	Abnormal p compartments [4]
All of the above	all variables and parameters	Earthquake cycle [5]

Table 4.2: Various types of coupled processes or non-constant material properties can result in rather complex or surprising behavior. Shown here are some examples of surprising dynamics that can arise in the crust, along with the variables involved and some references to each example. Reference superscripts are: [1]Cryer, 1962; [2]this thesis, chp. 3; [3]Yilmaz, et al., 1994; [4]Walder and Nur, 1984; [5]Byerlee, 1996.

drive fluid flow (Ingebritsen, 1998). Fluid flow can also drive mechanical processes, either directly (through poroelastic effects) or indirectly through thermal advection and chemical reactions. Walder and Nur (1984) have shown that as long as the crust contains pore fluids, it is not in equilibrium. The crust exhibits several characteristics that contribute to the overall complexity of crustal processes: coupling of two or more processes, spatially heterogeneous material properties which evolve in time, and nonlinear terms in the governing equations. Some examples of each of these and their potential dramatic effects are discussed now. Table 4.2 gives some examples in summary form.

4.2.1 Coupled Processes

It is possible for two simple linear processes to exhibit nonlinear, unpredictable behavior when coupled together. A striking example of this is the coupling of flow through an elastic porous medium. A comparison between simple fluid diffusion and coupled poroelastic diffusion was done by Cryer (1963) which illustrates how surprising behavior can arise from simple linear processes that are dynamically coupled. This effect was first discussed in the soil mechanics literature by Mandel (1953).

Cryer's study compared fluid diffusion as modeled by Terzaghi's consolidation theory (Terzaghi, 1943) with Biot's poroelastic theory (Biot, 1941) for coupled stress and fluid diffusion. Terzaghi's theory is essentially a simple diffusion equation for a

porous medium. The three dimensional Terzhagi consolidation equation, as given in Cryer (1963) is

$$c_v \nabla^2 p = \frac{\partial p}{\partial t}$$

where c_v is the hydraulic diffusivity of the soil and p is the excess hydrostatic pressure in the water.

Biot's theory couples pore fluid flow with elastic deformation. The equations as originally written by Biot are

$$N\nabla^2 p + (N+S)\,\nabla(\nabla\cdot\mathbf{u}) + (1/f)\,\nabla\sigma = 0 \quad (4.1)$$

$$f^2(2N+S)\,\nabla^2(\nabla\cdot\mathbf{u}) = b\frac{\partial(\nabla\cdot\mathbf{u})}{\partial t} \quad (4.2)$$

together with six elasticity relations for the stress tensor σ_{ij}, where $\mathbf{u}$ is the displacement vector (hence, $\nabla\cdot\mathbf{u}$ is the volumetric contraction or expansion), p is the pressure in the water, f is the porosity of the material, σ is the hydrostatic stress borne by the water (thus, $\sigma = -fp$), and N and S are Lame coefficients of the skeleton. Cryer derived analytic solutions for the simple fluid diffusion model of Terzaghi and the coupled poroelastic model of Biot. The remarkable result was that in the Biot model, fluid pressure at the center of the sphere initially *rises* before decaying to the steady-state pressure. This problem will be examined in more detail in the next chapter.

4.2.2 Heterogeneous Properties

The prediction of contaminant movement and the flow of fluids in a petroleum reservoir rely heavily today on the use of geostatistical methods to quantify the role of heterogeneities in controlling fluid flow in the crust (Tompson, 1998). Measurements of the hydrologic properties of faults have revealed their heterogeneous character (see especially the collection of articles edited by Hickman, et al. (1994). These studies demonstrate not only that permeability is quite heterogeneous in and near fault zones, but is also strongly anisotropic. In some cases, heterogeneous permeability may combine with poroelastic effects to cause unexpected abnormally high pore pressures.

This phenomenon, which is related to the Mandel-Cryer effect, will be examined in the next chapter.

4.2.3 Nonlinearities

Nonlinear behavior is one of the predominant characteristics of complex dynamical systems. Yilmaz, et al. (1994) showed that even fairly mild nonlinearities can cause significant deviations from expected linear behavior when permeability is a nonlinear function of pressure. This may be an appropriate physical model of flow in materials where the permeability is due primarily to fractures. Fractures tend to be much more compliant than pore spaces in granular rocks and will tend to open or close in response to the pressure of the fluid that is flowing through them. The regions around many major faults may be composed largely of micro-fractured rock. When the permeability depends strongly on the fluid pressure, a shock-wave type of pressure front may result (Yilmaz, 1994), similar to nonlinear thermal waves that occur in high-temperature plasmas when radiation heat conduction is the dominant heat transfer mechanism (Zeldovich, 1966, p. 653). Thus, qualitatively accurate simulations of the poroelastic response of fractured materials requires that nonlinear permeability be considered in simulations.

4.2.4 Time Evolution of Material Properties

The properties of a porous material change over relatively short timescales. The primary agent in the rapid alteration of rocks in the earth is moving water. The time scale for chemical alteration of the flow properties of crustal rocks may be short enough to play a significant role in a number of geological processes in the shallow crust, including earthquakes. Byerlee (1996), for example, presents a model for the earthquake cycle which depends upon evolving permeability and porosity in and near the fault zone. Computer simulations to test such hypotheses must include the effects of evolving material properties.

4.2.5 Computational Science versus Engineering Computing

To understand the behavior of complex systems we must be able to carry out numerical experiments and manipulate each of the parameters of the model so as to determine their effect on the whole system under various conditions. The use of the computer as an experimental tool to explore the consequences of competing physical models is often referred to as *computational science*. I would like to distiguish this activity from the use of the computer as a giant calculator that is used to "compute the answer" to a problem where the physical model is either known or accepted. For convenience, we will refer to this latter activity as *engineering computing*. There is no intention at all here to place a value judgement on the different ways of using a computer. Both can be equally challenging mathematically, both can stretch the capabilities of the largest supercomputers to their limit, and both are very important to the advancement of pure and applied science. Though there may be some overlap in these definitions, there is a basic distinction which I wish to make.

Engineering calculations require that the underlying physical models, hence the mathematical equations that are being solved, be known and relatively stable. Commercial software packages generally offer the best means by which to solve such problems, because the codes required to solve complex engineering problems can represent many programmer-years of effort to build. Scientific codes sometimes require as much effort to build, yet we see scientists, graduate students, and industrial researchers often building their own codes from scratch, perhaps with the help of math libraries for tasks such matrix solvers. The reason for this is found in the task: scientific codes (as I have defined them) are used to experiment with various physical and mathematical models, compare different constitutive laws, and test the consequences of alternative theoretical ideas. It is necessary for the scientist to be able to change fundamental aspects of the code in order to carry out the numerical experiments. This is why so much effort is expended in scientific circles to write and rewrite numerical codes.

Some of the numerical experiments presented in this paper can be done with commercial codes, such as Dyna3D and Abacus. Some, however, cannot. For scientific research, it is important to be able to test the consequences of new physical theories. For example, one theory about stress transfer in the upper 100 km of the earth,

including the brittle crust and the upper mantle, has been proposed by Nur (personal communication). The idea involves an exponential relation between strain rate and stress, where the exponential is a function of temperature. It desirable to compare the consequences of this physical model against other models by simulation. There are no commercial codes available to test this theory.

Furthermore, what I am attempting to do here is to build a new foundation of software *components* for numerical experimentation in the solid earth sciences. By building software components which can readily be coupled together with other components and altered to test new ideas, I hope to gain some of the advantages of commercial or publically available codes that are already built, tested, and working, whilst retaining the scientific need for adaptability and flexibility. A discussion of the software design strategy will be given in an appendix. Now I will present the fundamental equations that I will need for my studies of the role of fluids in crustal geophysics using poroelastic theory.

4.3 Theoretical Development: Thermoporoelasticity

The goal of this section to formulate the equations that describe the evolution of a chemically reactive, coupled poroelastic crust in a form that is not only suitable for numerical simulation, but is framed in a way that allows for relatively easy experimentation with new equations for both the dynamical equations and material properties. The numerical implementation must also be efficient computationally and allow the possibility of porting from workstations and personal computers to large parallel computers as the need arises.

The theory for fluid flow in a homogeneous, linear, porous, elastic medium was first derived by Biot (1941; 1956) and restated by Rice and Cleary (1976) . The theory presented in these classic works assumes that the material properties of the medium are constant in both space and time. The importance of spatially heterogeneous permeability in controlling flow in aquifers and reservoirs is well-known. Less well-known

is the fact that pressure-dependent permeability, such as might be found in fractured media, can significantly alter the flow behavior of the pore fluid. Furthermore, chemical dissolution/precipitation can significantly alter the pore space of the medium through which it flows on timescales that are commensurate with the flow field evolution. Since reaction rates often depend strongly on temperature, thermal advection and diffusion can also critically affect fluid flow. A number of theories concerning crustal behavior invoke changes in material properties to account for earthquake cycles, episodic pore pressure buildup and release, and various pre- and post-seismic poroelastic phenomena. Thermal stresses are also significant in many situations.

Before computers became widely available as routine tools for computational experimentation, the equations for poroelasticity were necessarily simplified into forms which could be solved analytically. The motivation for this paper is the current availability of powerful computer hardware and, more importantly, numerical software to enable the exploration of the behavior of coupled and nonlinear complex processes in the crust. Computational experimentation with the complex systems of equations that describe the dynamics of the earth's crust will contribute to the determination of when various nonlinearities, heterogeneities, and time-dependent terms are significant and under what circumstances. This is essential to constructing predictive physical models of the dynamics of earth processes.

It is thus appropriate to re-derive the equations of poroelasticity with a view toward numerical simulation. In the following development, we will assume that the material properties may be functions of space, time and the state of the system (pressure, temperature, stress), may be nonlinear, and may be tensor quantities rather than scalars. Of course, inclusion of these complexities in the equations is certainly not exhaustive. But we must choose how general our model will be at this time and attempt to understand the dynamics of the crust at this level before including more detail in the equations. As Charlez points out, it is necessary to "discern between what is essential and what is unnecessary in order to solve practical problems as simply as possible" (Charlez, 1998, p. 47). The resulting set of coupled partial differential equations are analytically intractable. However, computational simulations have progressed to the point where the interesting physics which results from coupled,

nonlinear equations and heterogeneous coefficients can be studied. It is this goal that motivates our present pursuit.

4.3.1 Mass Balance Equations

The fundamental equations governing fluid flow, heat transport and elastic deformation in a fluid-saturated porous medium will be developed now. I will not repeat a rigorous derivation of equations that can be found in other papers and texts (Rice and Cleary, 1976, is a classic paper, for example; Charlez, 1998, gives a particularly thorough development of thermoporoelasticity; Detournay, 1993, and Wang, 1998, treat isothermal poroelasticity), but review only those aspects of the derivations that differ from standard treatments. This primarily involves coefficients (permeability, porosity, elastic moduli) or state variables (temperature, pore pressure) which are usually assumed to be constant in space and time, restrictive assumptions which will not be made here. Only the case of a single fluid phase which saturates the porous material will be considered in the present study. Generalization to multiphase flow requires essentially the same development as for any multiphase flow problem, with the modifications made here. Multiphase fluid flow is not necessary for many problems concerning large-scale crustal processes. The goal of this section is to present the set of equations which describe important physical processes that control the dynamics of the crust in a form suitable for numerical discretization and computer simulation. It is believed that the crust is a complex dynamical system and quantitative understanding will only be achieved if geophysics moves beyond linear, homogeneous models.

Darcy's law states that the flux of fluid in the x_i direction is

$$q_i = \phi v_i = -\frac{k_{ij}}{\mu}\left(\frac{\partial p}{\partial x_j} + \rho g_j\right) \tag{4.3}$$

where q_i is the volumetric flux per unit area, ϕ is the porosity, v_i is the fluid velocity, ρ is the fluid density, g_j is the acceleration vector due to gravity, k_{ij} is the absolute permeability tensor, μ is the viscosity, and p is the fluid pressure. Fluid mass

conservation is expressed as the divergence equation:

$$\frac{\partial m}{\partial t} - \rho \frac{\partial q_i}{\partial x_i} = 0 \tag{4.4}$$

Substituting equation 4.3 into equation 4.4 yields an equation for flow in porous media:

$$\frac{\partial m}{\partial t} = \rho \frac{\partial}{\partial x_i} \left(\frac{k_{ij}}{\mu} \left(\frac{\partial p}{\partial x_j} + \rho g_j \right) \right) \tag{4.5}$$

Viscosity, μ, may depend significantly on the temperature of the fluid, which is spatially variable in general. Hence, the viscosity term must remain inside the spatial derivative.

The time derivative of the fluid mass requires careful evaluation. The fluid mass per unit volume is the product of the fluid density and the local porosity of the material. Since our intent is to simulate crustal behavior on a macroscopic scale, grid blocks, which define elementary volumes in simulations, will be assumed to be large enough to treat porosity and other material properties as well-defined continuum variables.

Fluid density will be assumed to depend on pressure and temperature. It may also depend on the concentration of dissolved species, but in this paper chemical species concentrations are treated as given quantities, either specified constant values or derived from an unspecified simulator.

Porosity will depend on the fundamental state variables pressure, temperature, and hydrostatic stress. It can also vary with time due to inelastic pore volume changes associated with material deposition and dissolution or plastic deformation. In functional notation,

$$\rho = \rho \left(p, T \right) \tag{4.6}$$

$$\phi = \phi \left(p, T, \sigma, t \right) = \widetilde{\phi} \left(p, T, \sigma \right) \phi_0 \left(t \right) \tag{4.7}$$

Note that the pore volume has been separated into a time-dependent porosity ϕ_0,which is assumed to vary by chemical changes and inelastic deformation and a multiplicative scaling porosity that is dependent upon pressure, temperature, and hydrostatic

stress. In the relaxed state, that is, when $p - p_{ref}$, $T - T_{ref}$, and $\sigma - \sigma_{ref}$ are zero, $\widetilde{\phi}$ will be equal to one.

The mass derivative with respect to time may be written

$$\frac{\partial m}{\partial t} = \frac{\partial (\rho\phi)}{\partial t} = \phi\frac{\partial \rho}{\partial t} + \rho\left(\phi_o\frac{\partial \widetilde{\phi}}{\partial t} + \widetilde{\phi}\frac{\partial \phi_0}{\partial t}\right) \tag{4.8}$$

$$= \phi\frac{\partial \rho}{\partial t} + \rho\phi_o\frac{\partial \widetilde{\phi}}{\partial t} + \rho\widetilde{\phi}\left(\frac{\partial \phi_0}{\partial t}\right)_{inelastic} \tag{4.9}$$

The pore volume scaling factor, $\widetilde{\phi}(p, T, \sigma)$, will generally be close to one for matrix porosity, but may vary over a considerable range in fractured media. In fact, if the anisotropic compressibility of fractures is to be considered, the full stress tensor rather than just the hydrostatic stress must be considered in order to evaluate the porosity change due to stress. In this case, the porosity (and consequently the permeability) will depend on the orientation of the stress field. There are many situations in which this will be significant for crustal dynamics (Zoback, 1992). In this situation, quantities derived from porosity, for example permeability, will depend on other parameters besides porosity, such as the stress orientation, pore pressure, mean fracture orientation, and so on. This level of complexity can be incorporated by making the material properties (coefficients in the equations) functions of the state variables. The role of inelastic porosity changes in generating abnormally high pore pressure and its consequences for tectonic processes was explored by Walder and Nur (1982).

Fluid density depends only on the pressure and temperature of the fluid; note that temperature and pressure are time-dependent, however. When dissolved minerals are present, the density may also be a function of aqueous species concentration. It will be assumed here that chemical concentrations are low enough that their effect on fluid density can be ignored. There are many cases when this is not true, for instance, when sea water intrudes a freshwater aquifer. But this is not important for tectonic processes. The deformation of the solid matrix does not affect the fluid density. Thus, the time derivative for fluid density is:

$$\frac{\partial \rho}{\partial t} = \left(\frac{\partial \rho}{\partial p}\right)\frac{\partial p}{\partial t} + \left(\frac{\partial \rho}{\partial T}\right)\frac{\partial T}{\partial t} \tag{4.10}$$

If the coefficients in parentheses are taken to be constants we have

$$\frac{\partial \rho}{\partial p} = \beta_\rho \rho \tag{4.11}$$

$$\frac{\partial \rho}{\partial T} = \alpha_\rho \rho \tag{4.12}$$

Similarly, the time derivatives for ϕ may be expanded as

$$\frac{\partial \phi}{\partial t} = \left(\frac{\partial \phi}{\partial p}\right)\frac{\partial p}{\partial t} + \left(\frac{\partial \phi}{\partial T}\right)\frac{\partial T}{\partial t} + \left(\frac{\partial \phi}{\partial \sigma}\right)\frac{\partial \sigma}{\partial t} + \frac{\partial \phi_0}{\partial t} \tag{4.13}$$

In many situations, it is correct to model the variation of porosity with pressure, temperature, and hydrostatic as constants also:

$$\frac{\partial \phi}{\partial p} = \beta_\phi \phi \tag{4.14}$$

$$\frac{\partial \phi}{\partial T} = \alpha_\phi \phi \tag{4.15}$$

$$\frac{\partial \phi}{\partial \sigma} = \gamma \phi \tag{4.16}$$

The elastic constants in equations 4.14 through 4.16 may be used in equation 4.8 and equation 4.13 to yield

$$\frac{\partial \phi}{\partial t} = \phi\left(\beta_\phi \frac{\partial p}{\partial t} + \gamma \frac{\partial \sigma}{\partial t} + \alpha_\phi \frac{\partial T}{\partial t}\right) + \widetilde{\phi}\left(\frac{\partial \phi_0}{\partial t}\right)_{in} \tag{4.17}$$

Combining these expressions yields:

$$\frac{\partial m}{\partial t} = \rho\phi\left(b\frac{\partial p}{\partial t} + \gamma \frac{\partial \sigma}{\partial t} - a\frac{\partial T}{\partial t}\right) + \rho\left(\frac{\partial \phi}{\partial t}\right)_{in} \tag{4.18}$$

where $b = \beta_\phi + \beta_\rho$ and $a = -\left(\alpha_\phi + \alpha_\rho\right)$. The value of these parameters in terms of commonly measured elastic and hydraulic parameters will be examined later. Note

that the variation of porosity due to inelastic pore space diagenesis in 4.18 uses the fact that $\widetilde{\phi}\frac{\partial(\phi_0)}{\partial t} = \frac{\partial(\phi)}{\partial t}$.

McTigue (1986) , following Rice and Cleary (1976), derives the following diffusion equation for a thermoporoelastic material (ignoring inelastic porosity changes):

$$\frac{\partial m}{\partial t} = \left(\frac{9\mu\left(\nu_u - \nu\right)}{2GB^2\left(1-\nu\right)\left(1+\nu_u\right)}\right)\frac{\partial}{\partial t}\left(P + B\sigma\right) - \left(\phi_0\left(\alpha_f - \alpha_s\right)T\right) \tag{4.19}$$

The thermal expansion coefficients are discussed in detail in McTigue (1985) and Charlez (1991). The other parameters are also discussed in Rice (1976) and Wang (1993). We can now identify the coefficients in 4.18 in terms of common material parameters. First, we introduce the following notation:

$$c = \frac{9\mu\left(\nu_u - \nu\right)}{2GB^2\left(1-\nu\right)\left(1+\nu_u\right)} \tag{4.20}$$

$$\gamma = \frac{9\mu\left(\nu_u - \nu\right)}{2GB\left(1-\nu\right)\left(1+\nu_u\right)} \tag{4.21}$$

$$a = -\phi\left(\alpha_f - \alpha_s\right) \tag{4.22}$$

Substituting equation 4.3 and equation 4.18 into equation 4.4 yields

$$c\left(\frac{\partial p}{\partial t} + B\frac{\partial \sigma}{\partial t}\right) + a\frac{\partial T}{\partial t} = \frac{\partial}{\partial x_i}\left(\frac{k_{ij}}{\mu}\frac{\partial p}{\partial x_j} + \rho g_j\right) - \left(\frac{\partial \phi}{\partial t}\right)_{in} \tag{4.23}$$

Since we want to allow for evolution of the pore space in our equations, that is, variable porosity ϕ, a more suitable form for the parameter c is that given in Charlez (1997):

$$c = \phi\left\{\left[\frac{1}{K_f}\right] + \left[\left(\frac{1-\alpha}{\phi}\right)\left(\frac{1}{K_B} - \frac{1}{K_M}\right) - \frac{1}{K_M}\right]\right\} \tag{4.24}$$

$$= \phi\left\{C_f + C_r\right\} \tag{4.25}$$

C_f and C_r are the fluid and rock compressibilities, respectively. The fluid compressibility can be assumed to be constant. For small porosity changes, the rock compressibility may also be assumed constant. However, in the equations formulated below, C_f may vary over time.

Two more equations are needed to resolve the system. These are derived from the strain compatibility conditions and from energy balance (that is, thermal advection-diffusion equation). It should be especially noted that we have not assumed that the permeability and elastic coefficients are constant. In the most general case, these coefficients may be spatially variable, may be nonlinear functions of pressure, temperature, and stress, and may change over time due to chemical alteration of the porous structure. The two additional equations required are derived below.

4.3.2 Heat Transport

A full treatment of the thermodynamics of fluids should include internal energy changes, mechanical work performed by the fluid, and work against friction arising from the viscosity of the fluid. For many tectonic problems, it is sufficient to represent some of the material properites by appropriate averages between solid (mineral) and fluid phases. The energy balance equation for thermal advection-diffusion of a single phase fluid is

$$\frac{c_e}{\rho c_p}\frac{\partial T}{\partial t} - \rho_f c_{pf} q_i \frac{\partial T}{\partial x_i} - \frac{\partial}{\partial x_i}\left(D_{ij}\left(\mathbf{x}\right)\frac{\partial T}{\partial x_j}\right) = Q_T\left(\mathbf{x}\right) \tag{4.26}$$

where c_e, ρ, c_p are the *effective* thermal conductivity, density, and specific heat, respectively, which may be taken to be the volume-fraction weighted averages of fluid and mineral properties. ρ_f is the fluid density, c_f is the specific heat of the fluid, D_{ij} is the effective thermal diffusivity tensor of the saturated porous medium, $Q_T\left(\mathbf{x}\right)$ is a heat source and q_i is the Darcy velocity which may be found from equation 4.3. The latter term couples thermal advection to equation 4.23. More precise descriptions of the thermal diffusivity are possible if the medium is considered to be a multiphase system where solid and fluid phases are present. Each phase, solid or fluid, then has a distinct thermal diffusivity and the mass fraction or saturation of each phase is a dependent variable that changes with time as flow proceeds and as chemical reactions alter the solid matrix. The thermal diffusivity will, in general, be spatially variable. Thus, it is important to keep the diffusivity parameter within the outer spatial derivative in equation 4.26.

To complete the system of partial differential equations, we need to introduce a constraint on the elastic deformation that ensures that the strains will be continuous across the domain. For this purpose, the Beltrami-Mitchell equations for a thermo-poroelastic medium are introduced. The derivation of these equations follows from the compatibility equations (Charlez, 1991; Rice, 1976). Summation of the Beltrami-Mitchell equations yields a compatibility condition, which has the form of a Poisson equation:

$$\frac{\partial^2}{\partial x_j^2}\left(\sigma + c_1 p + c_2 T\right) = 3g\left(\phi\rho + \left(1-\phi\right)\rho_r\right) \tag{4.27}$$

where the constants c_1 and c_2 may be expressed in terms of commonly-known material parameters by:

$$c_1 = \frac{2\left(\nu_u - \nu\right)}{B\left(1-\nu\right)\left(1+\nu_u\right)} \tag{4.28}$$

$$c_2 = \frac{4G\left(1+\nu\right)}{9\left(1-\nu\right)}\alpha_T \tag{4.29}$$

α_T is the effective bulk thermal expansion coefficient for the fluid-saturated medium in the drained case. The body force term on the right side of the equation is the gravitational force on the mean density of rock mass and fluid mass. ρ is the fluid density and ρ_r is the rock density. The latter may be spatially variable.

4.3.3 Elastic Deformation

Elastic deformation may be computed from the stress equilibrium equations with pore pressure and temperature as applied forces (equation 4.30). If the fully coupled poroelastic diffusion equations are used, as described above, the mean stress derived from solving the stress equilibrium equations will be exactly equal to the mean stress that is evolved in the two coupled poroelastic equations, equations 4.23 and 4.27. It is computationally efficient to solve the coupled poroelastic equations and the stress equilibrium equations in this decoupled manner. However, this approach assumes that boundary and initial conditions can be assigned to p, σ and T. If boundary

conditions for the mean stress cannot be supplied, then the poroelastic equations for p and T must be solved simultaneously with the three equations for displacement in 4.30

The three equations for the displacements in terms of pore pressure and temperature are:

$$\frac{\partial}{\partial x_i}\left(\left(\lambda+G\right)u_{k,k}\right)+\frac{\partial}{\partial x_k}\left(Gu_{i,k}\right)=\frac{\partial}{\partial x_i}\alpha\left(p-p_{ref}\right)-\frac{\partial}{\partial x_i}\alpha_T\left(T-T_{ref}\right)+\rho_r\left(\mathbf{x}\right)g_i \tag{4.30}$$

where u_i are the three components of the displacement vector, λ is the Lame coefficient, and G is the shear modulus. Note that both of these may be spatially variable. The Biot-Willis parameter, α, is a function of Skempton's coefficient and the drained and undrained Poisson's ratios: $\alpha=2\left(\nu_u-\nu\right)/B\left(1-2\nu\right)$. α_T is the effective bulk thermal expansion coefficient for the fluid-saturated medium as above. The right side of equation 4.30 is expressed in terms of the deviation of the pore pressure from a reference value, p_{ref}. In the following equations, p_{ref} is assumed to be zero and dropped for convenience. Similarly, T in the following equations will represent the deviation from the reference state. The gravitational force vector, g_i, will have only a z-component. ρ_r is the density of the fluid-saturated rock at $\mathbf{x}$. If the independent variables are *deviations* from a reference value the gravitational force terms will be zero. Note that the elastic moduli are inside of the spatial derviatives.

4.3.4 Summary of Thermoporoelastic Equations

The set of general equations for a thermoporoelastic material with six unknowns, P, σ, T, and the three components of displacement u_i, are as follows:

$$\phi\left(C_f+C_r\right)\left(\frac{\partial p}{\partial t}+B\frac{\partial\sigma}{\partial t}\right)+\phi\left(\alpha_f-\alpha_s\right)\frac{\partial T}{\partial t}=\frac{\partial}{\partial x_i}\left(\frac{k_{ij}}{\mu}\frac{\partial p}{\partial x_j}+\rho g_j\right)-\left(\frac{\partial\phi}{\partial t}\right)_{in} \tag{4.31}$$

$$\frac{c_e}{\rho_e c_{pe}}\frac{\partial T}{\partial t}=\rho c_{pf}q_i\frac{\partial T}{\partial x_i}+\frac{\partial}{\partial x_i}\left(D_{ij}\left(\mathbf{x}\right)\frac{\partial T}{\partial x_j}\right)+Q_T \tag{4.32}$$

$$\frac{\partial^2}{\partial x_j^2}\left[\sigma + \left(\frac{2\left(\nu_u - \nu\right)}{B\left(1-\nu\right)\left(1+\nu_u\right)}\right)p + \left(\frac{4G\left(1+\nu\right)}{9\left(1-\nu\right)}\alpha_T\right)T\right] = 3g\left(\phi\rho + \left(1-\phi\right)\rho_r\right) \tag{4.33}$$

$$\frac{\partial}{\partial x_i}\left(\left(\lambda + G\right)u_{k,k}\right) + \frac{\partial}{\partial x_k}\left(Gu_{i,k}\right) = \frac{\partial}{\partial x_i}\alpha\left(p - p_{ref}\right) - \frac{\partial}{\partial x_i}\alpha_T\left(T - T_{ref}\right) + \rho_r g_i \tag{4.34}$$

where

$$q_i = -\frac{k_{ij}}{\mu}\left(\frac{\partial p}{\partial x_j} + \rho g_j\right) \tag{4.35}$$

in equation 4.32.

The full set of coupled partial differential equations may only be solved in its present general formulation by numerical approximation on a computer. Various assumptions allow simpler formulations of the thermoporoelastic problem which admit analytical solutions or straight-forward numerical solutions analogous to heat diffusion problems. Because the permeability is not assumed to be constant, equations 4.31 and 4.33 cannot be combined in the manner done by Rice (1976) and others cited previously to give an evolution equation in a single variable $m = P + B\sigma$.

4.3.5 Constitutive Relations

The strain tensor and stress tensor may be computed as derived quantities from the above equations using

$$\varepsilon_{ij} = \frac{1}{2}\left(\frac{\partial u_i}{\partial x_j} + \frac{\partial u_j}{\partial x_i}\right) \tag{4.36}$$

$$\sigma_{ij} = 2G\varepsilon_{ij} + \left(\left(K_B - \frac{2G}{3}\right)\frac{\partial u_k}{\partial x_k} + \alpha p + \alpha_T K_B T\right)\delta_{ij} \tag{4.37}$$

4.3.6 Material Properties

The mechanical and hydrologic properties of porous rocks may be modified quite rapidly on a geologic time scale by the flow of water through the pores. Porosity is the primary variable in our mathematical equations that is modified. However, permeability, the elastic modulii, and most of the other parameters are functions of the porosity of the material. Mathematically, time-evolving material properties cause the fundamental equations derived previously to become nonlinear. The mathematical model presented here assumes that the material coefficients may be functions of time (either directly or via dependence on temperature or pore pressure), spatial location, and the independent variables, which include fluid pressure, stress, and temperature. The numerical scheme which will be outlined is general and methods for both linear equations (constant coefficients) and nonlinear (nonlinear, time-varying coefficients) are presented.

Geochemistry is a vast subject and will not be dealt with here, though we envision the possibility of coupling a reactive chemistry model to the thermoporoelastic model in a sequential manner. By this we mean that reactive chemistry takes as input the state variables (fluid pressure, temperature, stress) at a given time and integrates ahead to the next time step. The output from the chemistry model is taken as input to the thermoporoelastic model, most likely as a new solid phase fraction which modifies the porosity. Pressure, mean stress, and temperature are then integrated forward in time, and so on. Porosity and fluid velocity values may be shared by each module or object as the whole system evolves in time. If a geochemical code is available, sequential coupling to the hydromechanical model presented here should be straightforward.

4.3.7 Representation of Faults

Faults present a difficult challenge for computer modeling. Poroelastic media are assumed to be relatively smooth continua, and this allows for straight-forward meshing of the domain of interest. Faults are geometrically complex and have discontinuous dynamics. One possibility for incorporating faults into a poroelastic continuum is by

means of a composite grid. Implementation of fault dynamics must include the dual nature of the fault. That is, faults exhibit both continuum dynamics (fluid flow, heat transport and diffusion) and non-continuum dynamics. The latter involves movement along planes according to prescribed friction laws or other models that govern slip movement.

A method for incorporating faults into a continuum model of the crust is to introduce a set of fault segments defined as sets of grid points on adjacent planes. The new points are incorporated into the continuum grid by forming a composite grid (see Daehlen, 1997 for more information on composite grids). The grid points are treated as boundary points for deformation (stress) calculations. Treating them as boundary points simply means that their displacements are not computed by the continuum equations. Rather, some other rules or physical laws are used as the basis for movement along fault segments. This method is related to the slip elements used by Ge (1994), but is somewhat more general in that fault segment points are incorporated into the continuum background for fluid flow or pore pressure calculations.

Extensive development and testing is still required to determine how best to implement many of the details and will be the subject of future research. Embedding faults into a continuum does not imply any particular fault rupture model. It provides a method for numerical experimentation with various fault models and friction laws within the context of a complex continuum.

4.4 Computational Method

There are two strategies for solving the coupled system of equations presented. In each case, the unknowns include pressure, temperature, mean stress and the three components of displacement. Of course, the mean stress may be computed from the displacements, so it's inclusion as an unknown might seem superfluous. One strategy is to evolve equations 4.31, 4.32, and 4.33 as a coupled system for pressure, temperature and mean stress. Then, at selected times of interest or at a later time, equations 4.34 can be solved independently for elastic displacements using the derived pressures and temperatures as input. The computation of σ is redundant in this

strategy because it can be computed from the displacements. However, separating the calculation into two systems of size 3N (pressure, temperature, mean stress in one system, three components of displacement in the other), where N is the number of computational nodes, may be preferable to solving a single system of size 5N for five unknowns (pressure, temperature, and the three displacements). Furthermore, there are a number of situations where the displacements are not of interest or need only be computed at selected times and not at every time step. In this situation, solving two systems is considerably more efficient.

Using the mean stress σ as an independent variable requires that initial and boundary values be available. If these cannot be assigned, then σ cannot be used as an independent variable. Instead, the Beltrami-Mitchell equation must be dropped and equations 4.31, 4.32, and 4.34 solved as a fully coupled system. σ in equation 4.31 will be computed at each time step from the displacements using the constitutive law for poroelastic materials:

$$\sigma = K_B \frac{\partial u_k}{\partial x_k} + \alpha p + \alpha_T K_B T \tag{4.38}$$

where K_B is the bulk modulus of the porous material.

4.4.1 Gridding

4.4.2 Finite Element Spatial Discretization

A thorough treatment of all of the numerical techniques needed to solve a complex set of coupled partial differential equations is beyond the scope of this paper. A brief overview of a finite element approach to the solution of the above set of equations is given here. We first write the general set of equations in the following form:

$$a_1 \frac{\partial \left(P + B\sigma + a_2 T\right)}{\partial t} = \frac{\partial}{\partial x_i}\left[\frac{k_{ij}}{\mu}\frac{\partial}{\partial x_j}P\right] + f \tag{4.39}$$

$$\frac{\partial^2}{\partial x_i^2}\left(b_1 P + \sigma + b_2 T\right) = 0 \tag{4.40}$$

$$c\frac{\partial T}{\partial t} = q_i\frac{\partial T}{\partial x_i} + \frac{\partial}{\partial x_i}\left(d_{ij}\frac{\partial T}{\partial x_j}\right) \tag{4.41}$$

where a_1, a_2, f, b_1, b_2, c, and d_{ij} are simply shorthand notations for the coefficients in equations 4.31, 4.32, and 4.33.

The finite element discrete form of these equations is derived by approximating the unknown functions P, σ and T by a linear sum of basis functions. Here we use the method of weighted residuals or Petrov-Galerkin formulation (Helmig, 1997) , where the weighting functions W_i and the basis functions N_i may be different. Petrov-Galerkin elements are used primarily to control numerical dispersion. In the standard Galerkin finite element formulation, $N_i = W_i$.

$$p \approx \sum_{i=1}^{n} p_i\,(t)\,W_i \tag{4.42}$$

$$\sigma \approx \sum_{i=1}^{n} s_i\,(t)\,W_i \tag{4.43}$$

$$T \approx \sum_{i=1}^{n} \tau_i\,(t)\,W_i \tag{4.44}$$

where n is the number of nodes, W_i are the finite element weighting functions and the p_i, s_i, τ_i are unknown values to be determined. A spatially discrete weak form of the system of equations is given by

$$a_1\mathbf{M}_{ij}\frac{d\,(p_j + Bs_j + a_2\tau_j)}{dt} + \mathbf{K}_{ij}p_j = d_i \tag{4.45}$$

$$\mathbf{B}_{ij}\,(b_1p_j + s_j + b_2\tau_j) = \gamma_i \tag{4.46}$$

$$c\mathbf{M}_{ij}\frac{d\tau_j}{dt} + \mathbf{D}_{ij}\tau_j = Q_i \tag{4.47}$$

where

$$\mathbf{M}_{ij} = \int_{\Omega} W_iN_jd\Omega \tag{4.48}$$

$$\mathbf{K}_{ij} = \int_{\Omega} \sum_{l=1}^{3} \sum_{k=1}^{3} \left(k_{kl}\left(\mathbf{x}\right) \frac{\partial W_i}{\partial x_k} \frac{\partial N_j}{\partial x_l} \right) d\Omega \tag{4.49}$$

$$\mathbf{D}_{ij} = \int_{\Omega} \sum_{k=1}^{3} \left[\left(\sum_{l=1}^{3} d_{kl}\left(\mathbf{x}\right) \frac{\partial W_i}{\partial x_k} \frac{\partial N_j}{\partial x_l} \right) + W_i q_k \frac{\partial N_j}{\partial x_k} \right] d\Omega \tag{4.50}$$

$$d_i = \int_{\Omega} f W_i d\Omega + \int_{\partial\Omega} g W_i d\Gamma \tag{4.51}$$

$$Q_i = \int_{\Omega} Q_T W_i d\Omega + \int_{\partial\Omega} q_T W_i d\Gamma \tag{4.52}$$

$$\mathbf{B}_{ij} = \int_{\Omega} \left(\frac{\partial W_i}{\partial x_k} \frac{\partial N_j}{\partial x_l} \right) d\Omega \tag{4.53}$$

$$\gamma_i = \int_{\Omega} \rho g W_i d\Omega \tag{4.54}$$

and the functions N_i are the finite element trial functions. Prescribed flux boundary conditions are the functions represented by g and g_T for pressure and temperature flux conditions. Mathematically, a fluid flux boundary condition, in the direction of $\widehat{n}$, is

$$q_n = \sum_{l=1}^{3} \sum_{k=1}^{3} \left(k_{kl} n_k \frac{\partial p}{\partial x_l} \right) \tag{4.55}$$

The prescribed heat flux has similar definition. In a computer code, g and q_T are simply defined flux values at the boundaries or at internal source points.

4.4.3 Time Discretization

Temporal discretization is accomplished by the *theta* method:

$$\frac{u^r - u^{r-1}}{\Delta t} = \theta g^r + \left(1 - \theta\right) g^{r-1} \tag{4.56}$$

When $\theta = 1$, for example, we recover the backward Euler approximation. $\theta = \frac{1}{2}$ gives the Crank-Nicholson scheme. For example, we can formally apply the theta method to equation 4.45 by writing it in the form

$$\frac{d\left(p_j + Bs_j + a_2 \tau_j\right)}{dt} = \frac{1}{a_1} \mathbf{M}^{-1} \left(\mathbf{d} - \mathbf{K}\mathbf{p}\right) \tag{4.57}$$

4.4.4 Linear and Nonlinear Solution Methods

Applying the theta scheme, we obtain a linear system for the unknowns at the time level r:

$$\mathbf{A}\mathbf{u}^r = \mathbf{c} \tag{4.58}$$

where

$$A_{ij} = \begin{pmatrix} a_1\mathbf{M}_{ij} + \theta\Delta t\mathbf{K}_{ij} & Ba_1\mathbf{M}_{ij} & a_1a_2\mathbf{M}_{ij} \\ b_1\mathbf{B}_{ij} & \mathbf{B}_{ij} & b_2\mathbf{B}_{ij} \\ 0 & 0 & c\mathbf{M}_{ij} + \theta\Delta t\mathbf{D}_{ij} \end{pmatrix} \tag{4.59}$$

$$u_j^r = \begin{pmatrix} p_j^r \\ s_j^r \\ \tau_j^r \end{pmatrix} \tag{4.60}$$

$$c_i = \begin{pmatrix} a_1\mathbf{M}_{ij}u_j^{r-1} + (\theta - 1)\,\Delta t\mathbf{K}_{ij}p_j^{r-1} + \Delta t d_i \\ \gamma_i \\ c\mathbf{M}_{ij}u_j^{r-1} + (\theta - 1)\,\Delta t\mathbf{D}_{ij}p_j^{r-1} + \Delta t Q_i \end{pmatrix} \tag{4.61}$$

The linear system in 4.58 becomes nonlinear when the coefficients, for example, the permeability tensor, depend on pressure, stress, or temperature, or evolve in time. The system of nonlinear equations may be solved using a Newton-Raphson iteration. In this method, the quantity $\mathbf{c} - \mathbf{A}\mathbf{u}^r$ is minimized using the the Jacobian (derivative) matrix of $\mathbf{c} - \mathbf{A}\mathbf{u}^r$. Details can be found in texts on numerical optimization such as Dennis and Schnabel, (1983).

Equation 4.34 can be discretized in a similar manner. The resulting linear system is

$$\mathbf{A}\mathbf{x} = \mathbf{b} \tag{4.62}$$

where $\mathbf{x}$ is the vector of displacements, $x = (u_1, v_1, w_1, u_2, v_2, w_2, ..., u_n, v_n, w_n)$. $\mathbf{A}$ is a 3n by 3n nonsymmetric matrix, which can be partitioned into n blocks of size 3×3

each. The general formula for block $\mathbf{A}_{ij}$, which represents the coupling between node i and j, is

$$\mathbf{A}_{ij} = \begin{matrix} \mathbf{a}_{ij}^{11} & \cdots & \mathbf{a}_{ij}^{13} \\ \vdots & \ddots & \vdots \\ \mathbf{a}_{ij}^{31} & \cdots & \mathbf{a}_{ij}^{33} \end{matrix} \tag{4.63}$$

and

$$\mathbf{a}_{ij}^{rs} = \int_{\Omega} \left[G \left(\sum_{k} N_{i,k} N_{j,k} \right) N_{i,s} N_{j,r} + \lambda N_{i,r} N_{j,s} \right] d\Omega \tag{4.64}$$

The corresponding partitioning for $\mathbf{b}$ is

$$\mathbf{b}_j = - \begin{pmatrix} \beta_j^1 \\ \beta_j^2 \\ \beta_j^3 \end{pmatrix} \tag{4.65}$$

where

$$\beta_j^r = \int_{\Omega} \left[(2G + 3\lambda) + \alpha_T \left(T - T_{ref} \right) N_{j,r} + \alpha \left(p - p_{ref} \right) \right] d\Omega \tag{4.66}$$

4.4.5 Boundary Conditions

Geologically realistic boundary conditions for temperature, pore pressure, mean stress, and the displacements must be prescribed. Boundary points can in fact be any grid points in the domain, though they are usually taken to be the boundary points in the geometrical sense. Dirichlet (fixed value) or Neumann (fixed flux) boundary conditions may be used for fluid pressure, mean stress, or temperature. For displacements, Neumann conditions take the form of constant pressure values which are normal to a specified surface. All boundary conditions may be time-dependent as well. Implementation details are not presented here.

Because it is often difficult to assign values to boundaries near a region of interest, boundaries are often taken to be sufficiently far away to assign some background value. This may not be sufficient for detailed studies of specific sites, but may be perfectly adequate for numerical experiments where general behavior of complex systems is

of interest. No-flux boundary conditions on the base and sides of a domain are often assumed for crustal simulations (see Person, et al., 1996). In general, available geologic data or theoretical constraints (for simulations of synthetic phenomena) will determine which boundary conditions are appropriate.

4.4.6 Initial Conditions

We will assume that the initial temperature field is prescribed. Either the mean stress or pore pressure must be prescribed in order to determine the remaining initial condition. The coupled temperature, mean stress and pore pressure fields must satisfy the compatibility equation (equation 4.33) for a thermoporoelastic material at all times. This boundary value problem must be solved in order to determine the initial values for mean stress or pore pressure given the other variable (assuming the initial temperature is known). Displacements are only needed at the boundary nodes, since they need satisfy only a boundary value problem (equation 4.34).

4.5 Some Special Cases

In this section we will derive some useful simplified forms for equations 4.31 through 4.34. Although the full poroelastic equations may always be used to model fluid flow and elastic deformation, the physical model can often be simplified considerably, thereby avoiding the increased computational burden incurred by more complex models. The purpose of numerical simulation must always be kept in mind when considering how complex a simulation to implement and carry out. The goal of a simulation is to gain insight into natural phenomena. Often a simple model will give as much insight as a more complex one.

4.5.1 Pressure Diffusion and Deformation

The simplest case involves isothermal flow in a matrix with constant material properties and constant mean stress. Constant mean stress implies that the mean stress is not changing with changes in pore pressure and the time derivative of mean stress

is zero. If the permeability is isotropic, that is, a scalar quantity, we obtain the equation for pressure diffusion in a porous medium. It is common to assume that fluid and material properties are homogeneous in space and constant in time. Though this is unrealistic for real materials, it is nevertheless a typical assumption when pore pressure is considered in crustal studies because permeability information is often lacking.

The governing flow equation is

$$(C_f + C_r)\,\phi\mu\frac{\partial p}{\partial t} = \frac{\partial}{\partial x_i}\left(k_{ij}\frac{\partial p}{\partial x_j} + \rho g_i\right) - \left(\frac{\partial \phi}{\partial t}\right)_{in} \tag{4.67}$$

Note that the coefficients here are not assumed to be constant; spatially variable or nonlinear coefficients may be used. A finite element discretization for this equation results in the following system:

$$\mathbf{A}\mathbf{p}^r = \mathbf{c} \tag{4.68}$$

where

$$\mathbf{A}_{ij} = a_1\mathbf{M}_{ij} + \theta\Delta t\mathbf{K}_{ij} \tag{4.69}$$

and

$$c_i = a_1\mathbf{M}_{ij}u_j^{r-1} + \Delta t d_i + (\theta - 1)\,\Delta t\mathbf{K}_{ij}p_j^{r-1} + \Delta t d_i \tag{4.70}$$

Elastic deformation due to pore pressure can be computed from the stress equilibrium equations in the usual manner using the pore pressure as a time-dependent force

$$\frac{\partial}{\partial x_i}\left(\left(\lambda + G\right)u_{k,k}\right) + \frac{\partial}{\partial x_k}\left(Gu_{i,k}\right) = \frac{\partial}{\partial x_i}\alpha\left(p - p_{ref}\right) + \rho_r g_i \tag{4.71}$$

The pore pressure evolves independently of the elastic deformation in this system of equations.

4.5.2 Coupled Isothermal Poroelasticity

The formulation by Rice and Cleary (1976) couples pore pressure and mean stress. This coupling is important particularly when fluids are pumped into or out of a reservoir under high pressure, as, for example, when induced seismicity results from injection or extraction of fluids (Segall, 1985). Elastic deformation may be felt almost instantly far from the fluid source due to the coupling between pressure and stress.

The system of equations shown in this section can be reduced to the equations of Rice and Cleary (1976) if the gravity and inelastic porosity change terms are dropped and permeability is assumed to be a scalar constant. The formulation in Rice and Cleary reduces to a system of two uncoupled equations in the two unknowns, pressure and hydrostatic stress. Numerically this is particularly advantageous. Since permeability heterogeneity is likely to be very important in any realistic simulation of the earth, we choose to treat the permeability as a function of space and possibly other variables. This prevents the reduction of Rice and Cleary (1976), leaving these fundamental equations:

$$\mu\phi\left(C_f + C_r\right)\left(\frac{\partial p}{\partial t} + B\frac{\partial \sigma}{\partial t}\right) = \frac{\partial}{\partial x_i}\left(k_{ij}\frac{\partial p}{\partial x_j} + \rho g_j\right) - \left(\frac{\partial \phi}{\partial t}\right)_{in} \tag{4.72}$$

$$\frac{\partial^2}{\partial x_j^2}\left[\sigma + \left(\frac{2\left(\nu_u - \nu\right)}{B\left(1-\nu\right)\left(1+\nu_u\right)}\right)p\right] = 0 \tag{4.73}$$

All of the components of the displacement can be determined as well in this simplification by solving the static equilibrium equations, equation 4.34, with the temperature set to zero on the right side.

4.5.3 Poroelasticity with Thermal Diffusion

When diffusive transport of heat dominates over advective transport, the temperature diffusion equation is decoupled from the other equations. Two equations with pressure and mean stress are solved as a coupled system, as above, with temperature as a known value in this case.

$$\mu\phi\left(C_f + C_r\right)\left(\frac{\partial p}{\partial t} + B\frac{\partial \sigma}{\partial t}\right) + \phi\left(\alpha_f - \alpha_s\right)\frac{\partial T}{\partial t} = \frac{\partial}{\partial x_i}\left(k_{ij}\frac{\partial p}{\partial x_j} + \rho g_j\right) - \left(\frac{\partial \phi}{\partial t}\right)_{in} \tag{4.74}$$

$$\frac{\partial^2}{\partial x_j^2}\left[\sigma + \left(\frac{2\left(\nu_u - \nu\right)}{B\left(1-\nu\right)\left(1+\nu_u\right)}\right)p + \left(\frac{4G\left(1+\nu\right)}{9\left(1-\nu\right)}\alpha_T\right)T\right] = 0 \tag{4.75}$$

A single uncoupled diffusion equation evolves the temperature field.

$$\frac{c_e}{\rho_e c_{pe}}\frac{\partial T}{\partial t} = \frac{\partial}{\partial x_i}\left(D_{ij}\left(\mathbf{x}\right)\frac{\partial T}{\partial x_j}\right) + Q_T \tag{4.76}$$

4.6 Software Implementation

Scientific computing involves three aspects, all of which are important when the computer is used as an experimental research tool. These are mathematical formulation of the physical processes, selection of appropriate numerical methods, and robust, maintainable, and extensible software implementation of the mathematical and numerical concepts. Too often the latter aspect is not given enough attention. The result is that, at best, much time is wasted in trying to maintain or adapt complex codes. Even worse, erroneous results creep in due to unmanagable code complexity and undetected bugs. New software design methodologies are developing to meet these needs. Though they are well-developed in some applications, the new ideas have been slower to take hold in scientific and engineering codes. An attempt is made here to sketch out an object-oriented design of a set of software components that may be flexibly used for complex crustal simulation experiments.

4.6.1 Managing Complexity in Sofware

The system presented here is designed to allow a hierarchical development of different models in each of the primary simulation components. Each hierarchy, such as the PorousMedium class hierarchy shown above, represents a set of different models that

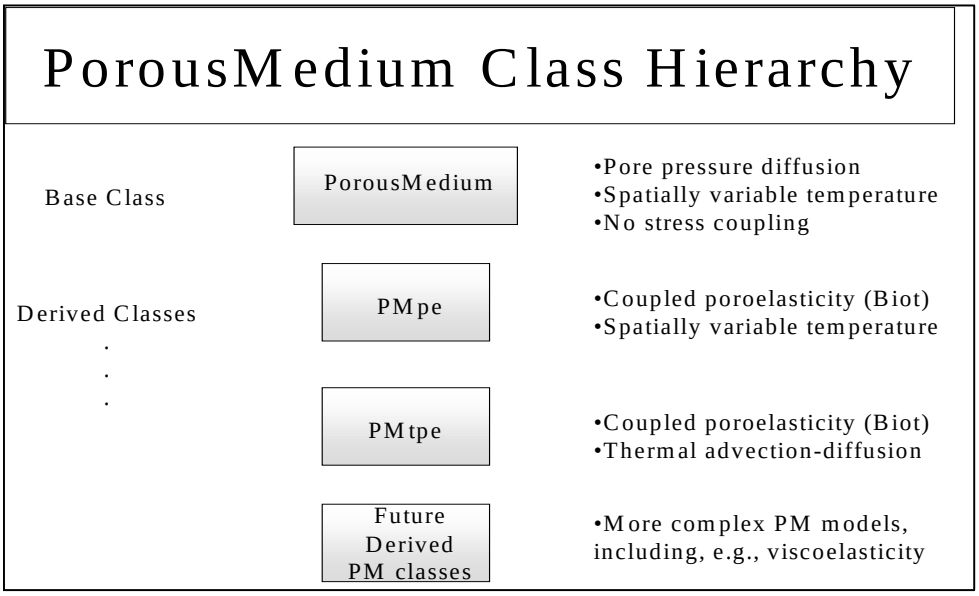

Figure 4.1: Diagram of the PorousMedium class hierarchy.

may be specified very easily by an input parameter. For example, one could choose to build a simulator which combines a PorousMedium component and a FaultSystem component. One could choose a coupled Biot model for the porous medium component, and test various fault models when coupled to or embedded in porous medium. This enables a researcher who is, for example, primarily interested in fault mechanics to utilize rather complicated software components built by others whose expertise is in poromechanics. This organization into software components allows the complexity of large software systems to be hidden and managed.

For the remaining chapters in this thesis, calculations are carried out with a prototype system which is diagramed in figure 4.4. Calculations of aftershock statistics, pore pressure and displacement profiles along lines, and other derived quantities are handled by the SimQuake component, which also coordinates the other components. The PorousMedium component has two sub-comonents. One computes only pore pressure using simple diffusion theory. The other implements fully coupled Biot

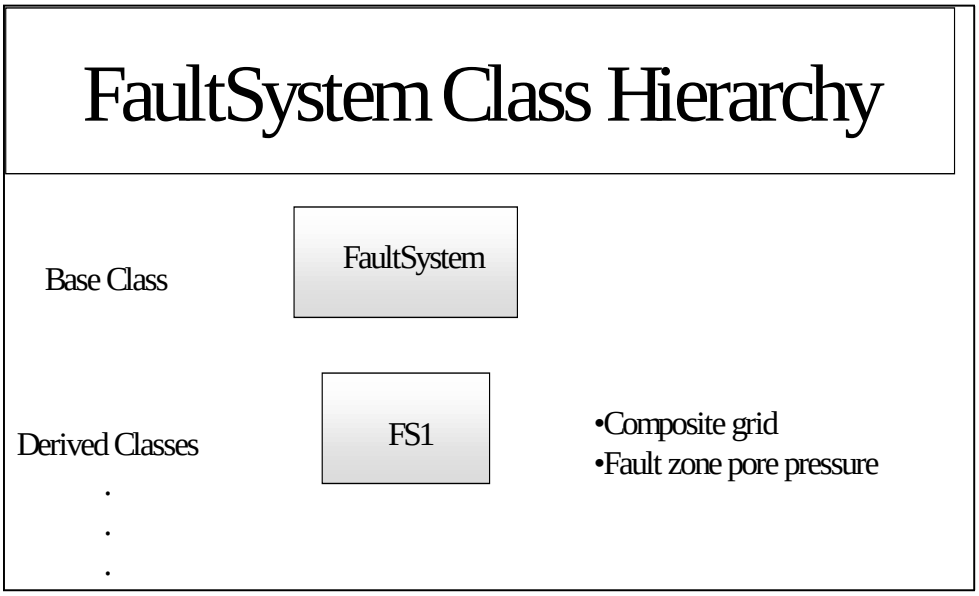

Figure 4.2: Diagram of FaultSystem class.

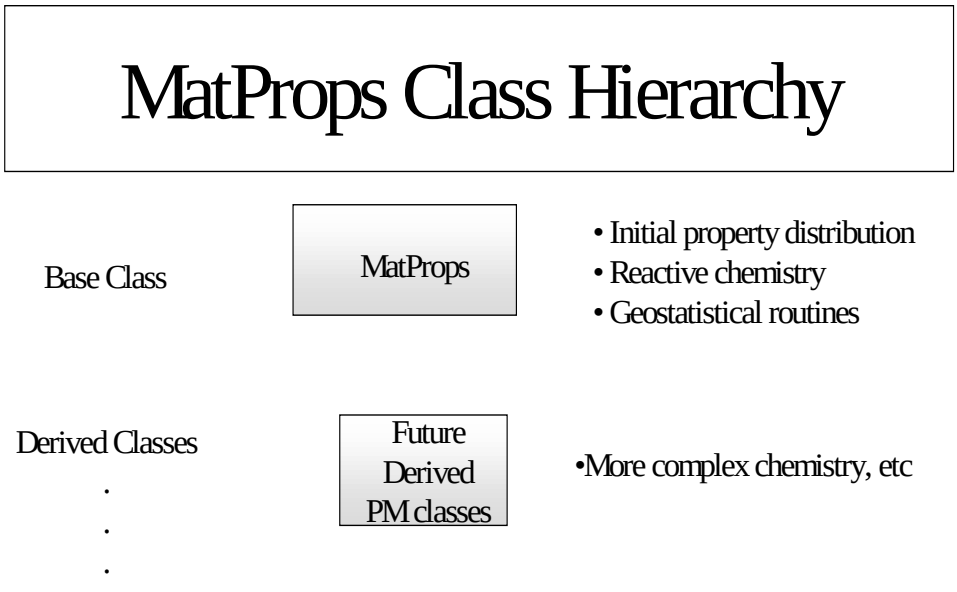

Figure 4.3: Material properties and reactive chemistry class.

poroelasticity. Either can be selected; if other models of a porous medium are written in the same framework, they can also be selected at run time and will be fully compatible with the other components.

Displacements are computed by the Elasticity component in the decoupled method described above. Pore pressure (and temperature, if desired) from PorousMedium are inputs to Elasticity. The FaultSystem shown here has only one component associated with it. It is the dislocation model of Larsen (1991). It is used only to compute coseismic stresses, from which initial pore pressure is calculated, on predetermined faults. Material properties are constants. Permeability is implemented as a spatially variable quantity which may be a full anisotropic tensor.

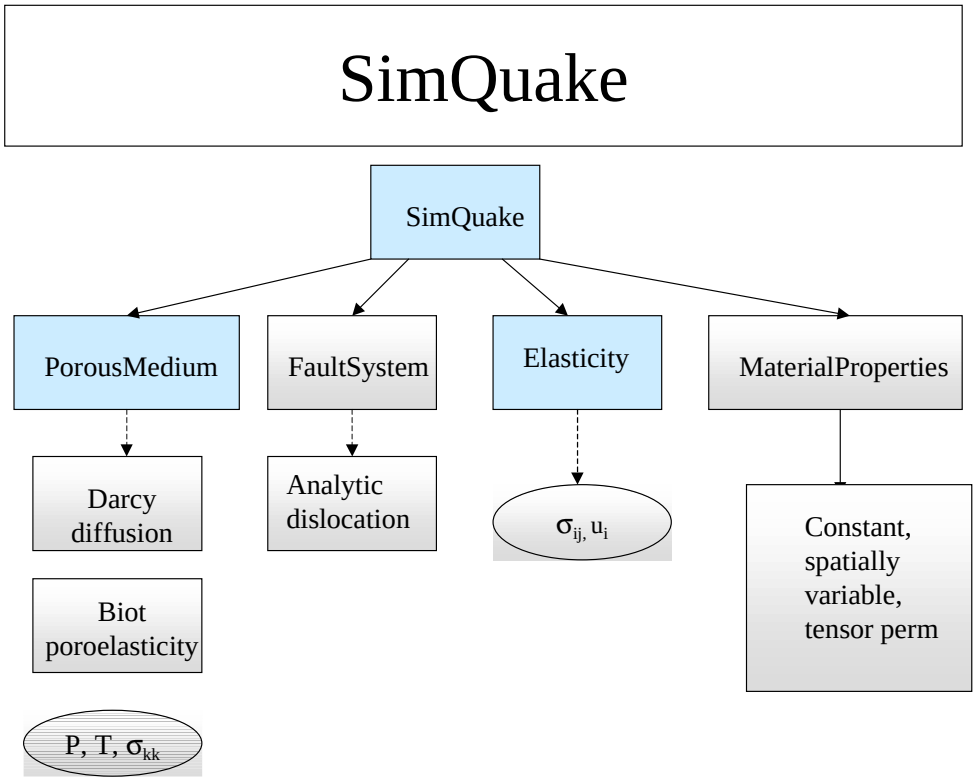

Figure 4.4: Diagram of the SimQuake simulator that was used for calculations in the rest of this thesis.

4.7 Summary

The equations for thermoporoelasticity have been derived and set forth in a manner suitable for numerical discretization. Spatially and temporally varying coefficients have been retained in keeping with the fundamental purpose of this paper to present a methodology for exploring complex dynamics in the brittle lithosphere by numerical experimentation. A numerical strategy for solving the equations was outlined and general classes were sketched which point the way to a maintainable system of software components for numerical experimentation.

4.8 Proposal for a General Earthquake Model

The organization of coupled systems of variables/equations into class hierarchies that was described above for thermoporoelasticity may be extended to more general systems in a direct manner. Each software component should resemble an analogous physical system in terms of state variables and dynamical behavior.

4.8.1 Goals

The goal of a general earthquake model is to provide a framework for numerically experimenting with various physical models for crustal dynamics (including the upper mantle) in order to determine likely physical mechanisms. This requires more than just a single complicated computer code. Rather, a set of software components which can be coupled together in various ways and from which new components can be derived. Such a set of components can be used by researchers and expanded in a way that makes new theoretical ideas - implemented in software - available to a wide community.

4.8.2 Earthquake Physics

From a general viewpoint, software components must derive from general templates that evolve certain state variables, such as stress, strain, displacements, pore pressure,

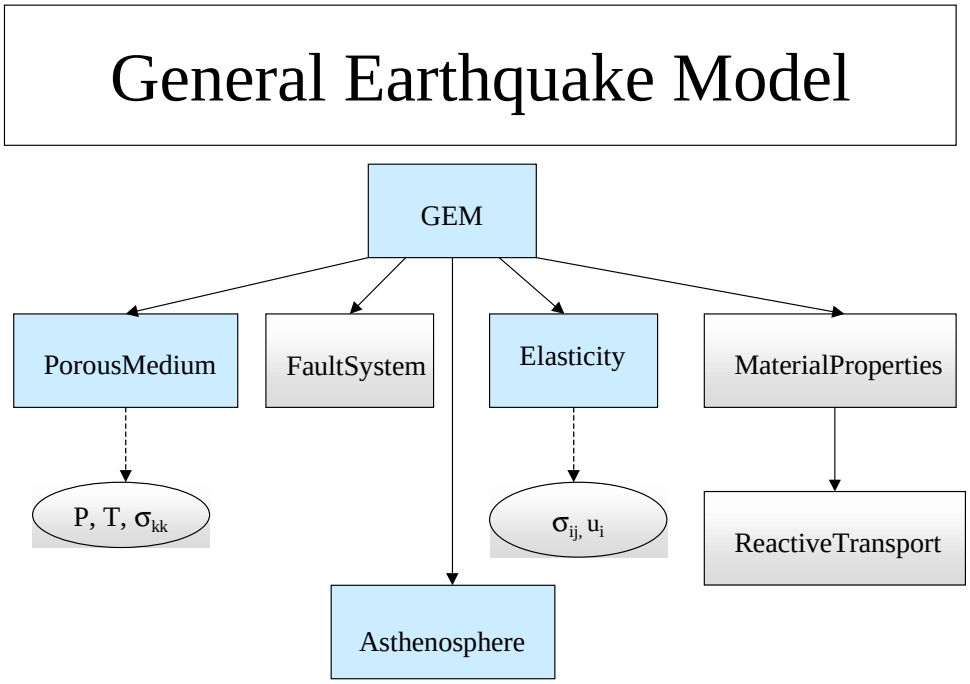

Figure 4.5: Class structure for a proposed GEM model.

and temperature, according to prescribed physical laws. These are the variables listed in table 4.1. The basic equations listed in the table are commonly used to model the earth and have been developed in this paper. Coupling together various parts of the thermoporoelastic model with different material properties and initial conditions is a very complex system whose dynamics will require many CPU hours (or years!) to explore. Some initial experiments are given in proceeding chapters to illustrate how such a system can be used.

The hierarchy of physical models organized into software components also provides a scientific computing system that will enable new physical models and equations to be implemented. Like electronic components, new models implemented as software components can be used in conjunction with other, already tested, components in order to explore dynamical behavior of new theories in a larger, more complex context. This is the goal, the first steps of which are presented here.

4.8.3 Fault Mechanics

Models of crustal dynamics must eventually include models of fault dynamics. One proposal for including faults in a continuum model of the crust, based on composite grids, was given. However, the same component software idea should be implemented for fault models. For example, a simplest fault model component (which is used to model the coseismic stress produced by the Landers earthquake in a later chapter), uses an analytic half-space dislocation model to compute stresses from prescribed slip on a fault. Generalizing, one could incoporate pre-existing, prescribed faults that can be made to "slip" at set times in a simulation or when some local stress condition is met. At that time, a modification to the evolving stress field can be computed using the analytic equations, for example.

There are many fault models that might be considered. The goal of the general earthquake model outlined here is not to select the best one in some sense and implement only that as our current best earthquake model. The point to made is that a mechanism must be provided whereby any model of interest can be implemented within a complex continuum model and its consequences explored. This is

how competing models can be compared and progress made toward understanding which physical laws are operative in the earthquake cycle.

Bibliography

Biot, M. A., Generalized theory of 3-dimensional consolidation, *J. Appl. Phys.*, *12*, 155–164, 1941.

Biot, M. A., General solutions of the equations of elasticity and consolidation for a porous material, *J. Appl. Mech., Trans ASME*, *78*, 91–96, 1956.

Byerlee, J., Earthquakes, *Journal of Geophysical Research*, 1994.

Byerlee, J., Model for episodic flow of high-pressure water in fault zones before earthquakes, *Geology*, *21*, 303–306, 1996.

Charlez, P. A., *Rock Mechanics Volume 1: Theoretical Fundamentals*, Editions Technip, Paris, 1991.

Charlez, P. A., *Rock Mechanics Volume 2: Petroleum Applications*, Editions Technip, Paris, 1997.

Cryer, C. W., A comparison of the three-dimensional consolidation theories of biot and terzaghi, *Quart. Journal of Mech. and Applied Math.*, *16*, 401–412, 1963.

Daehlen, M., and E. A. Tveito, *Mathematical Models and Software Tools in Industrial Mathematics*, Birkhauser, 1997.

Dullien, F. A. L., *Porous Media: Fluid Transport and Pore Structure*, 2nd ed., Academic Press, New York, 1992.

Ge, S., and G. Garvin, A theoretical model for thrust-induced deep groundwater expulsion with application to the canadian rocky mountains, *Journal of Geophysical Research*, *99*, 13851–13868, 1994.

Helmig, R., *Multiphase Flow and Transport Processes in the Subsurface*, Springer-Verlag, New York, 1997.

Hickman, S., R. Sibson, and R. Bruhn, eds., *The Mechanical Involvement of Fluids in Faulting*, Menlo Park, CA, U. S. Geological Survey, 1994.

Ingebritsen, S. E., and W. E. Sanford, *Groundwater in Geologic Processes*, Cambridge University Press, New York, 1998.

J.E. Dennis, J., and R. B. Schnabel, *Numerical Methods for Unconstrained Optimization and Nonlinear Equations*, Prentice Hall, New York, 1983.

Larsen, S. C., Geodetic measurements of deformation in southern california, Ph.D. thesis, California Institute of Technology, 1991.

McTigue, D. F., Thermoelastic response of fluid-saturated porous rock, *Journal of Geophysical Research*, *91*, 9533–9543, 1986.

Person, M., J. P. Raffensperger, S. Ge, and G. Garven, Basin-scale hydrogeologic modeling, *Reviews of Geophysics*, *34*(1), 61–87, 1996.

Rice, J. R., and M. P. Cleary, Some basic stress diffusion solutions for fluid-saturated elastic porous media with compressible constituents, *Rev. Geophys. Space Phys.*, *14*(2), 227–241, 1976.

Scholz, C. H., *The Mechanics of Earthquakes and Faulting*, Cambridge University Press, New York, 1990.

Segall, P., Stress and subsidence resulting from subsurface fluid withdrawal in the epicentral region of the 1983 coalinga earthquake, *Journal of Geophysical Research*, *90*, 6801–6816, 1985.

Terzaghi, K., *Theoretical Soil Mechanics*, John Wiley and Sons, New York, 1943.

Tompson, A. F. B., R. D. Falgout, S. G. Smith, W. J. Bosl, and S. F. Ashby, Analysis of subsurface contaminant migration and remediation using high performance computing, *Advances in Water Resources*, *22*, 203–221, 1998.

Walder, J., and A. Nur, Porosity reduction and crustal pore pressure development, *J. Geo. Res.*, *89*(B13), 11539–11548, 1984.

Yilmaz, O., R. Nolen-Hoeksema, and A. Nur, Pore pressure profiles in fractured and compliant rocks, *Geophysical Prospecting*, pp. 693–714, 1994.

Zeldovich, Y. B., and Y. P. Raizer, *Physics of Shock Waves and High-Temperature Hydrodynamic Phenomena*, Academic Press, New york, 1966, Nonlinear thermal waves discussed in Volume 2, pp652-676.

Zoback, M. D., and J. H. Healy, In situ stress measurements to 3.5 km depth in the cajon pass scientific research borehole: Implications for the mechanics of crustal faulting, *Journal of Geophysical Research*, *97*, 5039–5057, 1992.

Chapter 5

The Mandel-Cryer Effect

5.1 Introduction

Some numerical simulations of fluid flow in poroelastic media are presented here in order to illustrate how the combined effects of heterogeneous properties and coupled processes sometimes yield quite unexpected results. The poroelastic sphere problem outlined by Cryer was discussed earlier in this paper. Sometimes referred to as the Mandel-Cryer effect, this problem will be serve as the fundamental example for this chapter. A detailed look at Cryer's result will show that the phenomenon is even more surprising than has been reported in the literature thus far (Mandel, 1953; Cryer, 1963; Wang, 1998). The dynamical principles exhibited by these simple examples demonstrate that in some circumstances the coupled effects of pore fluid pressure, elastic deformation, and heterogeneous properties must be considered if the dynamical behavior of the crust is to be properly modeled. Thermal effects, chemical evolution of rock properties, and various nonlinearities due to the presence of fractures will not be considered here, though the addition of these processes will only serve to underscore the fundamental point of this paper: the known chemistry and physics of crustal processes, when considered as coupled processes, must be explored as a total system by extensive computer simulation in order be fully understood. Simulations of realistic crustal dynamics problems can result in remarkably complex systems behavior that

may exhibit characteristics of the complex dynamics observed in the earth.

5.2 Review of poroelastic equations

The isothermal poroelastic equations, which were presented in chapter 4, are:

$$\beta\left(\frac{\partial p}{\partial t}+B\frac{\partial \sigma}{\partial t}\right)=\frac{\partial}{\partial x_i}\left(k_{ij}\left(x\right)\frac{\partial p}{\partial x_j}\right) \tag{5.1}$$

$$\frac{\partial^2}{\partial x_j^2}\left[ap+\sigma\right]=0 \tag{5.2}$$

where

$$a=\frac{2\left(\nu_u-\nu\right)}{B\left(1-\nu\right)\left(1+\nu_u\right)} \tag{5.3}$$

and

$$\beta=\mu\phi\left(C_f+C_r\right) \tag{5.4}$$

Here, p is the pore pressure, $\sigma=\sigma_{kk}/3$ is the mean stress, B is Skempton's coefficient, ν_u and ν are the undrained and drained Poisson's ratios, μ is the fluid viscosity, ϕ is the porosity, C_f and C_r are the fluid and rock compressibilities, respectively. A further simplification that is generally made in the literature is to assume that the permeability tensor is a spatially homogeneous scalar quantity. This simplification is necessary if the equations are to be combined into a single diffusion equation in $m=(P+B\sigma_{kk}/3)$ as Rice and Cleary (1976) and others have done. As the following analysis will show, the heterogeneous nature of permeability can have significant consequences for poroelastic problems.

Two cases for consolidation and pore pressure diffusion in a porous medium will be considered. In the first, which was explored by Terzaghi (1943) in the context of soil mechanics, assumes that the pore fluid diffuses in such a way that the pore pressure and the mean stress are constant multiples of each other at all times. The mean

stress can thus be eliminated from the governing equations and the problem solved as a simple diffusion problem. This is equivalent to setting $B = \alpha = 0$ in equations 7.6 and 5.2. In Biot's theory, the mean stress is coupled to the pore pressure in a more complicated manner and two differential equations must be solved simultaneously to derive the correct dynamical behavior.

5.3 The Mandel-Cryer effect

Cryer (1963) compared the consolidation models of Terzaghi and Biot by considering a poroelastic sphere saturated with fluid at an initial pressure p_0. The boundary of the sphere at time t_{o^+} was set to zero pressure, with zero strain in the interior of the sphere and normal stresses on the boundary equal to the interior pore pressure. Two analytic solutions were presented to describe the pore pressure at the center of the sphere at $t > 0$. Pore pressure at the center of the porous elastic sphere in the Terzaghi model remained close to p_0 for some time after the initial instant, then slowly decreased as the influence of the boundaries diffused inward. In the Biot model the pore pressure at the center instantly began to *increase* above the initial pressure, then eventually declined as the boundary effects diffused inward. This surprising behavior is due to the initial collapse of the pore volume near the boundary of the sphere as pore fluid exits. In Biot's poroelastic theory, stress is transferred inward as the fluid near the boundaries escapes. Fluid in the center of the sphere is trapped and cannot escape immediately, so the pore pressure increases due to the compressive stress on the interior of the medium.

In this paper, we simulate Terzaghi and Biot consolidation numerically on a rectangular grid with 10 cells per side. The pressure on the interior of the cube is initially 1 Pa. The side boundaries are held at 0 Pa. The top and bottom of the cell were assigned no-flow boundary conditions. Flow is thus through the sides of the cube only.

The equations solved in this simulation are the coupled fluid flow equation for pore pressure and mean stress and the Beltrami-Mitchell (compatibility) equation, equations 7.6 and 5.2. A Galerkin finite element discretization was used to solve these

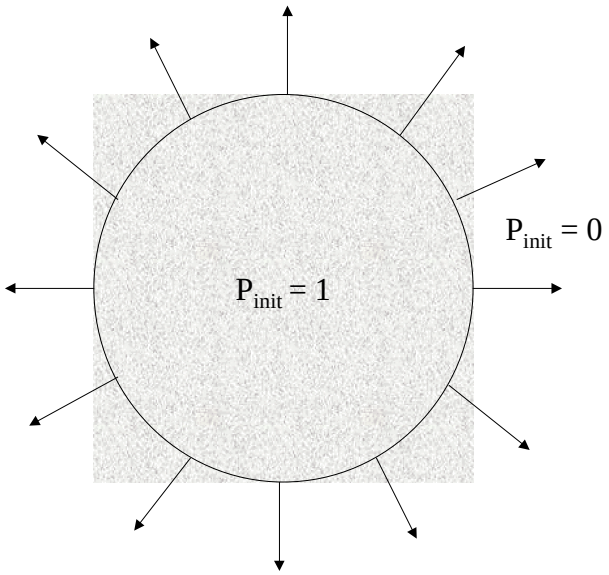

Figure 5.1: Cryer's sphere problem, used to compare the consolidation theories of Terzaghi and Biot.

equations. Two parameters were varied in the simulations, the diffusivity $D = \frac{k_{ij}}{\beta}$ and the elastic parameter α. When the elastic parameters α and B are set to zero, fluid flow follows the simple diffusive flow model as in equation 7.6. As expected, the pore pressure in the center of the cube remains at the initial value p_0 for a period of time, then decays roughly exponentially. The rate of decay depends on the diffusivity. When α is nonzero, the pore pressure at the center rises above the initial pressure at first, then falls. Figure 5.2 shows the effect of varying the parameter α on pore pressure at the center of the cube. The $\alpha = 0$ curve is the Terzaghi result.

The maximum height of the pore pressure peak above the initial value is controlled by the elastic parameters of the material, which is controlled by the difference between the drained and undrained Poisson ratios, which is expressed in the parameter a (cf. equation 5.3).

When the diffusivity is high, fluid can escape readily from the center of the cube and the pressure rise is short and small. When the diffusivity is low, pore pressure rise in the center of the cube is long and slow. It becomes higher when the diffusivity

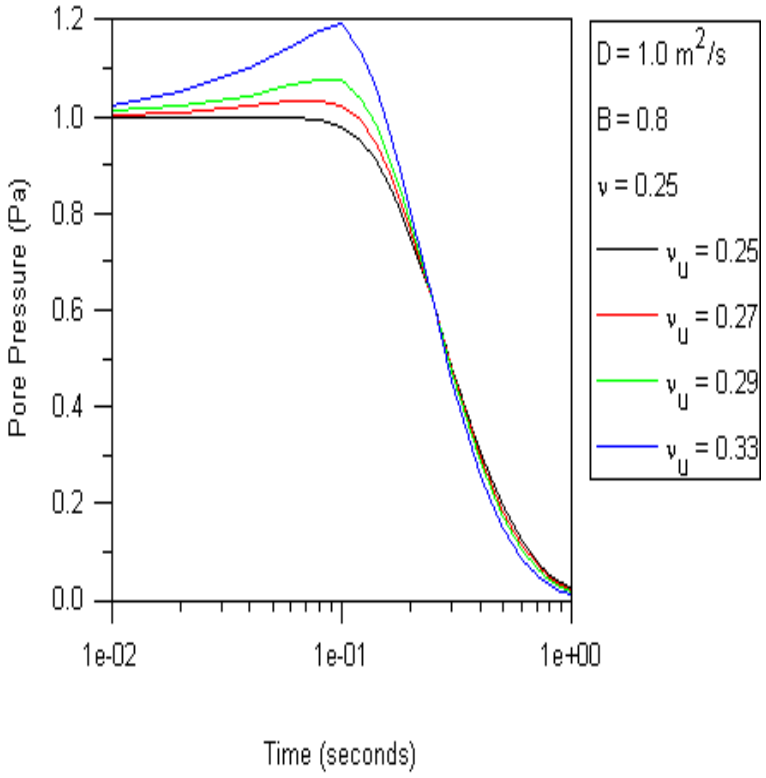

Figure 5.2: Pore pressure at the center of a square showing the Mandel-Cryer effect for several values of the parameter a, which is a function of drained and undrained Poisson ratios. Diffusivity $D = 2$, domain size $= 2m \times 2m$, $B = 1$, $a = 0.1$, $\Delta x = \Delta y = 0.2m$.

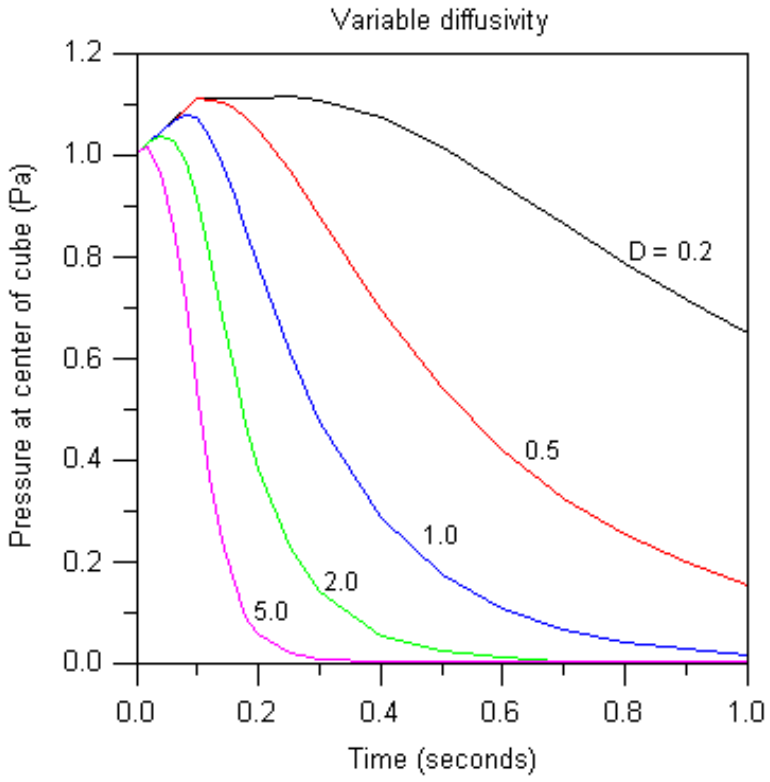

Figure 5.3: Pore pressure at the center of a square showing the Mandel-Cryer effect for several diffusivity values. Domain size is $2m \times 2m$; $B = 1$, $a = 0.1$, $\Delta x = \Delta y = 0.2m$.

is small than when it is large. Figure 5.3 shows the pore pressure development over time in the center of the cube when the elastic parameter $a = 0.05$ and the diffusivity is the same as in the previous case. TIme snapshots of pore pressure values for the whole cube are shown in figure 5.4.

Some examples of the pressure field that resulted from a simulation with $a = 0.05$ and $k = B = \beta = 1.0$ are shown in figure.

The size of the region will greatly affect the duration of elevated pore pressure. In figure 5.5, we see that pore pressure rises to abnormally high levels near the interior of the domain and remains at high levels for a relatively long time. The reason for this is clear: fluid trapped in the center of the region doesn't feel the effects of the boundary for a long time. Low pressure at the boundaries takes a long time to diffuse

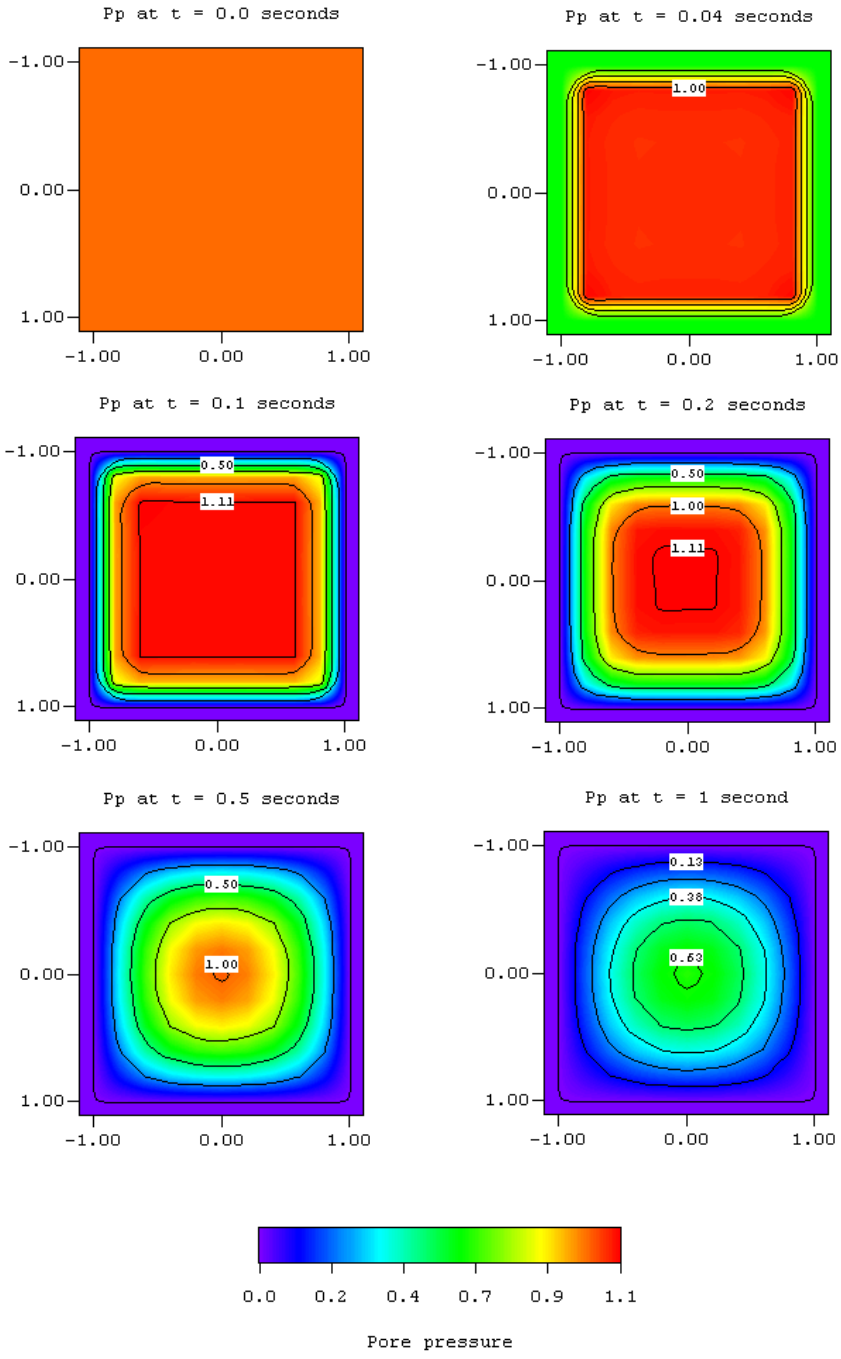

Figure 5.4: Snapshots of pore pressure evolution showing the Mandel-Cryer effect. Domain size is $2m \times 2m$; $B = 1$, $a = 0.1$, $\Delta x = \Delta y = 0.2m$, $D = 2$. Note that pore pressure in the interior of the cube exceeds the initial value.

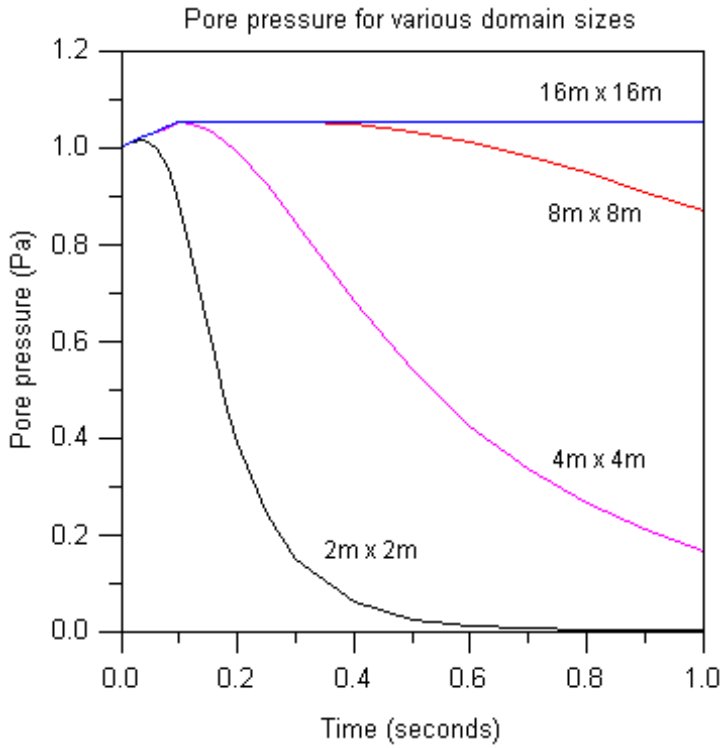

Figure 5.5: Pore pressure at the center of a square showing the Mandel-Cryer effect for several domain sizes. Diffusivity $D = 2$, $B = 1$, $a = 0.1$, $\Delta x = \Delta y = 0.2m$.

over the distance to the center.

The abnormally high pore pressure that is generated by poroelastic effects can be attributed to the trapping of fluid in a region while mean stress is transferred from surrounding regions. To demonstrate that the region of abnormally high pressure need not be centered in a symmetric domain, such as a sphere or cube, we assigned low permeability values to a circular region offset from the center of a square. This trapped the fluid in the low permeability region. Stress transfer due to the Mandel-Cryer effect caused pore pressure to rise above the initial value before starting to dissipate. In contrast, for the simple fluid diffusion case, pore pressure never rises above the initial value. Results are shown in figure 5.6.

Next, permeability values between 0 and 1 were randomly assigned to grid points

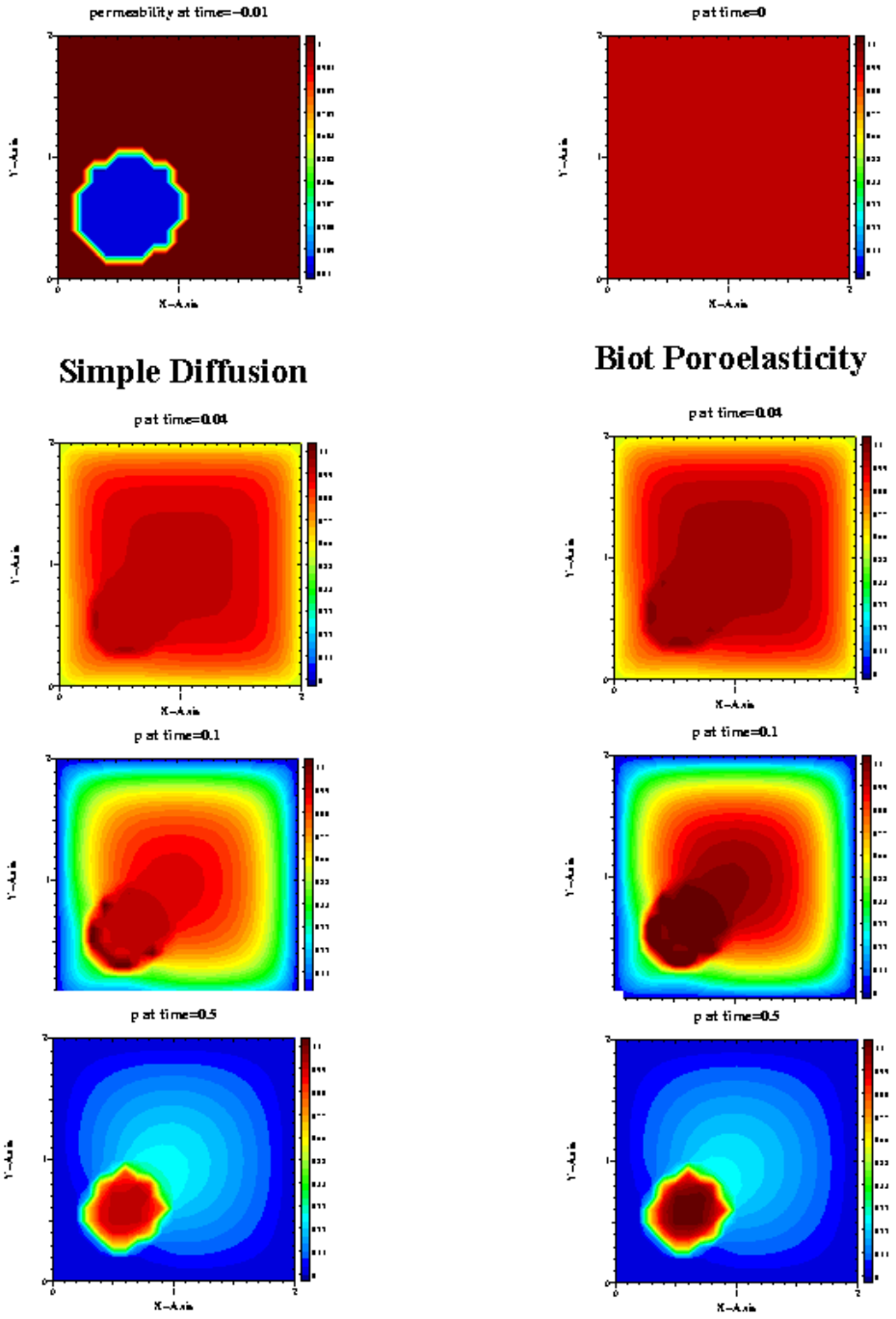

Figure 5.6: Pore pressure evolution with an isolated low-permeability pocket. Background permeability=1, low-perm value=0.01; total diffusivity=permeability.

in a two-dimensional 20×20 grid. For this simulation, no-flow boundary conditions were assigned to the top and bottom of the domain. The permeability distribution and pore pressure snapshots are shown in figure 5.7. The region of high pore pressure is in the center strip of the square, but the effects of the random permeability distribution are evident.

5.4 Fluid Flow in Fault Zones

The San Andreas fault is weak (Rice, 1992; Wang, et al., 1995; Zoback, 1987). By this it is implied that the fault is in a state of near failure. Several explanations may be given for the weakness of the San Andreas (see Scholz, 1990 and Evans, 1992, for example). The existence of high pore pressure within the fault zone is a commonly-mentioned explanation. A quantitative measure of the strength of a fault is the Coulomb failure criterion. The Coulomb failure criterion, which was adopted from soil mechanics, where it was called the Drucker-Prager criterion. (Drucker, 1952), states that when the shear stress τ exceeds the slip criterion, fault slip will occur. The Coulomb failure criterion may be written quantitatively as

$$\tau \geq \tau_o + \mu_f \left(\sigma_n - p\right)$$

where τ is the shear stress on the fault, τ_0 is the cohesion, μ_f is the coefficient of internal friction or simply the frictional strength, σ_n is the normal stress on the fault, and p is the pore pressure in the fault. Increasing pore pressure effectively reduces the normal stress and thus reduces the shear stress needed to exceed the slip criterion. The quantity $(\sigma_n - p)$, often referred to as the *effective stress.* More accurately, the effective stress is $(\sigma_n - \alpha p)$, but the Biot parameter $\alpha \approx 1$ is frequently assumed. A discussion of the role and meaning of the Biot parameter can be found in Nur (1971). An important point to made here is that when a fault is weak or critically stressed, only a small perturbation to the effective stress is needed to exceed the Coulomb slip criterion.

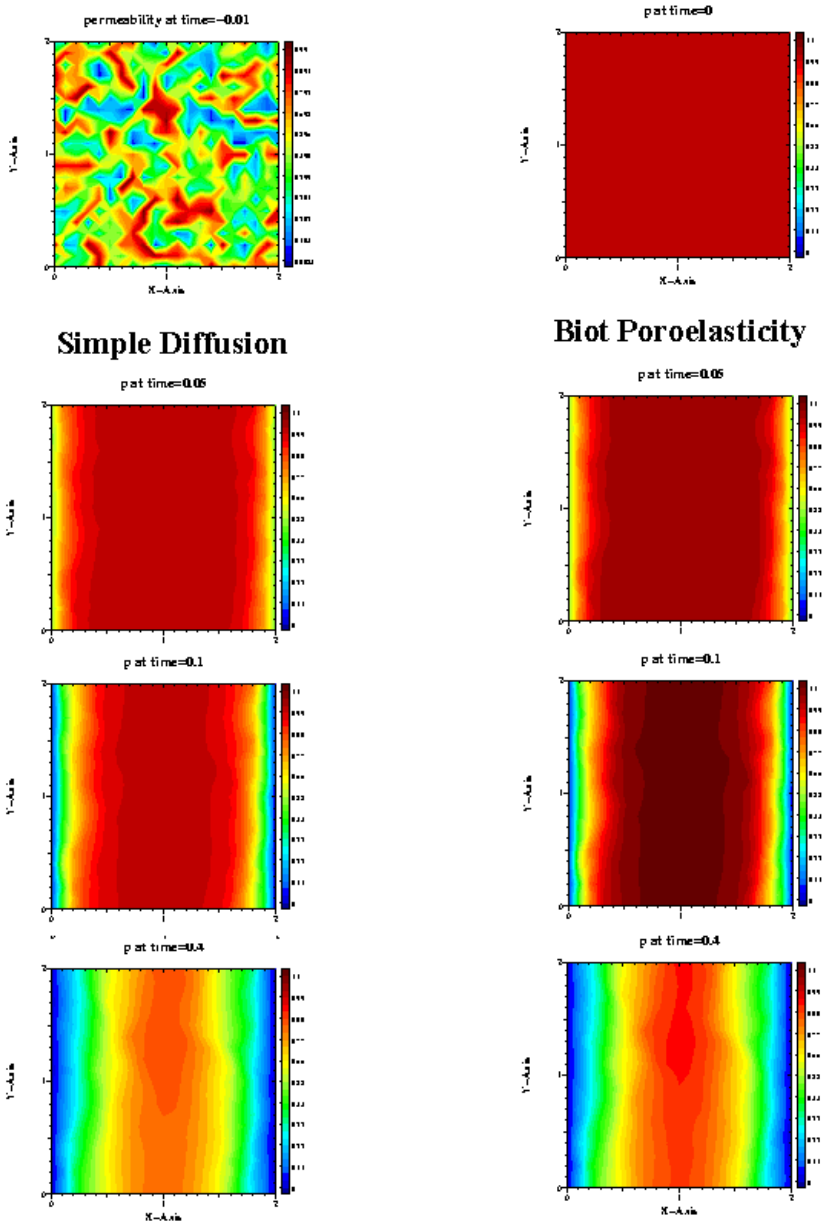

Figure 5.7: Random values of the diffusivity parameter D between 0 and 1.0 were assigned to cells in this simulation. The permeability distribution is shown in the top left image. The last three rows of images compare Terzaghi and Biot diffusion.

Under certain conditions, poroelastic effects can cause pore pressures within hydraulically confined regions, such as some faults, to attain pressures that are abnormally high. Furthermore, the results of the preceeding Mandel-Cryer simulations suggest that pore pressure within the fault zone can increase markedly beyond an initial value even when no apparent source of fluid or stress change is present. This idea is tested in a simple model of a fault zone here.

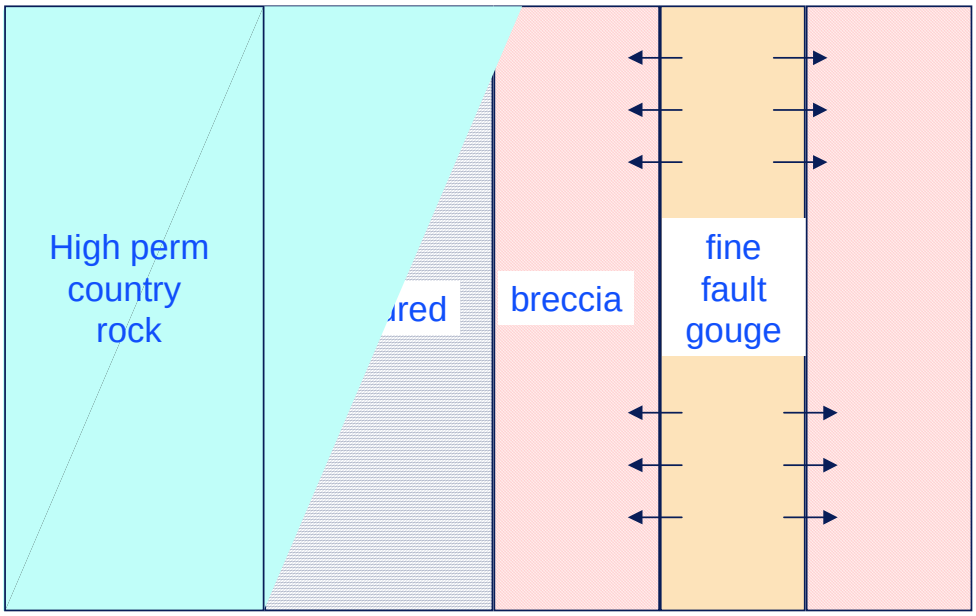

Figure 5.8: Schematic picture of Byerlee's fault model.

One model for a typical fault zone suggests that the permeability in the fault gouge is low, while the permeability in the surrounding damage zone is relatively high due to the presence of breccia and extensive microfractures (Bruhn, 1994). Byerlee's model (Byerlee, 1994) for the involvement of fluids in the earthquake cycle hypothesizes that permeability varies spatially in the region of a fault and also that it evolves in time. A schematic diagram of a fault such as this is shown in figure 5.8.

A simple experiment with a two-permeability simulation as shown in the first frame of figure 5.9 was performed. With a constant normal stress applied and zero pore pressure on the sides, and zero-flux boundaries on the top and bottom, the fluid

flows primarily in the horizontal direction. Figure 5.10 shows the pore pressure at various times along a line normal to the center of the fault zone and at the center of the domain throughout the duration of the simulation.

The essential point of this simulation result is that pore pressure can attain values higher than expected if the permeability near faults is low. Low permeability normal to a fault is a reasonable assumption in some cases. As will be discussed in chapter 7, pore fluids play an important role in causing aftershocks. Simulations that attempt to reproduce the Coulomb stress function in the region surrounding a major earthquake should not make simple assumptions about the pore pressure. Rising pore pressure in the fault vicinity may be an indicator of aftershock probability. In general, pore pressure will rise following an earthquake in regions of dilational mean stress (negative pore pressure deviation). However, the Mandel-Cryer effect may also cause transient pore pressure increase in regions of initial compressive mean stress. That is, pore pressure may continue to rise where it would not be expected to rise on the basis of simple (Terzaghi) diffusion theory. This has important implications for earthquake physics and for efforts to construct numerical models of stress evolution in the crust.

5.5 Conclusions

This study demonstrates that the Mandel-Cryer effect can be simulated numerically and that it's occurrence is not restricted to any particular geometry. Previously published discussions of the effect are restricted to spherical and cylindrical geometries because of the need to find analytical solutions to the governing system of equations. Computer simulation removes the domain restriction, and allows experimentation with heterogeneous property distributions. The primary result of this paper has been to demonstrate the importance of fluids in crustal rheology. The fascinating Mandel-Cryer effect may have important implications for critically-stressed faults that are saturated with fluids. In particular, computer models of crustal dynamics and fault mechanics should include the effects of pore fluids.

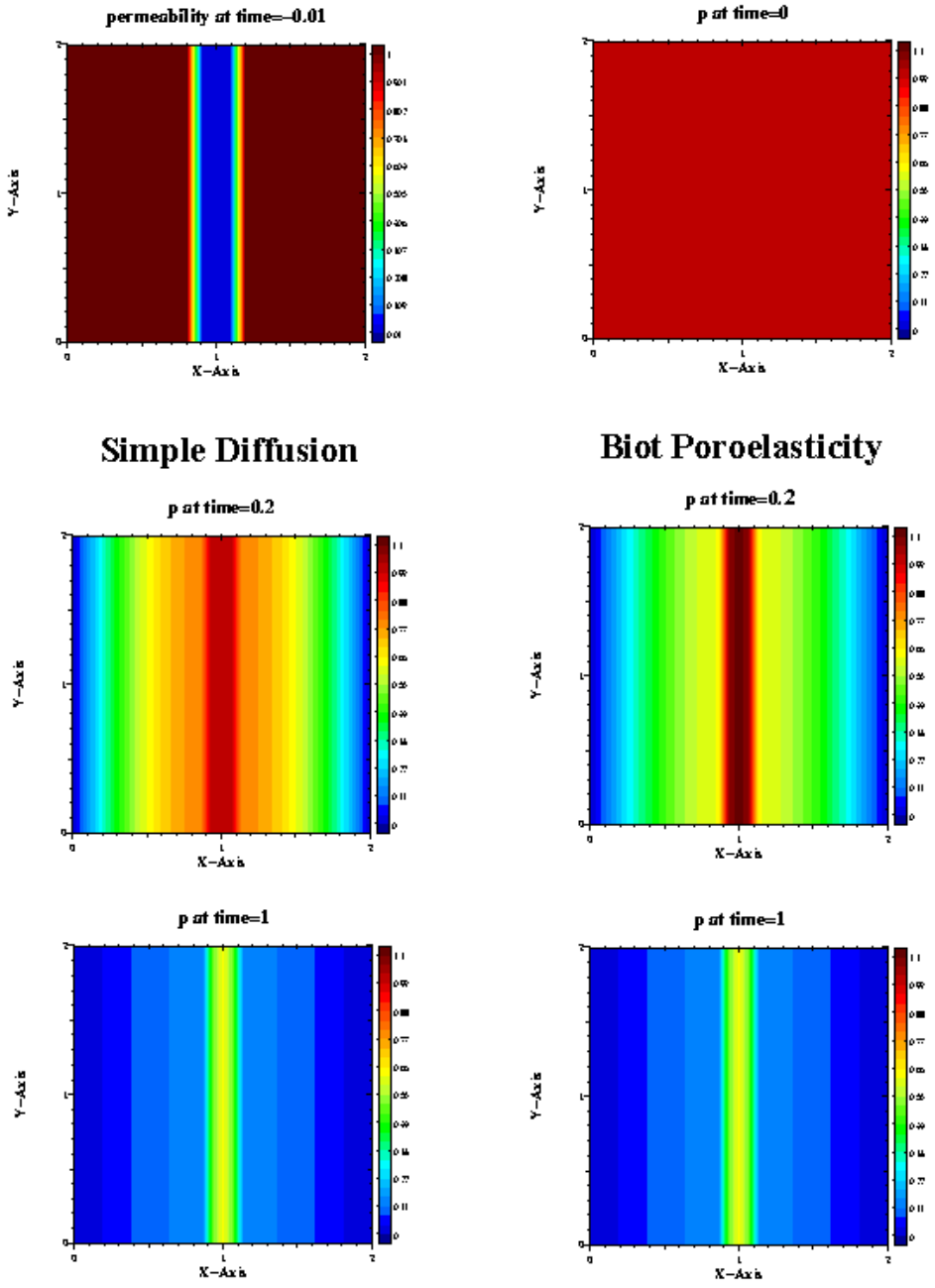

Figure 5.9: Illustration of a simple two-permeability fault zone model and the resulting fluid pressures when fluid is allowed to diffuse out the sides. The permeability in the fault zone is equal to 0.01 m^2 and in the surrounding region 1.0 m^2. The diffusivity is equal to the permeability in magnitude. For the poroelastic simulation, $a = 0.1$. The normal stress on the sides $x = 0, 2$ is constant and equal to 1 Pa throughout the simulation. Boundary pore pressure is 0 on those sides. The top and bottom boundaries are zero-flux.

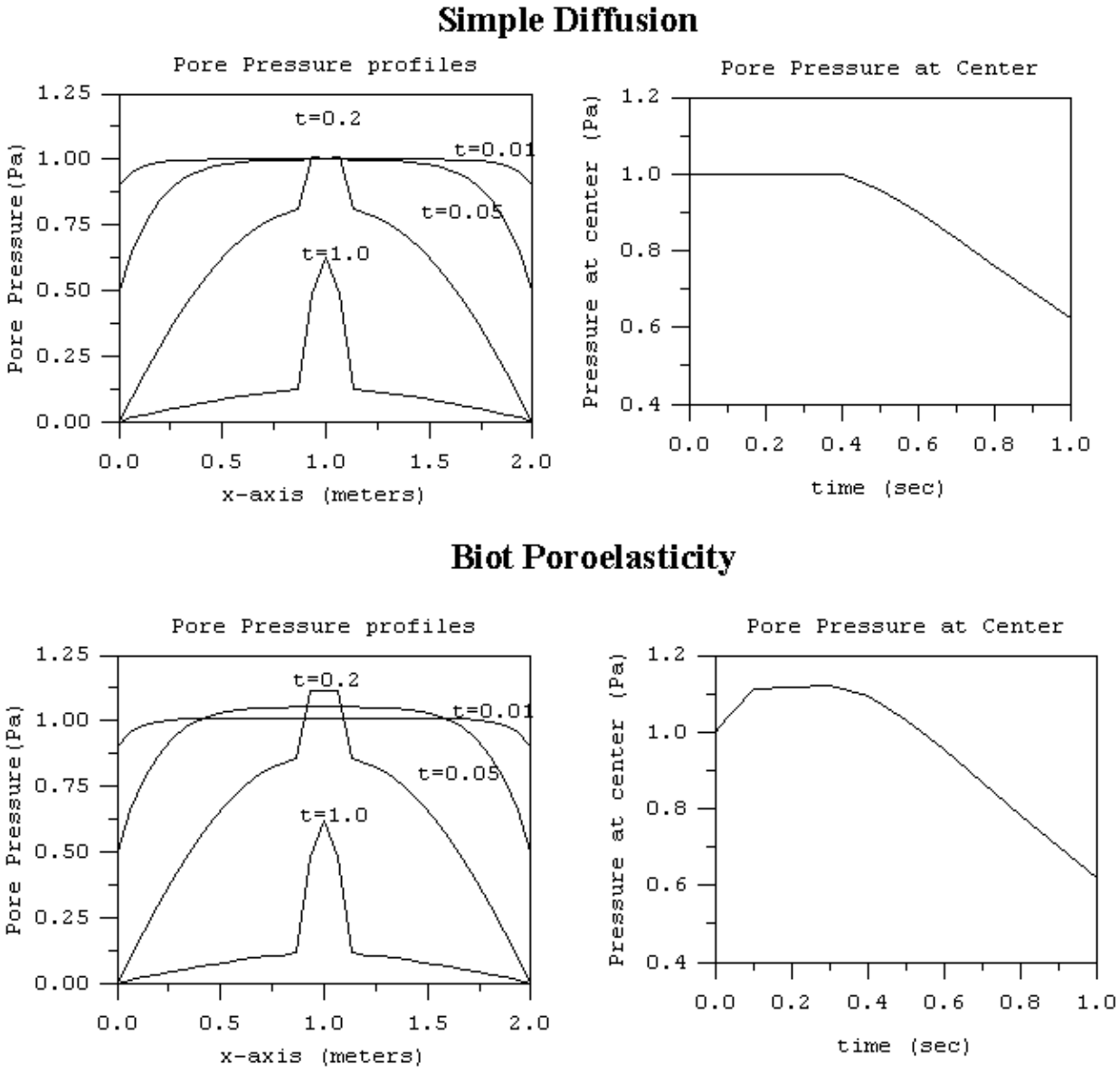

Figure 5.10: Plots of pore pressure (left-side) along a line through the fault zone at several times and (right-side) at the center of the domain for the whole time of the simulation.

Bibliography

Bruhn, R. L., W. T. Parry, W. A. Yonkee, and T. Tompson, Fracturing and hydrothermal alteration in normal fault zones, *PAGEOPH*, *142*, 609–644, 1994.

Byerlee, J., Earthquakes, *Journal of Geophysical Research*, 1994.

Cryer, C. W., A comparison of the three-dimensional consolidation theories of biot and terzaghi, *Quart. Journal of Mech. and Applied Math.*, *16*, 401–412, 1963.

Drucker, D. C., and W. Prager, Soil mechanics and mechanical analysis or limit design, *Applied Mathematics Quarterly*, *10*, 157–165, 1952.

Mandel, J., Consolidation des sols (etude mathematique), *Geotechnique*, *3*, 287–299, 1953.

Nur, A., and J. D. Byerlee, An exact effective stress law for elastic deformation of rock with fluids, *Journal of Geophysical Research*, *76*(26), 6414–6419, 1971.

Rice, J. R., Fault stress states, pore pressure distributions, and the weakness of the san andreas fault, in *Fault Mechanics and Transport Properties of Rocks*, edited by B. Evans and T.-F. Wong, pp. 475–503, Academic Press, New York, 1992.

Wang, C.-Y., Y. Cai, and D. L. Jones, Predicting the areas of crustal faulting in the san francisco bay region, *Geology*, *23*(9), 771–774, 1995.

Wang, H. F., Poroelasticity, unpublished manuscript.

Zoback, M. D., and T. Others, New evidence on the state of stress of the san andreas fault system, *Science*, *238*, 1105–1111, 1987.

Chapter 6

Landers Postseismic Deformation

6.1 Introduction

Pore fluids are believed to be involved in many dynamical processes related to seismic activity. These include the faulting process itself as well as postseismic phenomena caused by stress changes which result from seismic fault slip. Pore pressure buildup and release may play a significant role in the seismic cycle and particularly in the initiation of faulting. Hickman, et al. (1994) and Evans, et al. (1992) contain many papers which discuss the role of pore fluids in faulting. In this paper we are interested in the fundamental behavior of the crust as a poroelastic material (Bosl, 1998b).

There is growing interest in the seismology community in developing a general earthquake model to use for numerical experimentation, as evidenced by the General Earthquake Model (GEM) Workshop held in Santa Fe, New Mexico in November, 1997. A better understanding of the crust as a fluid-saturated poroelastic material is necessary in order to understand the physics of the entire earthquake cycle. Pore fluid pressure is often treated as a secondary effect when pre- and post-seismic stress changes are investigated. The goal of this paper is to demonstrate that pore fluids have a significant effect on the elastic properties of the crust and must be included in stress evolution models. To do this, pore pressure changes that would result from the 1992 Landers earthquake are computed. From this, fluid diffusion and the consequent elastic deformation changes are simulated. Vertical and horizontal displacements

are interpolated from the evolving postseismic poroelastic model and compared with measurements of the same quantities. The importance of pore fluids in postseismic crustal stress evolution can be evalutated from this comparison.

Elastic deformation due to sudden stress changes in the region surrounding faults causes changes in pore fluid pressure. The coseismic pore pressure distribution results in spatial pressure gradients which cause pore fluid movement. Seismically induced hydrologic effects that have been observed include increased streamflow, water table changes, and well level fluctuations (Roeloffs, 1996). Other observable coseismic and transient postseismic phenomena, such as vertical deformation (Peltzer, et al., 1994; Peltzer, et al., 1996; Zebker, 1994), horizontal displacement (Hudnut, et al., 1994; Wyatt, et al., 1994) changes in aftershock location and frequency (Nur, 1972), and changes in seismic wave velocities in the fault region (Li, 1997), are also likely to be or possibly related to pore fluid flow, but the direct physical link is less certain.

Viscoelastic relaxation of the lower crust and upper mantle, as well as afterslip, have been hypothesized as the physical cause for postseismic deformation. Deng (1998) used a viscoelastic model consisting of an elastic upper crust on top of a relatively weak lower crust and strong (high viscosity) upper mantle to simulate observed vertical and horizontal deformation following the Landers earthquake. In order to get significant vertical deformation, some vertical motion on the fault plane was required. Published slip models (Cohee and Beroza, 1994; Hudnut, et al., 1996; Wald and Heaton, 1994) determined only strike-slip faulting, so it appears that the strong mantle model is insufficient. Pollitz (1998) used a 3-layer viscoelastic model to simulate Landers postseismic deformation. This model consisted of an elastic crust, a weak lower crust (viscosity $= 4 \times 10^{18}$ Pa-s) and a weaker upper mantle (viscosity $= 2 \times 10^{18}$ Pa-s) and was able to match measured horizontal and vertical deformation reasonably well. As Pollitz points out (Pollitz, 1992), modeling of postseismic deformation is the only way to estimate asthenospheric viscosity. Thus, tuning a viscoelastic model assumes the correctness of the physical model. This paper shows that poroelastic effects are significant, particularly near the fault zone and should be included in models of the upper crust.

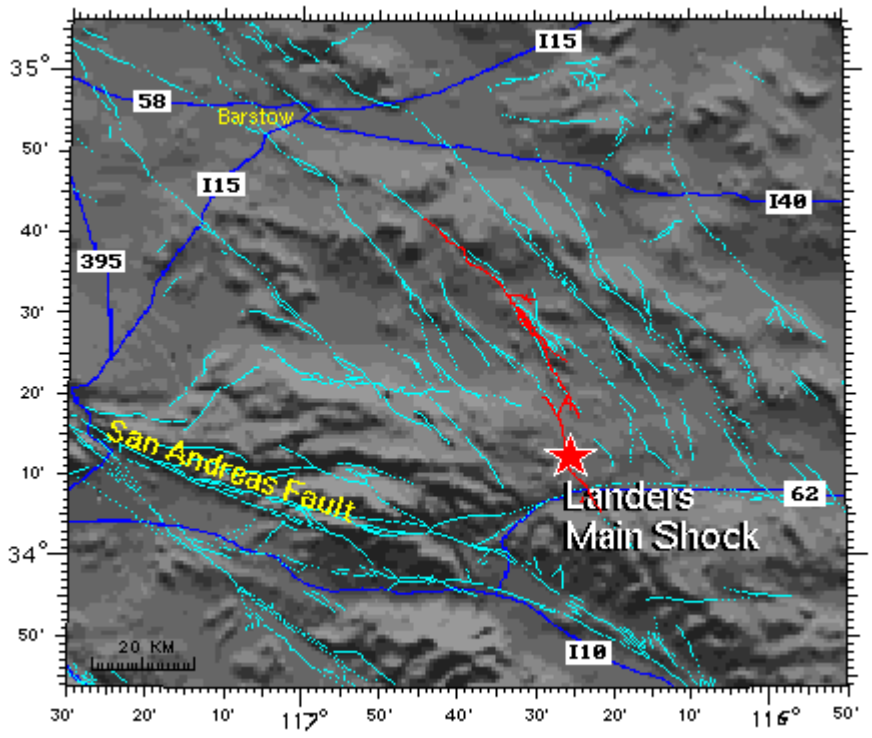

Figure 6.1: Map of the Mohave region showing the trace of the Landers fault rupture in red and the location of the epicenter.

6.2 The 1992 Landers Earthquake

The 1992 Landers earthquake was the largest earthquake in southern California in several decades. The faults that ruptured in this earthquake are located in the Mohave Block of southeastern California. The region is dominated by northwest-trending, right-lateral strike-slip faults. The densest cluster of faults in this region, known as the Eastern California Shear Zone (ECSZ) is estimated to accomodate between 9 and 23% of the relative motion between the Pacific and North American tectonic plates.

Rupture during the Landers earthquake occurred along several major faults that were thought to be disconnected. It thus provided an example of how stress changes caused by one fault can cause rupture along adjacent faults. A major aftershock

occured on the Big Bear fault approximately three hours later and 40 km to the west of the Landers rupture. The Big Bear earthquake had a different orientation and slip than the Landers earthquake; it was roughly conjugate to the Landers event. The Landers surface rupture produced right-lateral displacement over a total rupture length of approximately 85 km. Average slip of two to four meters was measured along the surface and the total magnitude was determined to be M_w=7.3.

Peltzer et al. (1996) used Synthetic Aperature Radar (SAR) interferometry to determine postseismic surface displacement in the region of the 1992 Landers earthquake. Line plots of vertical displacement along ~10 km segments spanning three different time intervals were constructed by combining SAR images from different time intervals over several years after the earthquake. Profiles were located along three lines which intersected the fault where the rupture changed direction or jumped to another fault branch. These segments formed two pull-apart structures and a compressive jog. Horizontal deformation measurements used in this study include a survey of a linear array of geodetic monuments by Savage and Svarc (1997) using the Global Positioning System (GPS) and relative displacement measurements by Shen, et al. (1994) between 16 GPS receivers located in the region around the Landers earthquake. These data sources are simulated with our computational model to test the theory that pore fluids are responsible for a significant part of the overall postseismic stress changes.

Although many postseismic hydrologic effects can be observed or measured, it is difficult to actually measure local pore pressure changes at the times and locations necessary to correlate pore pressure changes with the observed effects. Commenting on the pore fluid diffusion hypothesis for explaining observed postseismic vertical displacements, Peltzer et al. (1996) state that "A critical test of this model would require pore pressure data that can be obtained by water-level measurement in wells near rupture zones. *Such data are lacking in the region of Landers*" (emphasis added). Computational simulation may be employed in this situation to test the plausibility of the pore fluid diffusion hypothesis.

6.3 Computational Model

6.3.1 Induced Pore Pressure Due to Fault Slip

The initial (coseismic) pore pressure distribution is assumed to be caused entirely by the elastic volumetric strain that results from slip along the fault segments. This is a reasonable approximation away from the fault zone, where the stresses are not so large as to exceed the elastic limit of the crust. Near the fault, however, it may be expected that inelastic response must occur when the yield strength of the rock is exceeded. This is not included in our current model. The slip parameters determined by Hudnut, et al. (1994) were used to compute the coseismic stress field produced by the major segments of the Landers rupture, as well as along the nearby Big Bear and Iron Ridge faults. The latter faults slipped soon after the main rupture, so the stress changes induced by them are included in our stress calculations. The fault parameters used in our model are shown in Table 6.1.

The coseismic hydrostatic stress field was computed from these fault parameters using a program which implements an analytic half-space elastic dislocation model (Larsen, 1991). The mean stress field computed using this model is shown in Figure 6.2. The fault segments used to compute the stress field are superimposed on the image. Note in the model parameters that slip along any segment was assumed to be uniform over the entire length of the segment and from the surface to 10 km depth. This assumption is a simplification of the real situation; slip solutions which have depth variation have been determined by, for example, Wald and Heaton (1994) and Cohee and Beroza (1994) . These studies did not provide the detailed slip parameters in tabular form that were needed as input for the calculations in this study, as did Hudnut, et al. (1994). However, for this study we are first interested in qualitative behavior of the crust. That is, we wish to examine whether or not pore fluid effects can account for observed postseismic phenomena. Uncertainty in material parameters, such as permeability and elastic coefficients, is perhaps greater than any errors that might be introduced by assuming uniform slip on each segment.

The coseismic pore pressure field which was computed for this study is shown in figure 6.2. One can discern the general four-quadrant structure of a typical edge

Segment	**Latitude**	**Longitude**	**Length (km)**	**Azimuth**	**Slip** (cm)
Camp Rock A	34.6791	-116.7070	8.140	-43.28	0
Camp Rock B	34.6344	-116.6619	4.963	-62.04	200
Emerson A	34.5913	-116.6114	8.671	-36.92	270
Emerson B	34.5549	-116.5634	3.439	-57.40	640
Emerson C	34.5319	-116.5432	2.887	-50.11	580
Emerson D	34.5126	-116.5240	2.680	-51.47	255
Emerson E	34.4873	-116.4996	4.512	-51.28	480
Emerson F	34.4538	-116.4741	4.370	-64.83	360
Transfer A	34.5099	-116.5331	2.698	-89.65	375
Transfer B	34.4881	-116.5148	3.359	-89.69	130
Transfer C	34.4157	-116.4677	4.581	-98.76	345
Homestead Valley A	34.5037	-116.5389	1.730	-50.72	150
Homestead Valley B	34.4853	-116.5239	3.225	-58.77	240
Homestead Valley C-1	34.4521	-116.5032	4.761	-65.34	225
Homestead Valley C-2	34.4133	-116.4816	4.750	-65.35	615
Slip Gap	34.3864	-116.4597	2.945	-42.43	90
Homestead Valley D	34.3704	-116.4483	1.576	-92.61	140
Homestead Valley E	34.3412	-116.4369	5.383	-66.29	380
Kickapoo	34.3375	-116.4521	5.796	-96.25	320
Johnson Valley A	34.3288	-116.4707	4.753	-53.89	0
Johnson Valley B	34.2973	-116.4481	3.465	-66.97	410
Johnson Valley C	34.2654	-116.4389	3.918	-84.85	280
Johnson Valley D	34.2299	-116.4380	4.011	-92.76	190
Johnson Valley E	34.1937	-116.4341	4.141	-77.32	310
Paxton	34.1506	-116.4076	7.156	-67.58	130
Eureka A	34.1027	-116.3849	4.282	-70.31	0
Eureka B	34.0587	-116.3673	6.050	-72.52	10
Big Bear	34.2042	-116.7833	28.000	42.00	-44
Iron Ridge	34.6337	-116.5625	11.614	9.66	-23

Table 6.1: Fault parameters for the Landers fault rupture determined by Hudnut, et al. (1994).

dislocation stress field, though there is considerably more small-scale structure in our model, especially near the fault. We used the convention that compressive stresses are negative; hence, regions of positive pore pressure correspond to regions of compressive stress.

The initial pore pressure distribution in our model is computed from the hydrostatic stress field by assuming undrained deformation. The term 'undrained deformation' implies that stress perturbations are imposed so rapidly that the fluid in an elemental volume or computational cell does not have time to move by diffusive transport to any neighboring cells. This is physically reasonable, because little pore fluid movement will occur during the brief time that the actual rupture is happening. Mathematically, undrained conditions mean that pore pressure is linearly related to hydrostatic stress by

$$P = -\frac{B}{3}\sigma_{disl} \tag{6.1}$$

where B is Skempton's coefficient, P is pore pressure, and $\sigma_{disl} = \sigma_{11} + \sigma_{22} + \sigma_{33}$ is the hydrostatic stress due to the fault dislocation. Compressive stresses are assumed to be negative. Skempton's coefficient is an elastic parameter that is commonly measured in the laboratory. Typical values for B range from approximately 0.5 for marble and Charcoal Granite to 0.85 for Westerly Granite and 0.88 for Ruhr Sandstone and effectively 1.0 for most unconsolidated soils (Rice and Cleary, 1976). For our simulations, we used $B = 0.8$.

6.3.2 Pore Fluid Diffusion and Elastic Deformation

Fluid flow in a poroelastic medium can be modeled by a set of partial differential equations first set forth by M. A. Biot (Biot, 1941) and reformulated by Rice and Cleary (1976) and others. The equations derived by Rice and Cleary and commonly used for poroelastic studies assume that the material parameters are constant. The simulations presented in this paper use constant material properties also. However, the formulation of the equations presented here and the implementation our code are more general and allow material parameters to vary spatially and temporally. We expect that the variability of material parameters, especially permeability, is

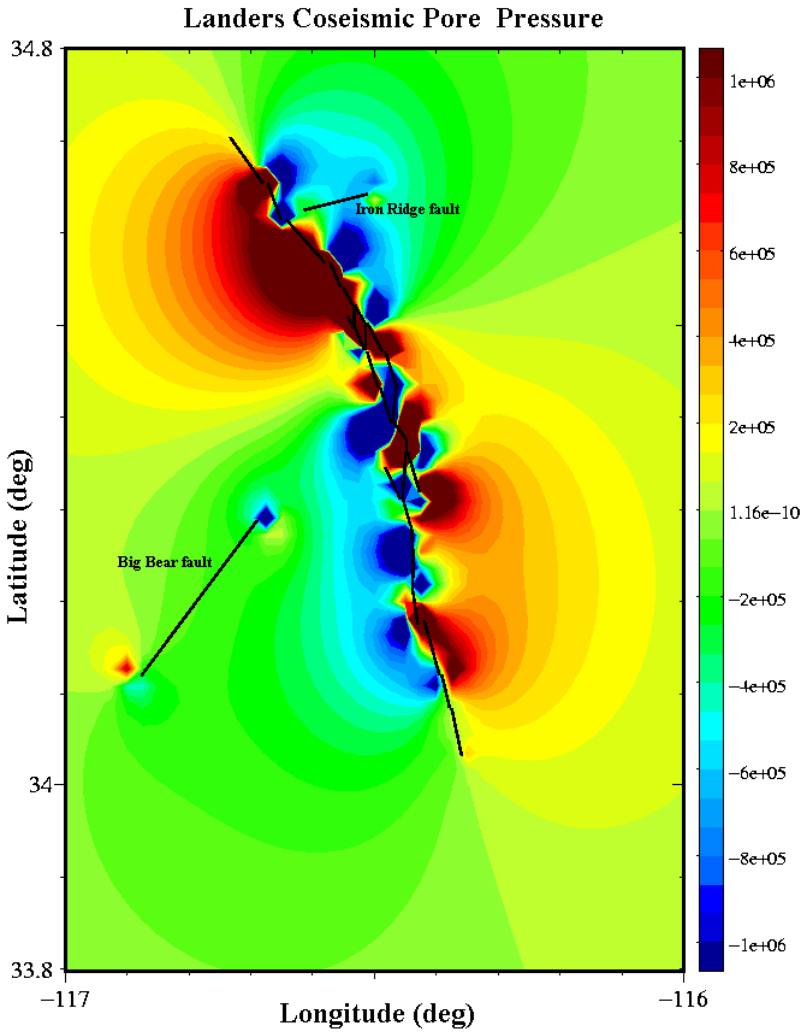

Figure 6.2: Landers coseismic hydrostatic stress field calculated using the half-space slip model *disl* (Larsen, 1991). Fault trace for the 27 segments of the Landers rupture, plus Big Bear and Iron Ridge faults are shown. Landers fault trace was derived from the parameters given in table 6.1.

probably significant in the region near the fault. The spatially heterogeneous nature of permeability and elastic properties and their alteration in time are important and will be investigated in a future paper.

The importance of the coupled nature of pore pressure and hydrostatic stress diffusion for crustal fluid flow remains an area of active research. It is clear that the coupling between elastic deformation and fluid pressure diffusion is significant in some situations, such as when seismicity is induced by fluid injection or extraction from the ground. (see for example, Segall 1994; Hsieh, 1981). In our calculations, we consider both simple diffusion and fully coupled poroelastic diffusion. Vertical displacements for both cases are presented. Horizontal displacement results are given only for the fully coupled poroelastic case, since the vertical simulation results indicated that the more realistic coupled equations gave significantly different results from the uncoupled case.

Our formulation of the poroelastic equations follows Rice and Cleary (1976), but is slightly more general in that we assume spatially variable coefficients and a full tensor permeability. Pore pressure is coupled to hydrostatic stress and obeys the following set of equations:

$$b\frac{\partial\left(P+B\sigma\right)}{\partial t}=\frac{\partial}{\partial x_i}\left[k_{ij}\left(x\right)\frac{\partial}{\partial x_j}P\right] \tag{6.2}$$

where P is the pore pressure deviation from a reference pressure, $\sigma=\left(\sigma_{xx}+\sigma_{yy}+\sigma_{zz}\right)/3$ is the mean stress deviation from the reference stress caused by the presence of the pore fluid, k_{ij} is the intrinsic permeability of the rock and b is a coefficient which includes the elastic properties of the rock and fluid density and viscosity:

$$b=\frac{9\mu\left(\nu_u-\nu\right)}{2GB^2\left(1-\nu\right)\left(1+\nu_u\right)} \tag{6.3}$$

ν and ν_u are the drained and undrained Poisson's ratios, respectively, G is the shear modulus, B is Skempton's coefficient, and μ is the fluid viscosity.

A second equation may be derived from the strain compatibility conditions and is equivalent to the Beltrami-Mitchell equation in elasticity theory:

$$\frac{\partial^2}{\partial x_i^2}\left(cP + \sigma\right) = 0 \tag{6.4}$$

where

$$c = \frac{2\left(\nu_u - \nu\right)}{B\left(1 - \nu\right)\left(1 + \nu_u\right)} \tag{6.5}$$

When $\nu = \nu_u$, c is zero, σ is constant in time and only P evolves in time, as in the case of simple diffusion of a compressible fluid through an incompressible porous rock. Physically, $\nu = \nu_u$ corresponds to the case where the rock elastic properties are uneffected by the presence of fluid. It should be emphasized that in equations 6.2 and 6.4 P represents the pressure deviation from the reference or pre-seismic pore pressure. σ in these equations is not the mean stress due to the fault dislocation, which was used to compute initial pore pressure. Rather, σ here is the mean stress deviation caused by the presence of the pore fluid pressure P. Thus, σ decays to zero as the pore pressure decays to zero.

Since the permeability has not been assumed constant in equation 6.2, it cannot be taken outside of the spatial derivatives. Mathematically, this prevents the decoupling strategy used by Rice and Cleary (1976) and others whereby the two equations are combined, resulting in a simple diffusion equation for the fluid mass excess or deficit, $m \sim P + B\sigma$. The equation is

$$b_{rice}\frac{\partial m}{\partial t} = \frac{\partial^2 m}{\partial x_i^2}$$

where b_{rice} combines constant elastic and fluid properties. This latter formulation is useful when constant material properties are assumed and when fluid mass is being pumped into or extracted from a well (Segall, 1985) . When permeability is spatially heterogeneous, the two equations cannot be combined.

The numerical solution of the set of poroelastic equations in our code is based on a finite element discretization scheme using Petrov-Galerkin elements in space and an upwind finite difference method in time. The equations are fully coupled in an implicit manner. A preconditioned iterative method, stabilized biconjugate

gradients (BiCGStab) with a relaxed incomplete LU preconditioning (RILU) is used to solve the linear system that results from the implicit discretization. Details on the fundamental numerical routines can be found in texts on finite element methods, such as those cited previously or on numerical linear algebra (e.g. Golub, 1989) . Helmig (1997) gives a clear discussion numerical methods for flow and transport equations with a level of mathematical rigor appropriate for engineers and scientists. Pande, et al. (1990) cover the application of finite element methods to rock mechanics problems. The publically-available Diffpack numerical libraries were used for the code framework (see `http://www.nobjects.com` for further information). The use of this commercially-available mathematically library allowed us to construct a sophisticated simulator using already-tested software components.

The domain for our problem is approximately 92 km by 110 km horizontally with horizontal grid spacing of 2 km for calculations of vertical displacement and the horizontal displacements of Savage and Svarc (1996). To match the results of Shen, et al. (1994), the domain was expanded to 274 km by 222 km with horizontal grid resolution of 4 km. The depth was 10 km over 2 cells (5 km vertical grid spacing) for all cases. The fault model used was identical for all simulations. Grid resolution was 2 km horizontally and 5 km vertically. If more information about material property variation was available near the fault a finer grid in this region would be desirable. Boundary conditions involved both fluid and elastic values. Zero flow boundaries were used to imitate far-away boundaries (Person, et al., 1996) . Displacement boundary conditions were zero normal stress along all sides. The latter boundary conditions would result in an ill-posed elliptic or boundary value problem; however, the coupled system of equations is an initial-value problem and is thus well-defined.

The initial conditions for pore pressure and mean stress deviation are found by assigning pore pressure values using the undrained assumption as in equation 6.1. The mean stress deviation due to the induced pore pressure is found by solving the compatibility condition, equation 6.4, which must always be satisfied.

Elastic deformation is computed from the stress equilibrium equations with the pore pressure as an applied force (equation 6.6). If the fully coupled poroelastic diffusion equations are used, as described above, the mean stress derived from solving

the stress equilibrium equations will be exactly equal to the mean stress that is evolved in the two coupled poroelastic equations, equations 6.2 and 6.4. We choose to solve the coupled poroelastic equations and the stress equilibrium equations in this decoupled manner for computational efficiency. The equations for the displacements in terms of pore pressure are

$$\frac{\partial}{\partial x_i}\left(\left(\lambda + G\right) u_{k,k}\right) + \frac{\partial}{\partial x_k}\left(G u_{i,k}\right) = \frac{\partial}{\partial x_i}\alpha\left(P_{total} - P_{ref}\right) \tag{6.6}$$

where u_i are the three components of the displacement vector, λ is the usual Lame coefficient and G is the shear modulus. Note that both of these may be spatially variable. The Biot-Willis parameter, α, is a function of Skempton's coefficient and the drained and undrained Poisson's ratios: $\alpha = 2\left(\nu_u - \nu\right)/B\left(1 - 2\nu\right)$. The right side of equation 6.6 is expressed in terms of the deviation of the pore pressure from a reference value, P_{ref}. In the following simulations $P = P_{total} - P_{ref}$ was assumed to be zero initially. That is, the state of stress and pore pressure just *before* the earthquake event was taken as the reference state.

Our basic algorithmic strategy is to evolve equations 6.2 and 6.4 in time as a fully coupled system. Only at designated times are the equations 6.6 solved, using the current value of pressure for the right hand side. This is computationally efficient because we need to solve a coupled system of size 2N, where N is the number of nodes, at each time step. Only at selected times, a system of size 3N is solved for the unknown displacements. If pressure and the three components of displacements are chosen as the unknown variables, a system of size 4N must be solved at every time step.

Values for elastic and hydrologic coefficients used in our simulations are shown in table 6.2. Reasonable values for material properties were chosen on the work of Hickman (1994), Rice and Cleary (1976), and Wang (1993). For this study, average values were assigned throughout the domain. This ignores the fact that the material properties are likely quite heterogeneous, especially near the fault. The undrained Poisson ratio is particularly sensitive since it is the difference between the two Poisson ratios that appears in all three governing equations. The values shown here for ν and

ν_u were taken from Peltzer, et al. (1996). Further computational experimentation is required to explore the sensitivity of the elastic response of the crust to the full range of possible material properties.

Parameter	Symbol	Value
Intrinsic permeability	k_{ij}	$(1, 1, 0.1)$ mD
Fluid Viscosity	μ	0.001 Pa-s
Shear modulus	G	22 GPa
Skempton's Coefficient	B	0.8
Poisson ratio	ν	0.25
Undrained Poisson ratio	ν_u	0.25 or 0.28
Derived quantities:		
$\frac{9\mu(\nu_u-\nu)}{2GB^2(1-\nu)(1+\nu_u)}$	b	10^{-14}
$\frac{2(\nu_u-\nu)}{B(1-\nu)(1+\nu_u)}$	c	0 or 0.075
Biot-Willis: $\frac{2(\nu_u-\nu)}{B(1-2\nu)}$	α	0.6

Table 6.2: Elastic and hydrologic parameters used in numerical simulation of fluid flow and deformation following the 1992 Landers earthquake.

6.4 Postseismic Vertical Displacement

6.4.1 SAR Measurements of Postseismic Rebound

Measurements of near-field postseismic surface displacement following the 28 June 1992 Landers earthquake rupture have been made by Peltzer, et al. (1996) using SAR interferometry. Measurements were made over three different time intervals in the region of the 85-mile surface rupture. The surface trace over which these measurements were taken is shown in figure 6.3. The vertical displacement profiles determined from the SAR measurements are shown in the enlarged subimages. The time intervals are shown in table 6.3.

Three aspects of the SAR profiles are to be noted. First, the magnitude of the displacements is on the order of 5 cm. Secondly, the shape of the profiles is rather complex. This is due not only to the complexity of the faults, but also to the heterogeneous hydrologic and mechanical properties of the crust near the fault. Thirdly, the

Line Profile	Time Period
1	Day 41 to 1183
2	Day 92 to 1304
3	Day 196 to 863

Table 6.3: Time intervals over which vertical displacement changes were measured and computed following the Landers earthquake. Day 1 is 28 June 1992, the day of the earthquake.

relaxation time was estimated to be 273 ± 44 days. This relaxation time is considerably less than the timescale that would be associated with relaxation due to viscous flow of the lower crust, which has been invoked to explain postseismic after-slip (for example, see Shen, 1994). Typical viscous relaxation of the lower crust occurs on a timescale more than an order of magnitude greater, approximately 36 years (Turcotte and Schubert, 1982).

6.4.2 Computed Postseismic Rebound

Using our coupled poroelastic code, we computed the vertical deformation in the region of the Landers earthquake over three time intervals corresponding to the time periods that were measure by Peltzer, et al. (1996) with SAR interferometry.

In Figure 6.4, computed vertical displacements are shown at times and locations that coincide with the times at which SAR measurements were made. Fluid flow in 6.4 followed simple diffusion ($b = 0$). In figure 6.5 we let $b = 0.075$, which corresponds to a poroelastic case in which the crustal rocks respond elastically to changes in pore pressure.

6.5 Postseismic Horizontal Deformation

Horizontal deformation following the 1992 Landers earthquake has been determined by a number of researchers (Shen, et al., 1994; Savage, et al., 1997; Wyatt, et al., 1994) , using GPS geodetic arrays, trilateration, and long-base strainmeters. Horizontal deformation caused by postseismic pore pressure evolution would be correlated

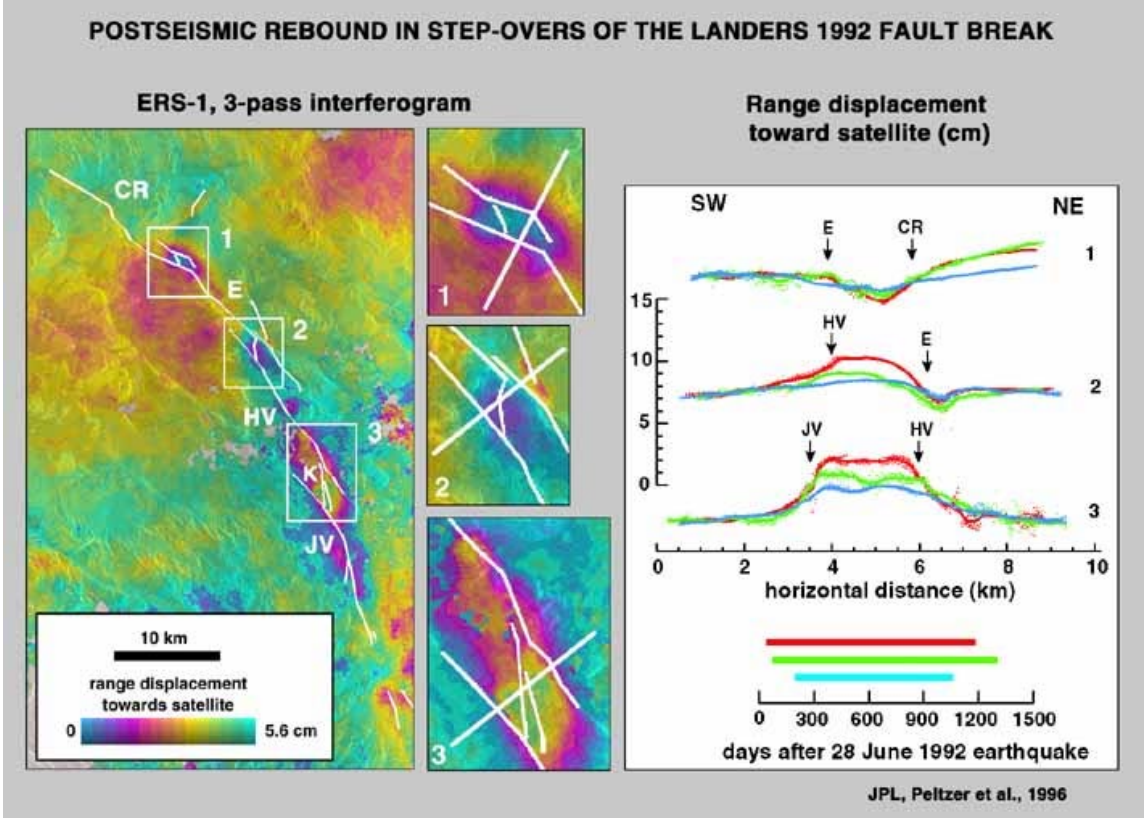

Figure 6.3: SAR measurements of Landers postseismic vertical displacement. Picture from Jet Propulsion Lab, Peltzer, 1996: http://www-radar.jpl.nasa.gov/sect323/InSar4crust/LandersPost.html. Used with permission of author.

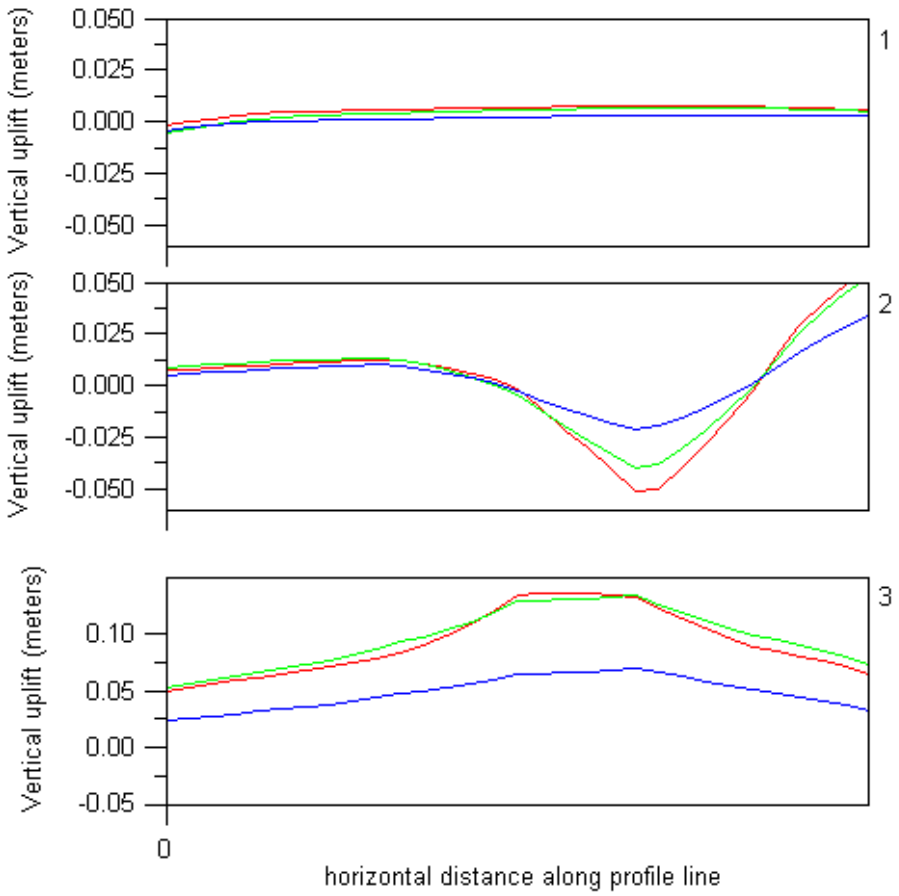

Figure 6.4: Computed postseismic vertical displacements along the profiles corresponding to the SAR measurements by Peltzer, et al. (1996), assuming simple diffusion of the fluid: $c = 0$. The time intervals for each profile correspond to those shown in table 6.3.

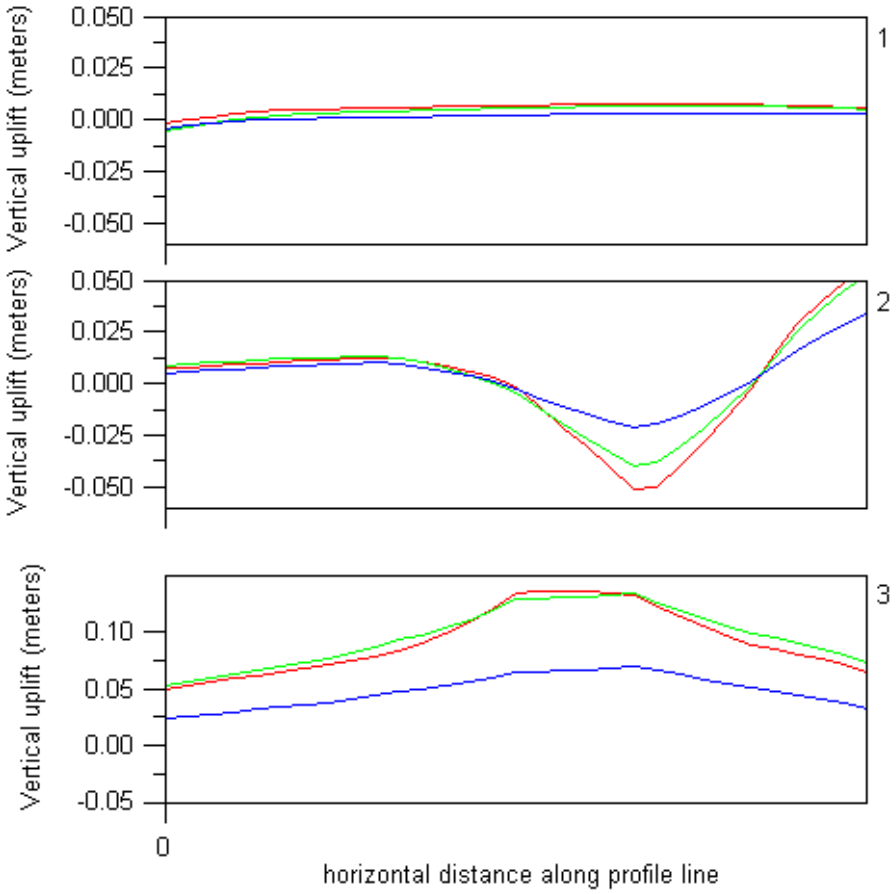

Figure 6.5: Computed postseismic vertical displacements along the profiles corresponding to the SAR measurements by Peltzer, et al. (1996), assuming poroelastic diffusion of the fluid: $c = 0.075$. The time intervals for each profile correspond to those shown in table 6.3.

to vertical deformation. Vertical uplift would be expected to occur where horizontal extension is occuring, while vertical subsidence would correlate to horizontal contraction. This contrasts with deformation caused by viscoelastic deformation in which vertical uplift would occur where horizontal *contraction* is occuring. This provides a way to determine the contribution of poroelastic diffusion to the total postseismic horizontal deformation following the Landers earthquake.

A comparision of vertical and horizontal deformation would be quite straightforward if comprehensive areal data were available for absolute vertical and horizontal displacements. Areal maps for vertical displacement and horizontal displacement could then be compared for correlations. Unfortunately, such data is not available. An alternative approach is to compare available horizontal displacement data to equivalent computed horizontal displacements, just as computed vertical displacements were compared to SAR measurements. It was clear that the vertical displacements due to pore fluid diffusion correlated rather well with SAR measurements. If computed horizontal displacements also correlate with measurements, we can conclude that poroelastic relaxation is at least a significant component of the total postseismic deformation.

In figures 6.6 through 6.8 the correlation between pore pressure changes, vertical displacement, and horizontal deformation are illustrated. Vertical and horizontal displacements in these figures are due entirely to the computed pore pressure changes. As expected, vertical uplift, horizontal expansion, and positive pore pressure changes occur in the same locations.

Shen, et al. (1994) used GPS receivers at a number of sites in the region of the Landers earthquake to determine relative displacements between stations over a period of approximately three years. Figure 6.9 shows the locations of stations used by Shen, et al. (1994). Red triangles represent the subset of stations that were selected for computer calculation.

Relative positions between selected pairs of survey markers at times up to approximately one year after the Landers earthquake event are plotted in figure 6.10. The analogous plots that resulted from computer simulation of poroelastic displacement are shown in figure 6.11.

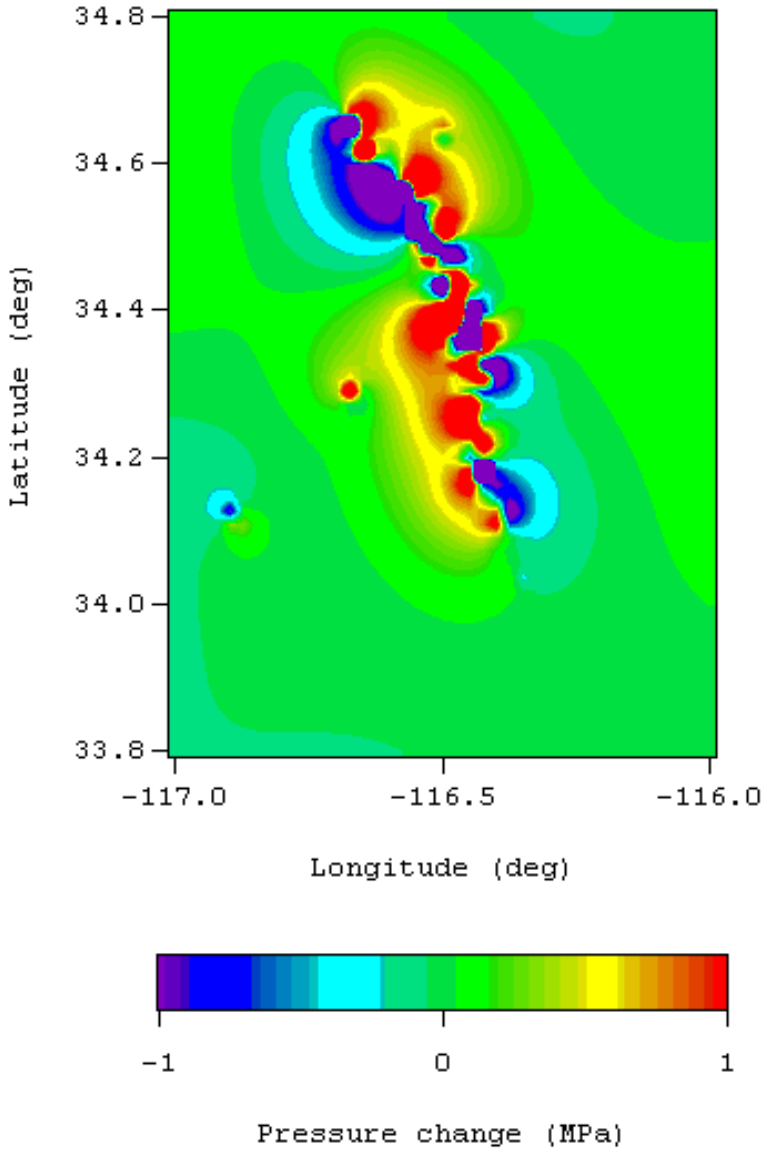

Figure 6.6: Pressure changes from day 0 (28 June 1992) to day 1226 following the Landers earthquake.

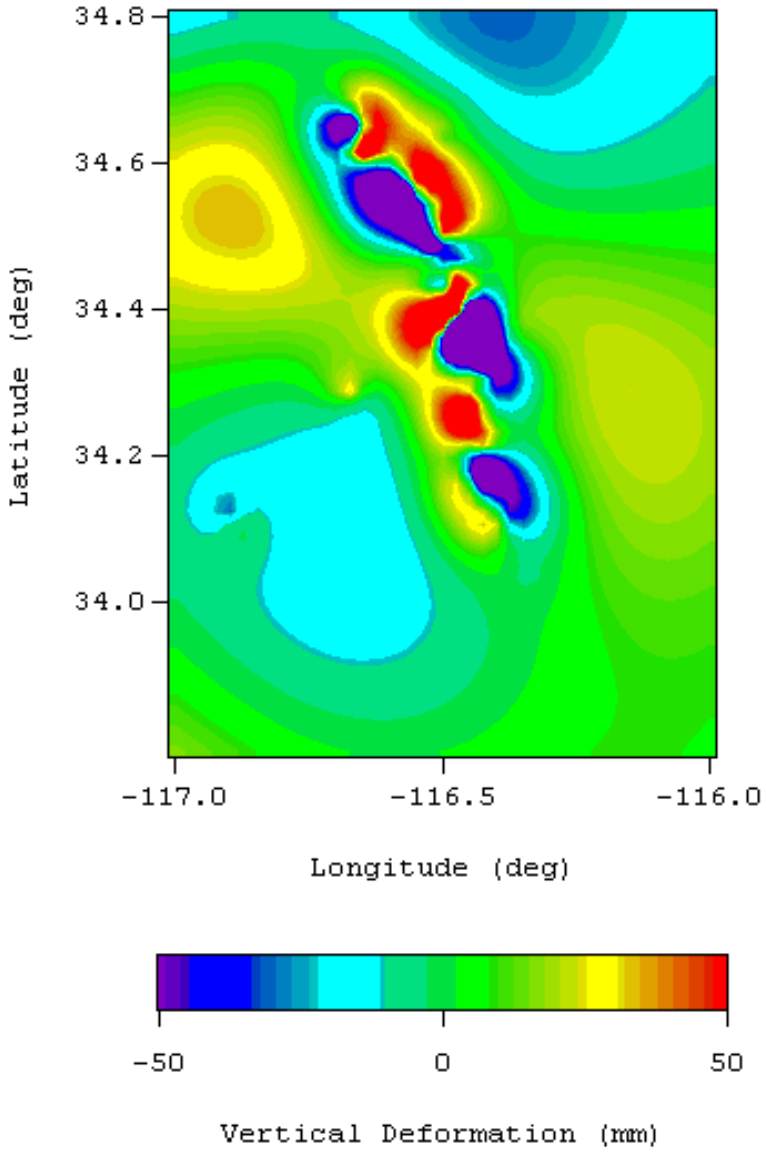

Figure 6.7: Vertical displacement from day 0 (28 June 1992) to day 1226 following the Landers earthquake.

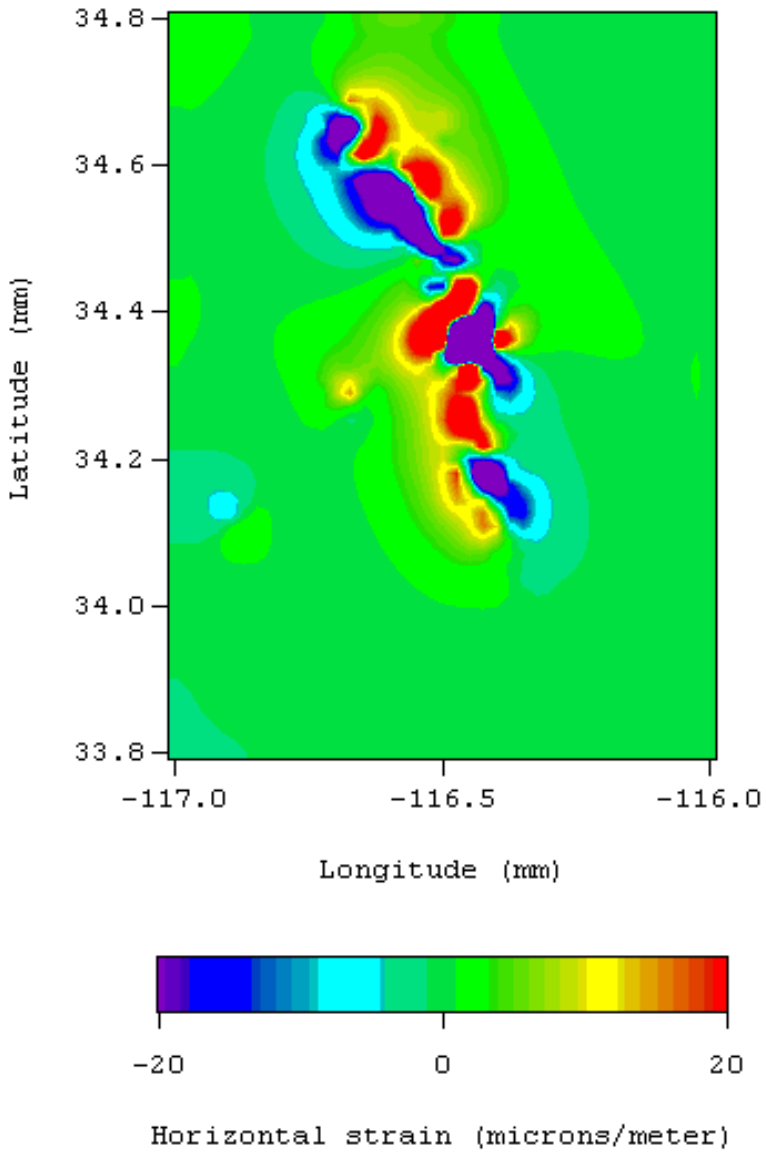

Figure 6.8: Horizontal strain change from day 0 (28 June 1992) to day 1226 following the Landers earthquake.

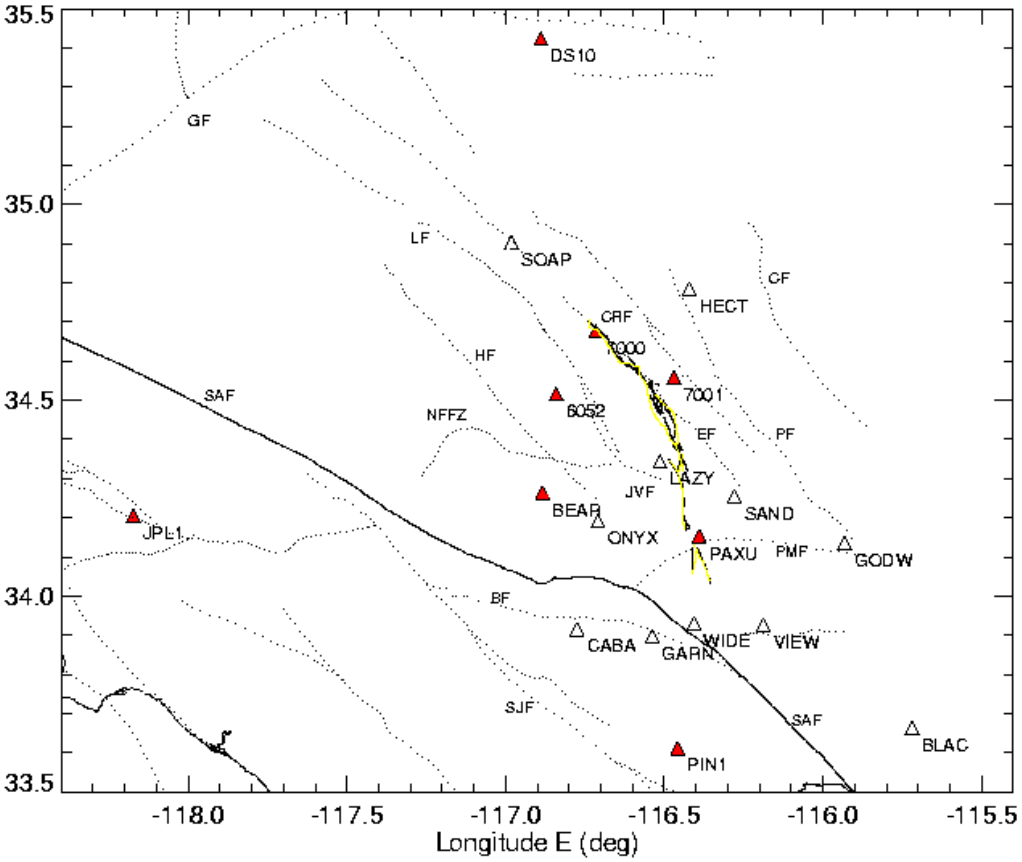

Figure 6.9: Map showing the surface trace of the Landers earthquake (yellow) and GPS postseismic monitoring stations (red triangles) used to compute horizontal deformation. Figure is from Shen, et al. (1994). Used with permission of author.

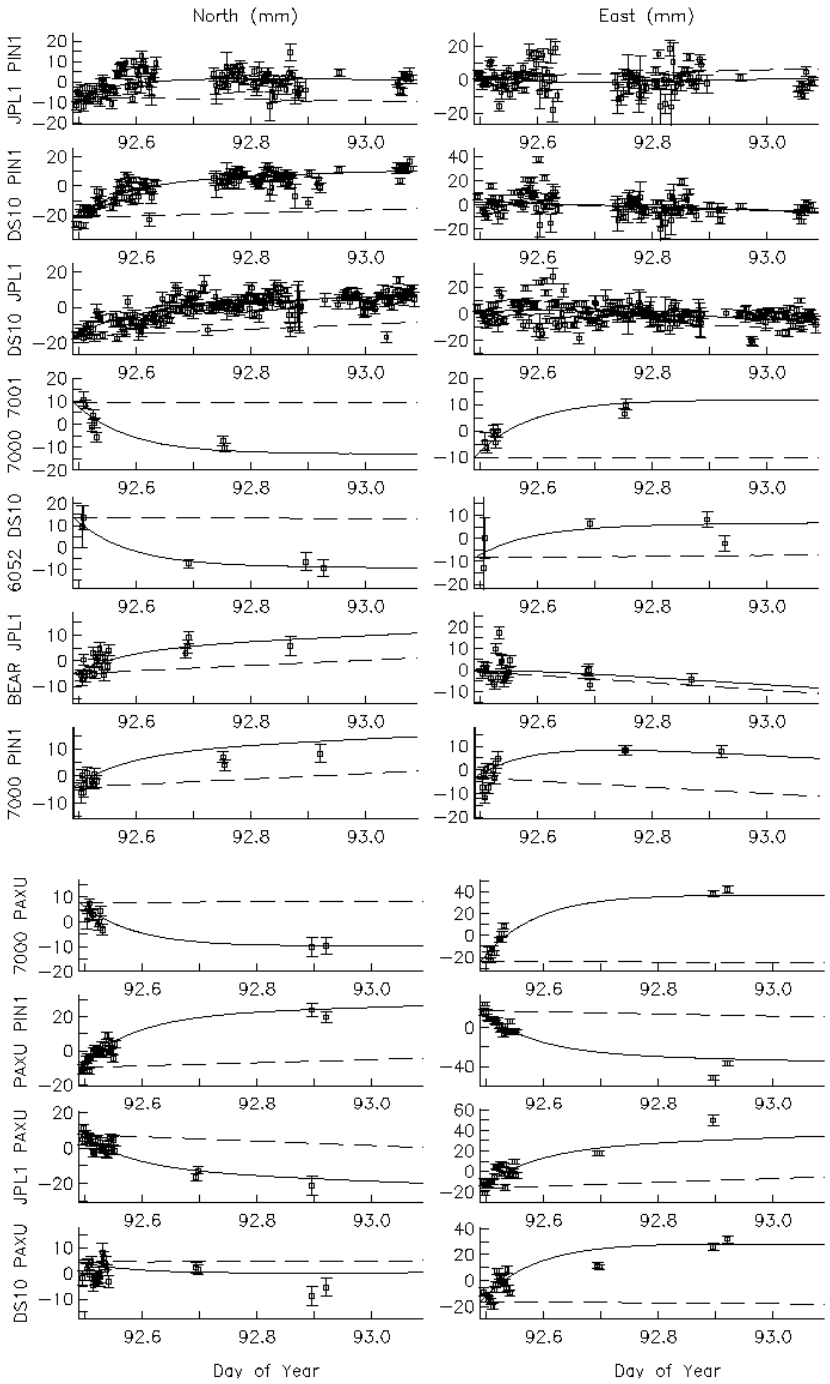

Figure 6.10: GPS baseline solutions from Shen, et al. (1994). Used with permission of the author.

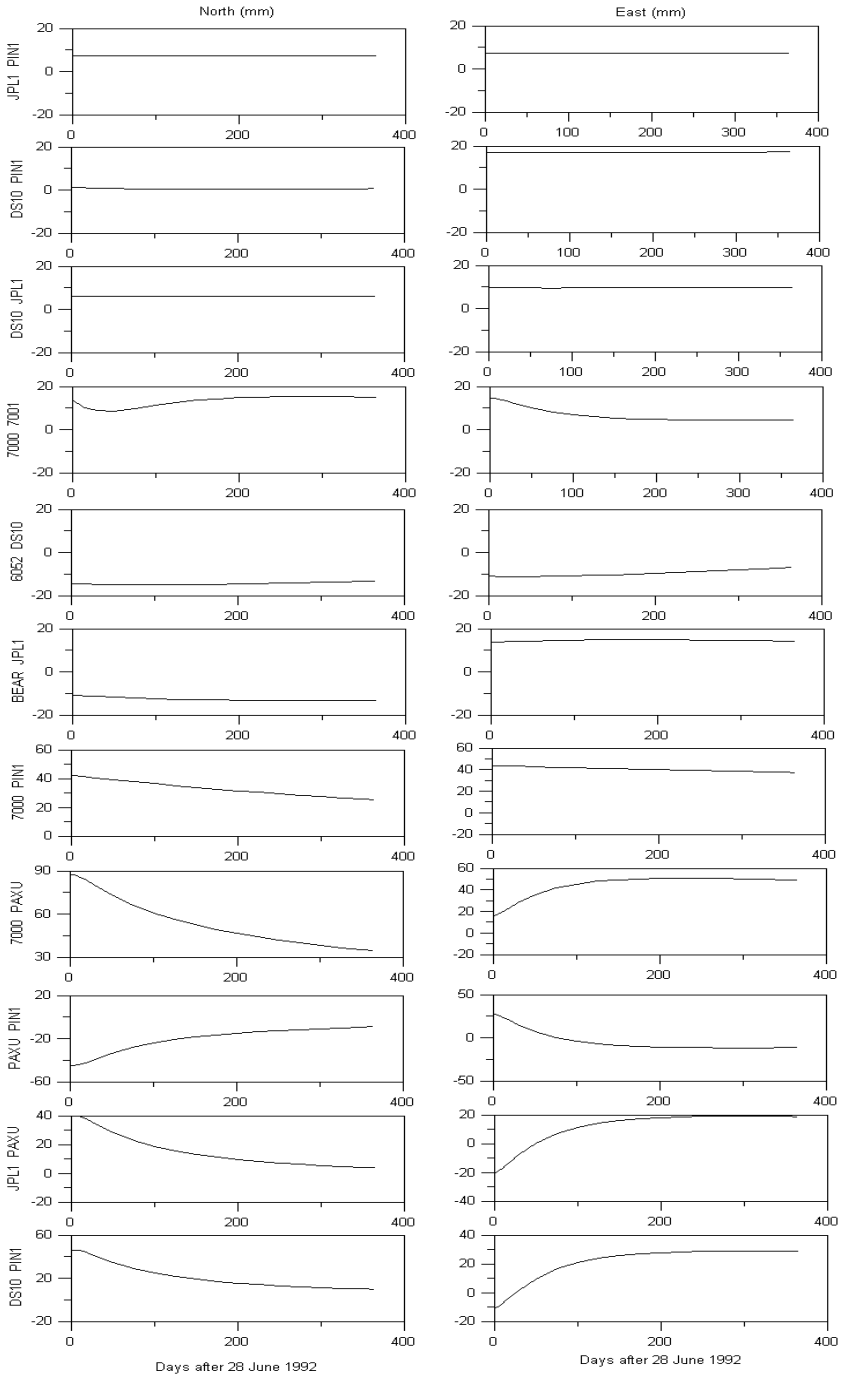

Figure 6.11: Computed horizontal (east and north) displacement differences. Stations are indicated on the vertical axis of the left (north) plot. These curves are analogous to the curves determined by Shen, et al. (1994) from GPS measurements.

Figure 6.12: Map of region near the Landers earthquake showing the geodetic array used by Savage and Svarc. Used with permission of the authors.

The first three sets of plots are for stations that are far from the fault and relatively far from each other (JPL1, PIN1, and DS10). Since pore pressures deviations are small far from the fault, relatively little change in position would be expected in the computed displacements. This is clearly seen in figure 6.11. The measured relative displacements for these three pairs is more significant in the northward direction, but relatively flat in the eastward direction. This indicates that some physical process in addition to poroelastic diffusion is operative far from the fault in the north-south direction. Stress perturbations due to aftershocks, viscoelastic relaxation, and continuing movement of tectonic plates on either side of the fault might all contribute to these north-south displacements.

The last four sets of plots all involve the station PAXU, which is located very close to the fault near the epicenter at the southern end. Pore pressure changes would be expected to be large at this location. Computed poroelastic displacements of four widely-dispersed stations (7000, PIN1, JPL1, and DS10) relative to PAXU are quite similar to the measured displacements in both magnitude and direction, suggesting that pore fluids contribute significantly to elastic deformation near the fault.

Computed displacements for sets four through seven (7000-7001, 6052-DS10, Bear-JPL1, 7000-PIN1) deviate from measured trends in at least one component. Three of these four pairs involve stations that are very near fault segments (7000, 7001, Bear). The grid resolution for the computational model (4 km horizontally) is greater than the distance to the fault at these stations. Since there is a great deal of variation in pore pressures along the faults at an apparently fine scale, calculations with finer resolutions might yield different results at these stations.

Savage and Svarc (1997) determined displacements of geodetic stations along an array relative to a fixed station. Figure 6.12 is a map of the region around the Landers fault trace with the geodetic station locations indicated.

Horizontal displacements parallel and normal to the fault trace, relative to the station labeled Sanh were determined. Plots of those measurements are shown in

figure **??**. It is immediately apparent that the movement of all stations along the geodetic array are in the same direction, relative to the Sanh station, both normal and parallel to the fault. This is particularly surprising since the array locations are on both sides of the fault. Stations on opposite sides of the fault would be expected to show displacements in different directions. This is confirmed by the displacement vectors in figure 6.14, which will be discussed later. Examination of the location of the geodetic array station in Savage (1997) and comparing this to the stress field in figure 6.2 reveals that the geodetic array lies approximately along the nodal line between quadrants in the coseismic mean stress field. Though stress and pore pressure will have different signs along the array on different sides of the fault, the magnitudes will not be as large as they would be in locations away from the nodal line. Thus, the relative displacements shown in figure **??** must be due largely to the displacement of the Sanh station.

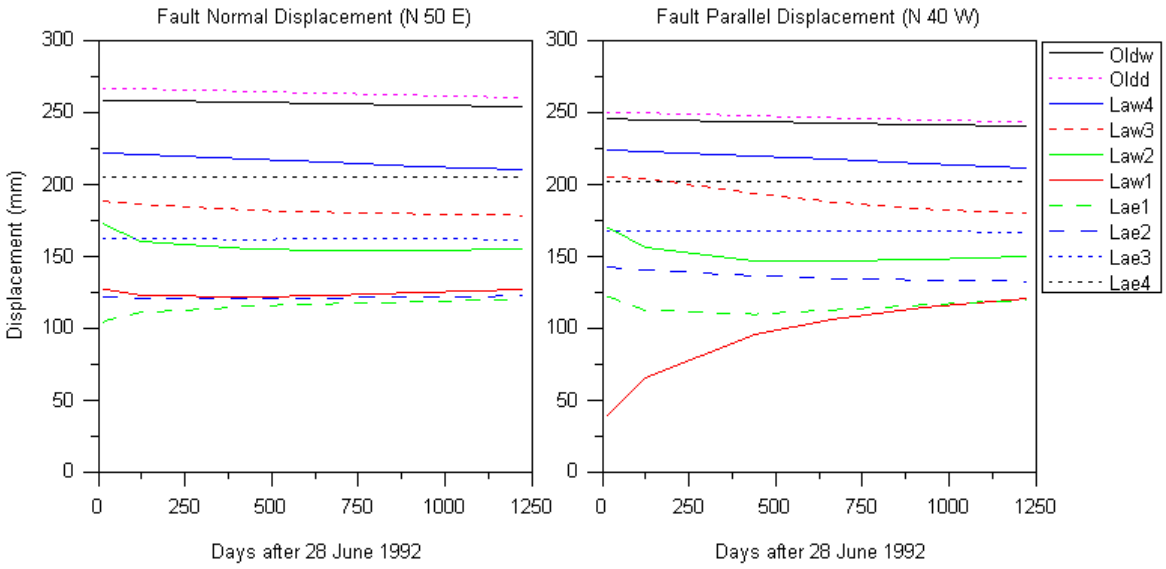

Figure 6.13: Computed displacements relative to Sanh due to pore fluid pressure

Computed displacements relative to Sanh along the geodetic array due to poroelastic relaxation are shown in figure 6.13. The magnitudes of the displacements and the general shape of the curves are similar enough to the measured displacements in

figure ?? to support the claim that poroelastic diffusion may contribute a significant amount to the total postseismic deformation. However, the curves do not fit the data well. Heterogeneities in the permeability field, which will greatly affect fluid flow, may contribute to this. It is also likely that other processes contribute to horizontal deformation and the data contains the combined effects of this. Deng, et al. (1998) shows results of viscoelastic deformation simulations and compares to Savage and Svarc's data.

Displacements along the array relative to the Gold station are shown in figure 6.14. The Gold station is relatively far from the fault, approximately 100 km from the north end of the Landers fault trace. The array displacements are approximately parallel to the fault and in the direction of fault movement (right-lateral). The displacements increase in magnitude away from the fault. and , the displacements along the array are in opposite directions on either side of the fault.

Computed horizontal displacements in the entire region surrounding the Landers fault are shown in figure 6.15. These are displacements changes relative to the coseismic displacement field and not relative to the location at Gold. The pore pressure changes at the remote Gold station would be quite small, so little if any differences result from this. Several aspects of the computed displacement field are of note. First, the displacements are largest near the fault, where the greatest mean stress and pore pressure changes occur. This contrasts with the measured displacements, which are largest away from the fault. Clearly, poroelastic diffusion, which will be largest near the fault, cannot be the only process causing deformation. Secondly, the displacement vectors have the same general direction as the measured displacement vectors in figure 6.14. Poroelastic deformation must contribute a significant component to the total deformation, especially near the fault. Finally, we note that pore pressure changes near the fault exhibit considerable spatial complexity and this is reflected in the displacement vectors near the fault. The few geodetic stations near the fault seem to also exhibit this kind of directional complexity.

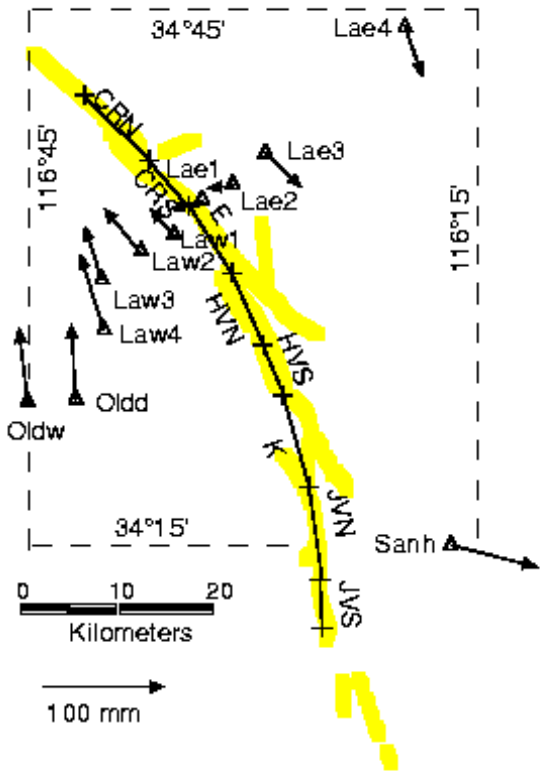

Figure 6.14: Map of the Landers region showing total displacement relative to Gold over the 3.4-year interval covered by the surveys. Figure taken from Savage and Svarc (1992). Used with permission of the authors.

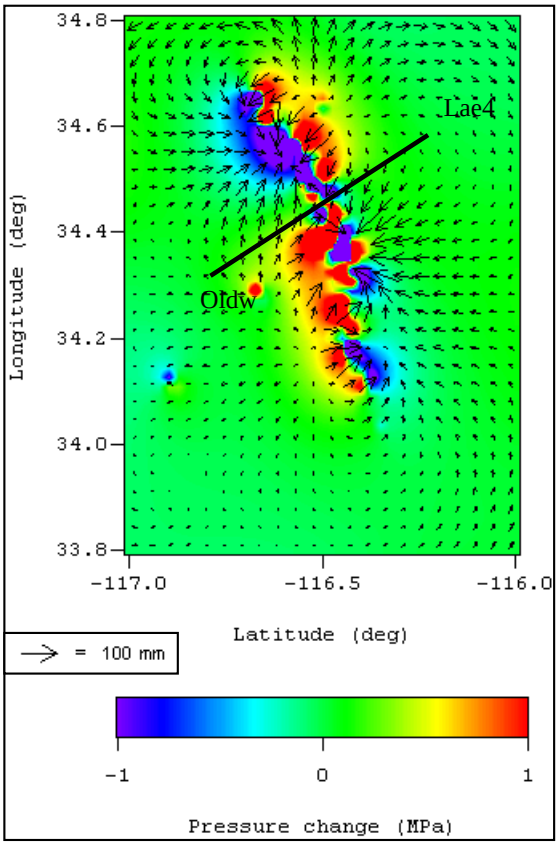

Figure 6.15: Changes in pore pressure and horizontal displacement from the moment after the Landers earthquake until 3.4 years (1226 days) after the earthquake are shown. Note that displacements are those due solely to elastic deformation caused by pore pressure changes. The heavy black line shows the location of the geodetic array used by Savage and Svarc (1997).

6.6 Discussion

Our computed vertical displacement changes have a magnitude and characteristic decay time that match measured values reasonably well. The coupled poroelastic simulations appear to give vertical displacement profiles that are qualitatively different from the simple diffusion case. This suggests that the coupled poroelastic effects may be significant, particularly near complex fault regions. Anelastic effects are likely to be quite important very near fault ends where stresses are high enough to cause failure of the rock, though these effects were not considered here. Variations in the effective elastic properties of the rock material near the fault would also affect the displacement profiles.

Computed horizontal displacements indicate that poroelastic deformation is a significant component of the total postseismic horizontal displacement field. It appears that other physical processes are also operating. Viscoelastic rebound has been suggested by several authors as a likely cause (Deng, et al., 1998; Savage and Svarc, 1996; Shen, et al., 1994; Wyatt, et al., 1994). Savage and Svarc (1996) note that dislocation models based on postseismic slip below 10 km can account for some of the observed horizontal deformation, but not all. It seems particularly likely that poroelastic deformation would be most significant near the fault and less important far from the fault. Postseismic slip below 10 km would also be less significant far from the fault.

Permeability variability is likely to have a profound affect on the poroelastic deformation in the fault region. In our simulations, permeability was homogeneous throughout the region of study. This is certainly not an accurate model of the permeability structure of faults. Studies indicate that the permeability structure near faults is quite complex and the magnitude of intrinsic permeability may vary over several orders of magnitude among fault gouge, the surrounding damage zone, and in the regional country rock (Forster, et al., 1994; Logan and Decker, 1994). Anisotropy is likely to be strong, particularly in the fault gouge. Furthermore, permeability may also be strongly affected by pore pressure in highly fractured rock (Yilmaz, et al., 1994). High pore pressure can open fractures and create locally high flow paths which

close as pressure decays. This effect would manifest itself as changing time scales of relaxation: fast decay near the fault in high stress/pore pressure regions, and slower decay later near the fault and at all times far from the fault. The latter would involve the complex interaction of pore pressure, principle stress orientation, and microfracture orientation. If heterogeneity, anisotropy and nonlinearity were included in our simulations it would certainly affect the shape of the displacement profiles that were computed. Additional simulations taking these properties into account are necessary to assess their importance in the overall dynamical evolution of the postseismic stress field.

Though we used a three-dimensional code, our simulations were effectively two-dimensional since the fault slip used to compute initial pore pressures was vertically constant. Information detailing vertical slip variation is available in the literature and might be included in a more detailed simulation (Wald and Heaton, 1994)(**?**). We believe that this would not affect the computed vertical deformation as much as permeability variations.

6.7 Conclusions

The purpose of this study was to demonstrate that the elastic deformation caused by pore fluid movement following the Landers earthquake was significant enough to be considered a first-order effect. The clear implication of our simulations is that pore pressure cannot be ignored in modeling studies of postseismic stress evolution, especially near the fault. The computer simulations presented here support the hypothesis by Peltzer, et al. (1996) that pore fluid flow can account for the postseismic vertical displacement measured by SAR imagery in the region of the 1992 Landers earthquake and the suggestion by Savage and Svarc, (1996). Shen, et al., (1994), Wyatt, et al., (1994) and others that poroelastic effects might be involved in the overall postseismic deformation process. Using reasonable values for material properties, our simulations produced vertical displacements having both magnitude and decay times that were similar to those that were measured. Computed horizontal displacements had magnitudes and directions that strongly indicate that poroelastic deformation

was a significant component of the displacement field, though it was apparent that other processes, particularly far from the fault, were also active.

To reproduce the measured displacement fields more precisely would require that the permeability structure and elastic properties near the fault be known and represented more accurately in our simulation model. Continuous deformation caused by postseismic viscoelastic relaxation and moving tectonic plates would contribute to the overall deformation over the several years that were considered in this study. The results presented here do, however, present compelling evidence that pore fluid diffusion is responsible for a significant part of the observed postseismic deformation in the region of the Landers earthquake.

6.8 Acknowledgemets

This work was partially supported by the the United States Geological Survey (USGS) National Earthquake Hazards Program (NEHEP).

Bibliography

Biot, M. A., Generalized theory of 3-dimensional consolidation, *J. Appl. Phys.*, *12*, 155–164, 1941.

Bosl, W. J., and A. Nur, Numerical simulation of postseismic deformation due to pore fluid diffusion, in *Poromechanics: A Tribute to Maurice A. Biot*, edited by e. A. J.-F. Thimus, pp. 23–28, A. A. Balkema, Rotterdam, 1998.

Cohee, B. P., and G. C. Beroza, Slip distribution of the 1992 landers earthquake and its implications for earthquake source mechanics, *Bull. Seism. Soc. Am.*, *84*, 692–712, 1994.

Deng, J., M. Gurnis, H. Kanamori, and E. Hauksson, Viscoelastic flow in the lower crust after the 1992 landers, california, earthquake, *Science*, *282*, 1689–1692, 1998.

Evans, B., and T.-F. Wong, eds., *Fault Mechanics and Transport Properties of Rocks*, Academic Press, Inc., San Diego, 1992.

Golub, G., and C. V. Loan, *Matrix Computations*, 2nd ed., Johns Hopkins University Press, Baltimore, 1989.

Helmig, R., *Multiphase Flow and Transport Processes in the Subsurface*, Springer-Verlag, New York, 1997.

Hickman, S., R. Sibson, and R. Bruhn, eds., *The Mechanical Involvement of Fluids in Faulting*, Menlo Park, CA, U. S. Geological Survey, 1994.

Hudnut, K. W., et al., Co-seismic displacements of the 1992 landers earthquake sequence, *Bull. Seis. Soc. Am.*, *3*, 625–645, 1994.

Li, Y., J. Vidale, K. Aki, F. Xu, and T. Burdette, Evidence of shallow fault zone healing after the 1992 m7.5 landers, california, earthquake, *Science*, 1997.

Nur, A., and J. R. Booker, Aftershocks caused by pore fluid flow?, *Science*, *175*, 885–887, 1972.

Pande, G. N., G. Beer, and J. R. Williams, *Numerical Methods in Rock Mechanics*, John Wiley and Sons, Inc., New York, 1990.

Peltzer, G., K. Hudnut, and K. Feigl, Analysis of coseismic surface displacement gradients using radar interferometry: New insights into the landers earthquake, *Journal of Geophysical Research*, pp. 21971–21981, 1994.

Peltzer, G., P. Rosen, F. Rogez, and K. Hudnut, Postseismic rebound in fault step-overs caused by pore fluid flow, *Science*, *273*, 1202–1204, 1996.

Person, M., J. P. Raffensperger, S. Ge, and G. Garven, Basin-scale hydrogeologic modeling, *Reviews of Geophysics*, *34*(1), 61–87, 1996.

Rice, J. R., and M. P. Cleary, Some basic stress diffusion solutions for fluid-saturated elastic porous media with compressible constituents, *Rev. Geophys. Space Phys.*, *14*(2), 227–241, 1976.

Roeloffs, E., Poroelastic techniques in the study of earthquake-related hydrologic phenomena, *Advances in Geophysics*, *37*, 135–195, 1996.

Savage, J. C., and J. L. Svarc, Postseismic deformation associated with the 1992 mw=7.3 landers earthquake, southern california, *Journal of Geophysical Research*, *102*, 7565–7577, 1997.

Segall, P., Stress and subsidence resulting from subsurface fluid withdrawal in the epicentral region of the 1983 coalinga earthquake, *Journal of Geophysical Research*, *90*, 6801–6816, 1985.

Shen, Z., D. Jackson, Y. Feng, M. Cline, M. Kim, P. Fang, and Y. Bock, Postseismic deformation following the landers earthquake, california, 28 june 1992, *Bulletin of the Seismological Society of America*, *84*, 780–791, 1994.

Wald, D. J., and T. H. Heaton, Spatial and temporal distribution of slip for the 1992 landers, california, earthquake, *Bulletin of the Seismological Society of America*, *84*(3), 668–691, 1994.

Wang, H. F., Quasi-static poroelastic parameters in rock and their geophysical applications, *PAGEOPH*, *141*(2/3/4), 269–286, 1993.

Wyatt, F. K., D. C. Agnew, and M. Gladwin, Continuous measurements of crustal deformation for the 1992 landers earthquake sequence, *Bulletin of the Seismological Society of America*, *84*, 768–779, 1994.

Zebker, H. A., P. A. Rosen, R. M. Goldstein, A. Gabriel, and C. L. Werner, On the derivation of coseismic displacement fields using differential radar interferometry: The landers earthquake, *Journal of Geophysical Research*, *99*, 19617–19634, 1994.

Chapter 7

Aftershocks and Pore Fluid Diffusion

7.1 Introduction

Aftershocks are an enigma. They are clearly associated with a preceding seismic event and their spatial distribution is fairly well correlated with coseismic stress changes (King, et al., 1994). Yet aftershocks do not happen immediately following an earthquake. The frequency of aftershocks decays like a diffusive process (Nur, 1972), indicating that a time-dependent physical process is at work. Nur and Booker (1972) proposed that pore pressure readjustment after an earthquake could explain the time delay in the occurence of aftershocks. Since the crust is believed to be saturated with water down to seismogenic depths (Walder,1984) and there are many clear examples to demonstrate that the crust behaves as a poroelastic medium, not simply an elastic medium (Roeloffs, 1996), it would seem that pore pressure effects must be considered in order to understand the time-dependent nature of faulting processes.

Aftershocks of the 1992 Landers are studied here using simulations of coupled poroelastic diffusion. It was found that postseismic Coulomb stress changes caused by pore fluid diffusion correlate better with aftershock location data better than either static Coulomb stress or pore fluid pressure alone. The poroelastic hypothesis is a physically satisfying explanation for aftershocks that reconciles coseismic Coulomb

stress and pore fluid explanations for aftershocks and offers a physical mechanism for afterslip and the expansion of aftershock zones. The hypothesis that pore fluid diffusion causes significant crustal stress changes after an earthquake is consistent with theories that posit pore fluid movement following the Landers earthquake as the cause for observed postseismic deformation (Bosl, 1998; Peltzer, 1996; Peltzer, 1998).

Various aftershock theories place the time element for aftershock occurence on changing fault properties (time-dependent friction laws). More intricate theories of earthquake and aftershock production (for example, Dieterich, 1994) seek to explain the occurrence of aftershocks by incorporating time-dependent fault constitutive properties (including state and rate-dependent friction laws) and time-dependent external (stress and pore pressure) changes in the crust. Both processes occur in faults and play a role in earthquake nucleation. Here we examine changes in stress and pore pressure on faults in the region of an earthquake as the dominate cause of aftershock production. This does not necessarily conflict with other models (such as Dieterich, 1994), but simply places the focus on external changes in the medium rather than fault property changes.

Li, et al. (1987) investigated the correlation between time-dependent Coulomb stress and aftershocks for three earthquakes. Their study was inconclusive. Important limitations in that study included simplified fault slip models, analytical poroelastic solutions which cannot account for heterogeneous diffusivities, and inaccurate aftershock locations. Our research has shown that detailed representations of fault slip, both horizontally and vertically, can greatly affect the location of pore pressure increase or decrease. This paper attempts to overcome these previous limitations in modeling postseismic poroelastic diffusion and re-examine the role of poroelastic fluid pressure and stress evolution following a major earthquake for which considerable data is available.

7.2 Nur and Booker Hypothesis

Pore fluid diffusion was first proposed by Nur and Booker (1972) as the time-dependent process responsible for causing aftershocks. Their idea was relatively simple: when

an earthquake occurs, there is an almost-instantaneous modification to the regional stress field. The change in strength of a fault (or rock), determined experimentally by Hubbert and Rubey (1959), was given by

$$\Delta S = \mu_f \left(\overline{\sigma} - p\right)$$

where μ_f is the coefficient of internal friction or simply the frictional strength, $\overline{\sigma}$ is the mean stress, and p is the pore pressure in the fault. Aftershocks will occur on faults where the shear stress exceeds the strength of the fault. Immediately following an earthquake, the pore pressure is changed by an amount proportional to the mean stress induced by the earthquake: $p = -B\overline{\sigma}$. In many studies, a first-order assumption is $B = 1$. After the earthquake, pore fluids will flow from regions of high pressure (compressional regions) to regions of low pressure (dilatational regions). The applied mean stress field will remain approximately constant, so the strength of the fault will change over time. The number of aftershocks, according to this theory, should be proportional to the time rate of change of pore pressure integrated over a region. Moreover, the theory predicts that aftershocks will occur where the pore pressure is *increasing*; that is, in regions of coseismic dilatation.

Consider a volume of the crust where an earthquake has occurred. If the confining pressure, $\overline{\sigma}$, and shear stress are constant, failure on regional faults that did not fail when the initial shock occurred will tend to occur where the strength of the faults is decreasing. That is, aftershocks will occur where pore pressure is increasing. The number of slip events (aftershocks) should be proportional to the total increase in pore pressure in the volume over a specified time interval. Quantitatively, this was expressed by integrating the time rate of change of pore pressure:

$$\frac{dN}{dt} = \frac{1}{c} \int_{\Omega} \left(\frac{\partial P}{\partial t}\right) dv \tag{7.1}$$

where c is a normalizing factor, P is pore pressure, N is the number of aftershocks, and Ω is the volume of rock.

7.3 The Coulomb Fracture Criterion

The frictional strength of faults is better represented by the empirical Coulomb fracture criterion than Hubert and Rubey's strength criterion, since it is the compressional stress normal to the fault plane that controls the frictional strength of a fault rather than the mean stress. The Coulomb stress is expressed mathematically by

$$\tau_c \equiv \tau - \mu_s \left(\sigma_n - P\right) \tag{7.2}$$

where τ_c is the Coulomb stress, τ and σ_n are the shear and normal stresses with respect to a given fault plane, and P is the fluid pressure in the fault. A fault tends to fail when $\tau_c > 0$. The Coulomb criterion is identical to the Hubert and Rubey strength if mean stress is replaced by the fault normal stress in the latter. Whereas the mean stress is isotropic, τ_c depends on the local stress field and the orientation of the fault of interest. Though the orientation of individual faults is usually unknown in a region, the average orientation of many faults in a region can often be inferred. Presumably, faults oriented so as to maximize the Coulomb stress will be most likely to fail (King, et al., 1994).

It is common to assume pore pressure is simply a multiple of the mean stress. This simplification implies that the *undrained* condition is applicable. A poroelastic medium is said to be in the undrained state when the stress modification that results from a dislocation occurs so quickly that fluids in the pores are essentially stationary and do not flow appreciably. Mathematically, undrained implies that $P = -B\overline{\sigma}$, where $\overline{\sigma}$ is the mean stress and the proportionality constant B is Skempton's coefficient. Skempton's coefficient is an empirically determined constant that quantifies the fraction of a compressive stress on a porous rock that is transferred to the pore fluid. Wang (1993) gives values for crustal rocks in the approximate range 0.55 to 0.9. If compression is primarily in the direction normal to a fault, then $\overline{\sigma} \approx \sigma_n$. This allows an effective friction coefficient to be defined, $\mu_e = \mu_f \left(1 - B\right)$, which incorporates pore pressure into an effective Coulomb stress:

$$\tau_e \equiv \tau - \mu_e \sigma_n \tag{7.3}$$

The effective Coulomb fracture criterion is a static quantity that can be computed once and for all, given a slip model or coseismic stress field for an earthquake. We will adopt the convention that compressive stresses are negative.

Unfortunately, the undrained assumption is false on time scales over which aftershocks occur. Typical diffusivities in the crust are on the order of 0.01 to 1.0 m^2/s (Charlez, 1997; Wang, 1993). Li, et al. (1987) used diffusivities in the range 0.1 to 10 m^2/s in their study of aftershocks. The time scale for diffusion over distances of 10 km is as little as 10 days with the larger of these values to several years for the smaller values. The appropriate time scale for aftershock studies is not the rupture time of an event, but the time period over which aftershocks occur following an earthquake. The undrained assumption does not hold in the crust over a period of days or months, and perhaps years, following an earthquake event. Pore fluids will flow from regions of high pressure to regions of low pressure following an earthquake. The resulting pore pressure redistribution is coupled to the stress field. Thus, the role of pore fluids in causing aftershock activity must be examined more closely.

We believe that pore pressure diffusion plays a particularly important role in causing aftershocks because it is the primary time-dependent term in the Coulomb criterion. Aftershocks do not all occur immediately following an earthquake; they occur with a time-dependent frequency that decays in a manner remarkably similar to fluid diffusion in porous media. We do not dispute the applicability of the Coulomb criterion to the prediction of future seismic activity. Rather, we believe that the time-dependent pore pressure which appears in the Coulomb criterion cannot be dismissed.

Assume that in a region surrounding an earthquake, faults have a uniform distribution of strengths. Then the number of faults that fail in a certain time interval will be directly proportional to the total increase of τ_c in the region over that time interval. Furthermore, only the regions where τ_c is increasing need to be considered since locations where the Coulomb stress is decreasing will not tend to have aftershocks. This may be expressed quantitatively by

$$N(\Delta t) \approx \int_{region} (\Delta\tau_c/\Delta t)\, dv \tag{7.4}$$

In the simplest approximation, we may assume in equation 7.2 that the shear

and normal stresses change relatively little after a mainshock and can be assumed constant over the period when most aftershocks occur. All changes to the Coulomb stress will then be due to changes in fluid pressure:

$$\frac{\partial \tau_c}{\partial t} = \frac{\partial P}{\partial t} \tag{7.5}$$

Replacing equation 7.5 in equation 7.4 yields equation 7.1.

There is some evidence to suggest that changes to the shear stress caused by pore fluid diffusion are significant. Booker (1974) showed that in the case of a simple edge dislocation, shear stresses along a fault may be strongly coupled to pore pressure and can change appreciably over time due to fluid diffusion. Li (1987) showed that pore fluid diffusion results in slow rotation of the stress shadow caused by an edge dislocation. These suggest that pore pressure is not the only significant time-dependent term in the Coulomb stress criterion that must be considered.

7.4 Equations for Fluid Diffusion in a Porous Medium

Pore pressure diffusion for a single phase fluid in a porous medium is modeled by

$$\mu\phi\left(C_f + C_r\right)\left(\frac{\partial p}{\partial t}\right) = \frac{\partial}{\partial x_i}\left(k_{ij}\left(x,p\right)\frac{\partial p}{\partial x_j}\right) \tag{7.6}$$

where p is the pore pressure, μ is the fluid viscosity, ϕ is the porosity, C_f and C_r are the fluid and rock compressibilities, respectively, and $k_{ij}\left(x\right)$ is the permeability tensor. Permeability is written in a general form here to indicate that it may be spatially variable, anisotropic, and may even depend on pore pressure. We will not examine the effects of all these variables in this study, but allow for this possibility in future studies by making our model general.

For convenience, the coefficients in equation 7.6 may be lumped into a single diffusivity coefficient

$$D = \frac{k_{ij}\left(x,p\right)}{\mu\phi\left(C_f + C_r\right)}$$

The permeability k is taken to be a scalar value which may be spatially heterogeneous. Typical values for D in the crust range from 0.01 to 1 m^2/s (Charlez, 1997; Wang,

1993). The difficulty in modeling flow in porous media, whether one is interested in the transport of contaminants in an aquifer, the flow of oil from a petroleum reservoir, or the diffusion of pore pressure following an earthquake, is in determination of the permeability of the porous rocks. In faulted regions, the permeability structure may be quite heterogeneous (Hickman, et al. 1994). Permeability in fault zones has been observed to be both anisotropic and asymetrically distributed (Seeburger, 1981). Zones of low permeability provides a mechanism for transient pore pressure increase in a fault even when the pore pressure in the surrounding rock is decreasing through the Mandel-Cryer effect (Bosl, manuscript in preparation; chapter 4 in this dissertation). For our study, we will have to assume fairly simple permeabilities, but note that much effort is expended by environmental and oil companies to determine the permeability of a reservoir because of its importance in controlling fluid flow. A conceptual model with more detailed and accurate representation of the actual permeability structure in the Landers region would yield a more realistic simulation of pore fluid diffusion effects.

Pore pressure may be coupled to elastic deformation in the simplest case by assuming only that pore pressure is a source term in the equations for linear elasticity and that the elastic deformation does not appreciably affect the rate of fluid diffusion. The equations for elastic displacement in terms of pore pressure are

$$\frac{\partial}{\partial x_i}\left(\left(\lambda + G\right) u_{k,k}\right) + \frac{\partial}{\partial x_k}\left(G u_{i,k}\right) = \frac{\partial}{\partial x_i}\alpha\left(P_{total} - P_{ref}\right) \tag{7.7}$$

where u_i are the three components of the displacement vector, λ is the usual Lame coefficient and G is the shear modulus. Note that both of these may be spatially variable. The Biot-Willis parameter, α, is a function of Skempton's coefficient and the drained and undrained Poisson's ratios: $\alpha = 2\left(\nu_u - \nu\right)/B\left(1 - 2\nu\right)$. The right side of equation 7.7 is expressed in terms of the deviation of the pore pressure from a reference value, P_{ref}. In the following simulations $P = P_{total} - P_{ref}$ was assumed to be zero initially. That is, the state of stress and pore pressure just *before* the earthquake event was taken as the reference state. From now on, P will be used to represent the change in pore pressure from the pre-seismic reference state. Strain and stress

can be computed from the displacement field in the usual way from derivatives of the displacement field.

In some cases, the stress field induced by pore pressure will influence the pore fluid diffusion significantly. Biot (1956) first derived the equations for coupled poroelasticity. Our formulation of the poroelastic equations follows Rice and Cleary (1976), but is more general in that we assume spatially variable coefficients and a full tensor permeability. Pore pressure is coupled to hydrostatic stress and obeys the following set of equations:

$$b\frac{\partial\left(P+B\sigma\right)}{\partial t}=\frac{\partial}{\partial x_i}\left[k_{ij}\left(x\right)\frac{\partial}{\partial x_j}P\right] \tag{7.8}$$

and

$$\frac{\partial^2}{\partial x_i^2}\left(cP+\sigma\right)=0 \tag{7.9}$$

where P is the pore pressure deviation from a reference pressure, $\sigma=\left(\sigma_{xx}+\sigma_{yy}+\sigma_{zz}\right)/3$ is the mean stress deviation from the reference stress caused by the presence of the pore fluid, k_{ij} is the intrinsic permeability of the rock and b is a coefficient which includes the elastic properties of the rock and fluid density and viscosity:

$$b=\frac{9\mu\left(\nu_u-\nu\right)}{2GB^2\left(1-\nu\right)\left(1+\nu_u\right)} \tag{7.10}$$

ν and ν_u are the drained and undrained Poisson's ratios, respectively, G is the shear modulus, B is Skempton's coefficient, μ is the fluid viscosity and

$$c=\frac{2\left(\nu_u-\nu\right)}{B\left(1-\nu\right)\left(1+\nu_u\right)} \tag{7.11}$$

When $\nu=\nu_u$, c is zero, σ is constant in time and only P evolves in time, as in the case of simple diffusion of a compressible fluid through an incompressible porous rock given by equation 7.6. Physically, $\nu=\nu_u$ corresponds to the case where the rock elastic properties are uneffected by the presence of fluid. It should be emphasized that in equations 7.6 and 7.9 P represents the pressure deviation from the reference

or pre-seismic pore pressure. σ in these equations is not the mean stress due to the fault dislocation used to compute initial pore pressure. Rather, σ here is the mean stress *deviation* caused by the presence of the pore fluid pressure P. Thus, σ decays to zero as the pore pressure decays to zero.

7.5 Aftershocks of the 1992 Landers Earthquake

7.5.1 Description of the 28 June 1992 event

In order to test our theories about aftershock triggering, we chose to look at the 1992 Landers earthquake. The 1992 Landers earthquake was a large and well-documented earthquake. The faults that ruptured in the Landers earthquake are located in the Mohave Block of southeastern California. The region is dominated by northwest-trending, right-lateral strike-slip faults. Rupture during the Landers earthquake occurred along several major faults that were previously thought to be disconnected. It thus provided an example of how stress changes caused by one fault can cause rupture along adjacent faults.

The Landers earthquake was preceded by two months of intense seismic activity in the region south of the mainshock fault trace (Yeats, et al., 1997, pp. 225-227). The largest of these foreshocks was the Joshua Tree earthquake which occurred on April 23, 1998 with a magnitude of M_w=6.1. Aftershocks of the Joshua Tree earthquake migrated northward in the two months between the Joshua Tree and Landers earthquakes. This activity continued to migrate to the vicinity of the Landers hypocenter until only hours before the main shock. It is suggested that this time-dependent behavior requires time-dependent dynamics for a causal explanation and that pore-fluid induced stress changes can account for this.

A major aftershock occured on the Big Bear fault approximately three hours later and 40 km to the west of the Landers rupture. The Big Bear earthquake had a different orientation and slip than the Landers earthquake; it was roughly conjugate to the Landers event. The Landers surface rupture produced right-lateral displacement over a total rupture length of approximately 85 km. Average slip of two to four

meters was measured along the surface and the total magnitude was determined to be M_w=7.3.

7.5.2 Slip models and fluid flow simulation

For this study it is important to have an accurate a slip model. Initial pore pressures are determined by the slip model and subsequent flow will depend to a large extent on the initial pore pressures. Hudnut, et al. (1994) used geodetic and surface rupture data to produce a detailed horizontal slip model of the Landers earthquake though it is limited by its assumption of uniform vertical slip. We use this model to compute the coseismic mean stress that would be produced by the earthquake. From this, the pore pressure changes due to the mean stress are computed from the undrained condition

$$P = -B\overline{\sigma}$$

This condition applies only at the moment of fault slip, before the fluid has time to diffusion appreciably. Subsequent fluid flow is then simulated by solving the coupled poroelastic equations shown above. It should be stressed that although the slip model of Hudnut et al.(1994), has considerable horizontal detail, it does not include vertical variability. In order to examine the effects of vertical variability in the slip model, we also used the slip model of Wald and Heaton (1994).

7.5.3 Regional aftershock frequencies

Regional aftershock frequencies according to the Nur and Booker hypothesis may be computed from simulated pore pressures at selected times by integrating numerically the time rate of change of pore pressure over a defined volume:

$$\frac{1}{c}\int_{\Omega}\left(\frac{\partial P}{\partial t}\right)d\mathbf{x} \approx \frac{1}{c}\sum_{i=1}^{N}\frac{P\left(t_n\right)-P\left(t_{n-1}\right)}{\Delta t}v_i \tag{7.12}$$

where Ω is the domain of interest, v_i is the volume of the i^{th} cell, and the summation is over all N cells in the domain. c is a scaling factor which relates the change in pore

pressure to the aftershock frequency. In this case the domain is the region bounded by longitude -117.0° to -116.0° and latitude 33.8° to 34.8°, a region approximately 92 km by 111 km. The rate at which pore pressure decays is controlled by the permeability of the crust. The scaling factor is set equal to one.

Figure 7.1 shows the initial (coseismic) pore pressure distribution that was computed from Hudnut's fault model, which is superimposed on the pore pressure image. Initial stresses were computed using the elastic dislocation code of Larsen (Larsen, 1991). The $46 \times 55 \times 3$ grid, which uses 2 km $\times$ 2 km $\times$ 5 km cells, appears to have enough resolution to capture most of the spatial variability of the pore pressure along the fault.

Figure 7.2 shows actual aftershock frequency data and the computed frequency based on the pore pressure diffusion hypothesis. This was accomplished by solving equation 7.6 numerically. At each time step, the pore pressure change from the previous time step was computed at every grid point. The pore pressure changes were then integrated over the entire domain using equation 7.12.

The scaling parameter $c = 8$ was determined empirically by fitting the theoretical curve to the aftershock data. The theoretical curve is approximately level until roughly 10 days, when it begins to follow a straight decline on the log-log plot. This corresponds approximately to the actual data. In the analytical solution shown in Nur and Booker's original work, the theoretical pore pressure diffusion curve is a straight line on log-log axes. Numerically, the pore pressure diffusion line cannot be straight on a log-log plot for finite grids for reasons that have been discussed. This corresponds physically to the fact that an elastic dislocation model fails when the theoretical elastic stress exceeds the strength of the rock. Pore pressures or coseismic stress have a finite limit in real rocks.

The predicted aftershock frequency curve corresponds quite well to the actual aftershock frequency data. Calculation of aftershock frequency curves for subdomains of the entire regions surrounding the Landers earthquake also agreed reasonably well with data. However, a much better test of the theory is to look at pore pressure tendency at the locations of individual aftershock events.

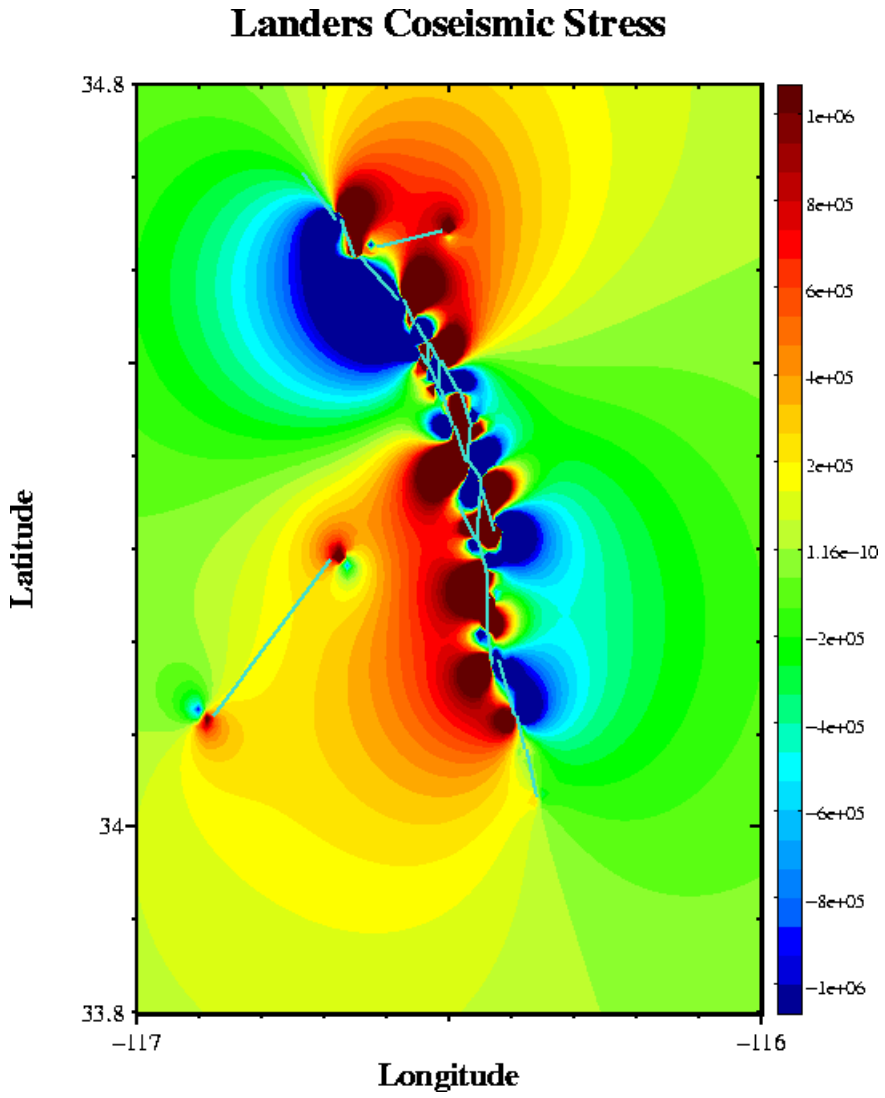

Figure 7.1: Coseismic mean stress field computed from Hudnut, et al. (1994) slip model. Fault trace is superimposed on the mean stress image. Negative mean stress is compressive.

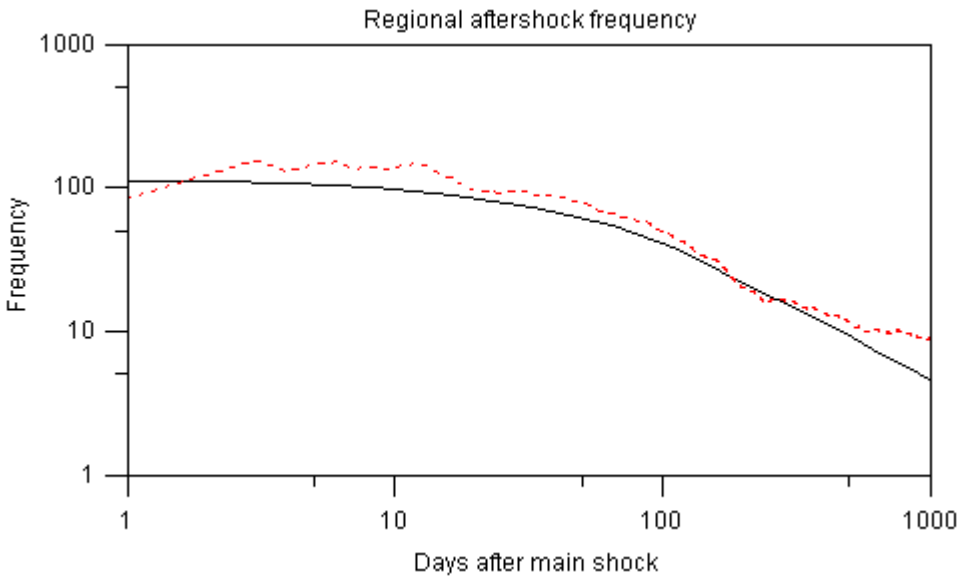

Figure 7.2: Regional aftershock frequency (events per day) following the 1992 Landers earthquake as a function of the days after the main shock. Dashed line is actual measurements. The solid line is the computed frequency based on the hypothesis of Nur and Booker.

7.5.4 Pore pressure tendency at aftershock locations

To directly test the hypothesis that aftershocks will tend to occur where pore pressure is increasing, the location in space and time of each aftershock in the first year following the main earthquake were read into our pore fluid diffusion model during execution. On each day of the simulation, the pore pressure trend at the location of each aftershock for that day was determined. Where the pore pressure was *increasing*, an event counter was incremented by one. In this way, the fraction of aftershocks that happened in a location where the pore pressure was increasing was recorded as a function of time. Overall, nearly two-thirds (65%) of the aftershocks occurred where pore pressure, at the time of the event, was increasing (figure 7.3). Outside of the fault zone, the percentage of aftershocks occuring where pore pressure is increasing approaches 80%.

As mentioned earlier, the permeability structure of fault zones can be anisotropic and heterogeneous (Hickman, et al., 1995). Within the fault zone, defined to be 10 km on either side of the fault trace, the fraction of aftershocks occuring where pore pressure was rising was slightly greater when the permeability was *increased* by a factor of four parallel to the fault and *decreased* by a factor of 100 normal to the fault. Enhanced permeability along the fault and decreased permeability normal to the fault has been observed (See the collection of papers on this subject in Hickman, 1994). Though one of the most difficult problems associated with simulations of fluid flow in the crust is assignment of permeability values, this exercise suggests that it is not a static coseismic state variable that is controlling aftershocks, but a dynamic variable that changes with the permeability. The fraction of aftershocks occuring where Pp is increasing was slightly higher (68%) in the fault zone with the anisotropic permeability. Outside the fault zone was unchanged. This indicates that the permeability of the fault zone and the surrounding region may have an effect on the location of aftershocks. Simulations using Wald and Heaton's slip model (1994), which includes variable slip with depth, did not improve our results.

A marked drop in the fraction of aftershocks occuring where pore pressure is increasing occurs at around 150 days after the mainshock. In figure 7.4 we find the cause of this drop. Aftershock locations were written to separate files at run

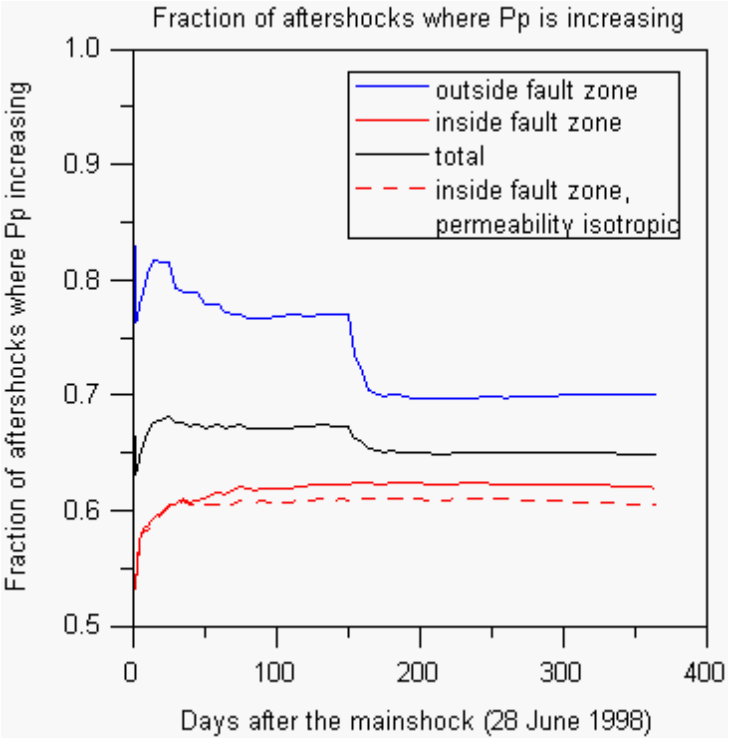

Figure 7.3: Fraction of aftershocks that occur where pore pressure is rising.

during our simulations depending on whether pore pressure tendency was positive or negative at the time of the aftershock. Black dots in figure 7.4 indicate the locations of aftershocks that occured when pore pressure was increasing at that location. Colored dots indicate those that occured where pore pressure was decreasing. Also shown, with large blue squares, are large aftershocks (>M5.0). On November 29 and December 4, two large aftershocks occured just north of the Big Bear fault. A cluster of aftershocks was apparently spawned by these two large events in a region where pore pressure was decreasing. The pore pressure field, however, would have been significantly altered by the large aftershocks. This effect was not included in our model. In fact, an accurate simulation would have to incorporate the stress and pore pressure changes for all moderately large events if it was to accurately model the actual pressure evolution of the region. This seems to account for the sharp drop on the curves in figure 7.3 that occurred near day 150.

It is significant that the aftershocks which do not agree with our hypothesis are not randomly scattered. They are primarily found in four distinct clusters: one just mentioned in association with the November 29 and December 4 aftershocks; one off the southern end of the Johnson Valley and Eureka Peak faults centered at (-116.4, 34.1); off the northern end of the Camp Rock fault, centered at (-116.7, 34.6); and a small cluster in the slip gap region that connects the Emerson and Homestead Valley faults, centered at (-116.5, 34.5). This suggests that pore pressure alone is not the cause of aftershocks.

7.5.5 Coulomb stress due to pore pressure

Booker (1974) suggested that pore fluid diffusion following a fault dislocation causes partial reloading of the stress on the fault. Another way to interpret this is that the presence of pore fluids in an elastic medium partially resists the stress imposed by the initial fault dislocation. Pore fluid is a shock absorber that mitigates, so some extent, the initial strain imposed by a fault dislocation. The fluid flow that follows relaxes the resistance and the strain goes asymptotically to the state that would have been attained initially if the fluid had not been present. We might expect, then that pore fluid

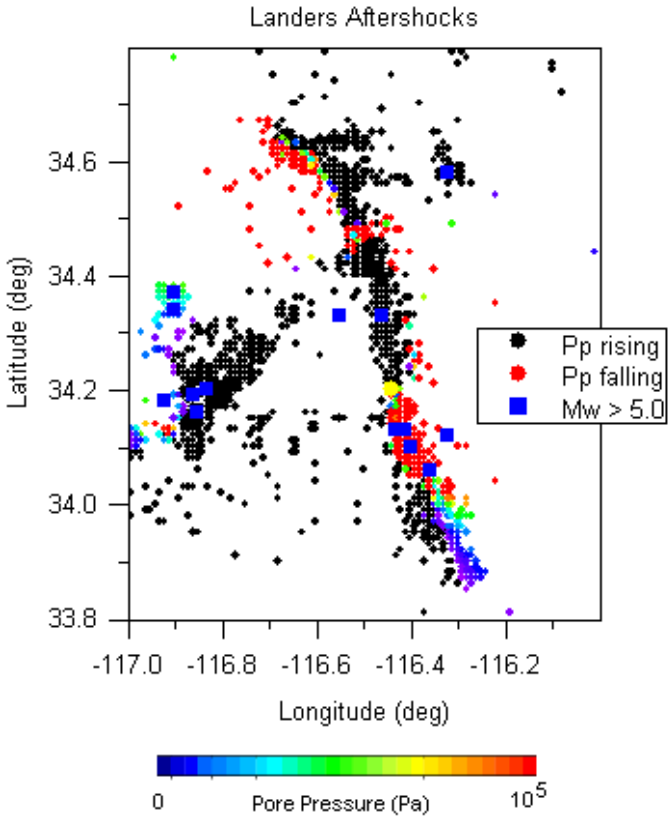

Figure 7.4: Aftershocks of the Landers earthquake. Yellow dot shows location of mainshock epicenter. Large blue squares indicate aftershocks with Mw $>$ 5.0. Black dots indicate aftershocks which occurred where pore pressure was rising. Colored dots are aftershocks that occurred where pore pressure was decreasing. Color indicates the magnitude of the pore pressure at the time of the aftershock event.

diffusion would tend to cause the Coulomb stress to increase over time in locations where the initial Coulomb stress was positive. The correspondence between locations of initial Coulomb stress and Coulomb stress increase due to pore fluid diffusion will not correspond exactly, since the movement of fluid will be controlled by permeability heterogeneities. Li, et al. (1987) showed that regions of positive Coulomb will rotate somewhat with time due to poroelastic effects. Similarly, Coulomb stress increases will tend to occur in regions where pore pressure is increasing, but the correspondence will not be exact. This can explain why predictions of aftershock location based on initial static Coulomb stress calculations (King, et al., 1994) and on pore pressure change (results presented in this paper) both give fairly good results. Physically, the variable of interest is the change in Coulomb stress due to pore pressure diffusion.

To test this hypothesis, we followed the above procedure to simulate flow following the Landers earthquake. Wald and Heaton's dislocation model was used (1994) to initialize pore pressures, primarily because King, et al. (1994) used this model for a study of Coulomb stress following the Landers earthquake. We then computed the Coulomb stress due only to pore pressure over the same region as our pore pressure study at every time step in our simulation. The change in Coulomb stress *due to pore pressure change* was computed at the time and location of each aftershock in the year following the mainshock. Within 10 km of the fault zone, where the majority of aftershocks occurred, more than 85 % occurred where Coulomb stress due to pore pressure was increasing. After the 18^{th} day, 100 % of the aftershocks in the fault zone occurred where $\tau_c(P)$ was increasing. For this calculation, we use 45° for the fault strike angle and assumed left lateral slip tendency. This crude estimate is approximately what was used by King, et al. to correlate aftershocks to the initial Coulomb stress field caused by the fault slip.

Landers aftershocks are shown in Figure 7.5. Black dots are aftershocks that occurred where $\tau_c(P)$ was increasing. We note that in the fault zone, those that disagree with our hypothesis are not randomly scattered, but are clustered at the north end of the Camp Rock fault, centered at (-116.65, 34.65). Stresses due to the Iron Ridge fault which are not properly modeled may account for this.

The fraction of total aftershocks occuring where $\tau_c(P)$ is increasing was around

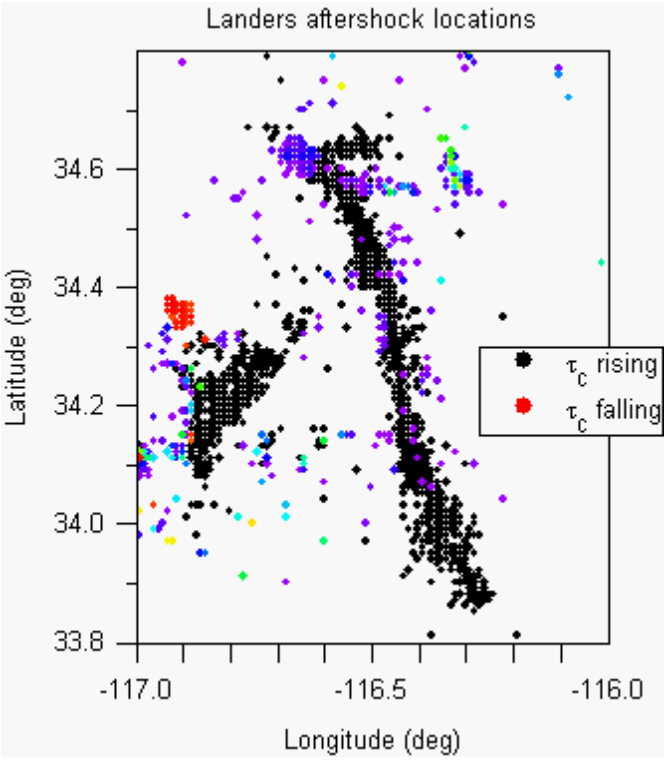

Figure 7.5: Aftershocks of the Landers earthquake compared to Coulomb stress tendency due to pore fluid diffusion. Black dots indicate aftershocks which occurred where $\tau_c(P)$ was rising. Colored dots are aftershocks that occurred where $\tau_c(P)$ was decreasing. Color indicates the time of the aftershock event; blue/violet are early, red are after 150 days.

80%. Aftershocks outside of the fault zone were largely associated with the large Big Bear aftershock. As with the pore pressure study in the previous section, a cluster of aftershocks north of the Big Bear fault occurs after day 150, following two large aftershocks in that location. The effects of those aftershocks should be taken into account in an accurate representation of the changing stress field.

The Coulomb stress tendency depends on the strike angle of the aftershock fault. Our use of a constant value of 44° gives remarkably good results, particularly inside the fault zone. A true test of our theory would require information about the slip mechanism for each aftershock.

7.6 Summary and Conclusions

Our first observation from our simulations is that most aftershocks occured where pore pressure was increasing. Furthermore, aftershocks which occur where pore pressure is decreasing are not randomly scattered. Instead, they occur in four distinct clusters. All of these clusters are located in regions of relatively low pore pressure deviation, along nodal lines separating the four main stress quadrants for the Landers earthquake. This led us to examine the Coulomb stress field caused by the presence of pore fluids and how it would change with time.

The time-dependence of aftershocks requires a time-dependent physical mechanism. Our simulations indicate that the overwhelming majority of Landers aftershocks were occuring where the Coulomb stress due to pore fluid diffusion was increasing. Because there is ample evidence to suggest that the crust behaves as a poroelastic medium, it is reasonable to expect that pore fluid diffusion will have an effect on the stress state of the crust. Pore fluids initially resist imposed stresses, then relax over time. This explains the reasonably good correlation between initial Coulomb stress and aftershocks. We emphasize, however, that the post-seismic Coulomb stress changes due to pore fluid diffusion are the essential time-delayed cause of aftershocks.

Theoretical studies of poroelastic response following edge dislocations by Booker (1974) and Li (1987) have shown that the Coulomb stress field in the region around a fault will change following rupture due to pore fluid diffusion. The complexity of real faults requires detailed numerical modeling to compare poroelastic simulation results with actual data.

Since permeability controls the direction and rate of fluid diffusion in a porous medium, more accurate knowledge of the permeability structure of faults and the surrounding regions will be required to make better calculations of the rate and magnitude of poroelastic stress changes due to pore fluid movement. The pressure dependence of permeability, spatial heterogeneities and anisotropy in and near the fault zone may dramatically affect fluid flow patterns and the evolution of the postseismic pressure field. The magnitude of the poroelastic effect depends also on the elastic parameters of the material, particularly the difference between drained and undrained

elastic moduli, or Poisson ratios, ν_u and ν. Nevertheless, the results of this study indicate that physical models of stress evolution in the crust must include pore fluids if effects with time scales of days to several years are of interest. Even approximate estimates for material parameters appear to support our poroelastic hypothesis. We suggest that poroelastic relaxation might also explain observed afterslip.

Greater use should be made of computer simulation to study the physics of crustal dynamics in order to better understand the earthquake process. This will require research into modeling techniques for the crust (and perhaps the upper mantle as well). Methods for modeling fluid flow in the crust have been studied for many years because of their economic and environmental importance. The role of permeability in controlling fluid flow in contaminated aquifers and in petroleum reservoirs is well known. Considerable research has been devoted to studies of how to model permeability heterogeneities through the use of geostatistics, various models for flow in fractured media, and new methods for measuring permeability directly or remotely. Crustal dynamics research will have to borrow fluid flow modeling methods from hydrology and reservoir engineering in order to determine more precisely how the physics of fluids must be integrated into the complex systems of fault mechanics and crustal seismicity.

7.7 Acknowledgements

This work was supported by USGS/NEHERP Grant #1434-HQ-97-GR-03 and DOE Basic Science Program Grant #FG03-86ER13601. The authors wish to thank Greg Beroza for helpful discussions about aftershocks.

Bibliography

Biot, M. A., General solutions of the equations of elasticity and consolidation for a porous material, *J. Appl. Mech., Trans ASME*, *78*, 91–96, 1956.

Booker, J. T., Time dependent strain following faulting of a porous medium, *Journal of Geophysical Research*, *79*, 2037–2044, 1974.

Bosl, W. J., and A. Nur, Numerical simulation of postseismic deformation due to pore fluid diffusion, in *Poromechanics: A Tribute to Maurice A. Biot*, edited by e. A. J.-F. Thimus, pp. 23–28, A. A. Balkema, Rotterdam, 1998.

Charlez, P. A., *Rock Mechanics Volume 2: Petroleum Applications*, Editions Technip, Paris, 1997.

Dieterich, J., A constitutive law for rate of earthquake production and its application to earthquake clustering, *Journal of Geophysical Research*, *99*, 2601–2618, 1994.

Hickman, S., R. Sibson, and R. Bruhn, eds., *The Mechanical Involvement of Fluids in Faulting*, Menlo Park, CA, U. S. Geological Survey, 1994.

Hudnut, K. W., et al., Co-seismic displacements of the 1992 landers earthquake sequence, *Bull. Seis. Soc. Am.*, *3*, 625–645, 1994.

King, G. C. P., R. S. Stein, and J. Lin, Static stress changes and the triggering of earthquakes, *Bulletin of the Seismological Society of America*, *84*, 935–953, 1994.

Larsen, S. C., Geodetic measurements of deformation in southern california, Ph.D. thesis, California Institute of Technology, 1991.

Li, V. C., S. H. Seale, and T. Cao, Postseismic stress and pore pressure readjustment and aftershock distributions, *Tectonophysics*, *144*, 37–54, 1987.

Nur, A., and J. R. Booker, Aftershocks caused by pore fluid flow?, *Science*, *175*, 885–887, 1972.

Peltzer, G., P. Rosen, F. Rogez, and K. Hudnut, Postseismic rebound in fault step-overs caused by pore fluid flow, *Science*, *273*, 1202–1204, 1996.

Peltzer, G., P. Rosen, and F. Rogez, Poroelastic rebound along the landers 1992 earthquake surface rupture, *Journal of Geophysical Research*, *103*, 30131–30145, 1998.

Roeloffs, E., Poroelastic techniques in the study of earthquake-related hydrologic phenomena, *Advances in Geophysics*, *37*, 135–195, 1996.

Seeburger, D. A., Studies of natural fractures, fault zone permeability, and a pore space-permeability model, Ph.D. thesis, Stanford University, 1981.

Stephen Hickman, R. B., Richard Sibson, Introduction to special section: The mechanical involvement of fluids in faulting, *Journal of Geophysical Research*, *100*, 12831–12840, 1995.

Wald, D. J., and T. H. Heaton, Spatial and temporal distribution of slip for the 1992 landers, california, earthquake, *Bulletin of the Seismological Society of America*, *84*(3), 668–691, 1994.

Walder, J., and A. Nur, Porosity reduction and crustal pore pressure development, *J. Geo. Res.*, *89*(B13), 11539–11548, 1984.

Wang, H. F., Quasi-static poroelastic parameters in rock and their geophysical applications, *PAGEOPH*, *141*(2/3/4), 269–286, 1993.

Yeats, R. S., K. Sieh, and C. R. Allen, *The Geology of Earthquakes*, Oxford University Press, New York, 1997.